Modelling far-field dredge plume dispersion

Master's thesis
Taco Tuinhof
Rotterdam, October 2014

Van Oord
Marine ingenuity

TU Delft
Delft University of Technology

Modelling far-field dredge plume dispersion

Report

Master's thesis

Taco Tuinhof
October 2014

Graduation committee

Prof.dr.ir. W.S.J. Uijttewaal	*TU Delft - Environmental Fluid Mechanics section*
Dr.ir. M. van Koningsveld	*Van Oord Dredging and Marine Contractors BV & TU Delft*
Ir. L. de Wit	*TU Delft - Dredging Engineering section*
Ir. E. van Eekelen	*Van Oord Dredging and Marine Contractors BV*

Student

T.J. (Taco Johannes) Tuinhof
Student number: 1392921
Email: tacotuinhof@gmail.com

This thesis is submitted to Delft University of Technology in fulfillment of the requirements for the degree of Master of Science in Hydraulic Engineering

The work in this thesis was supported by Van Oord Dredging and Marine Contractors BV. Their cooperation is hereby gratefully acknowledged.

Cover photo: Dredging operations

Acknowledgment

This Master's thesis is written in the scope of my Msc graduation project which is carried out as finalising part of the Master of Science program Hydraulic Engineering, at the faculty of Civil Engineering and Geosciences of the Delft University of Technology. The graduation project is carried out in corporation with Van Oord Dredging and Marine Contractors BV. The topic was put forward by the environmental engineering department of Van Oord. In close cooperation with professor Uijttewaal we were able to set up an interesting research topic. This research on dredge plumes has given me great insight in the environmental considerations of dredging activities. I am Van Oord grateful for offering me this opportunity.

First I thank all colleagues at the engineering department and my fellow students at Van Oord for the nice working environment. Also, I thank Erik van Eekelen for his supervision during the project. His knowledge on, and enthusiasm about, the topic were highly motivating. Our discussions every now and then helped to stay focused. Furthermore, I thank the other graduation committee members, Lynyrd de Wit and Mark van Koningsveld. Their comments during the meetings were very useful, especially because of their diverse but detailed knowledge on the topic. Also, I thank the chairman of the graduation committee; Professor Uijttewaal. His advice and suggestions helped to stay on track.

Finally, I thank my family, friends and girlfriend Saskia. Not only for their help while writing this master's thesis, but especially for their unconditional support during all my academic years in Delft.

Enjoy reading!

Taco Tuinhof
Rotterdam, October 2014

Abstract

By its very nature dredging is an environmental impact, since dredging includes the excavation and/or relocation of sediment in a river, sea or estuary. One of the environmental impacts related to dredging is increased suspended sediment concentration (SSC) levels, forming plumes of sediment. These so called dredge plumes originate from spillage of dredged material. Especially the fine sediment can stay in suspension on long time and spatial scales. Environmental Impact Assessments (EIAs) are conducted prior to the project's start to assess impact of dredging activities. One of the concerns of an EIA is to determine dredge induced rise of SSC levels. Forecast modelling is often applied to simulate dredge plumes in order to verify SSC and sedimentation levels. However, due to large uncertainties about the project, input parameters and ambient parameters, forecast modelling of dredge plumes is often challenging.

In the development of a dredge plume a distinction is made between the near- and the far-field, based on the differences in governing spreading mechanisms. Corresponding variation in time and spatial scales demand separate modelling approaches for the two areas. Far-field modelling can be performed using numerical modelling packages as Delft3D-FLOW, simulating both hydrodynamics as well as sediment transport. Near-field measuring or modelling campaigns can be used to determine the amount of sediment entering the far-field. Coupling of the two areas is crucial in dredge plume modelling. The aim of this research is to identify and test the influence of the most important parameters involved in modelling far-field dredge plume dispersion. Hereby, informed selection of modelling techniques and model input regarding forecast modelling spread of SSC in the far-field is supported.

The theoretical framework resulted in identification of influencing parameters, divided into three sets; model, input and ambient parameters. Model parameters are related to the formulations used in the model, model input and the schematisation of the considered area, being; the computational approach, computational grid size, time step, turbulent viscosity and diffusivity and erosion and deposition parameters. The input parameters are associated with the source term. This research illustrated that the use of a virtual source at the location of the dredging activity is inappropriate. Influence of near-field processes need to be accounted for, demanding the use of a far-field source term at the location of the transition zone. Input parameters regarding this far-field source term are the source term magnitude, input location, sediment properties, lateral and vertical source term distribution. Ambient parameters follow from the ambient conditions in the considered area; e.g. stratification, wind, water depth and flow velocity. In this research the influence of flow velocity and water depth are investigated. The effects of each of the model, input and ambient parameters are determined through a numerical model experiment, simulating uniform stationary channel flow.

The experiment revealed a clear distinction in results based on plume age and parameter of interest. Influencing parameters for a young plume, resulting from a continuous source input and located relatively close to the source, might in some cases be different from an old dredge plume. For an old dredge plume the source input has stopped and the 'released' plume has been advected further in the far-field. Also, the distinction between concentration and flux results is relevant, as both parameters are related to different environmental impacts.

Table 1 shows an overview of the effects of tested parameters on fluxes and concentrations, regarding both old as well as young dredge plumes. Comparison of the parameters gave insight in their relative importance on modelling far-field dredge plume dispersion. For instance, the computational approach has largest effect on both far-field flux and concentration results. Especially for the old dredge plume the fluxes strongly dependent on the chosen computational approach. This is caused by varying sedimentation rates in 1D, 2D and 3D, for equal settling velocities. Adjustment of the settling velocity can be applied to counteract these different sedimentation rates, hence leading to equal results.

Effects of the vertical distribution of the source term on far-field results was small compared to other contributors (computational approach and grid size). Vertical mixing of the sediment happened within several hundred meters from the source, minimising its influence on far-field dredge plumes. On the other hand, the lateral distribution of the source did have large effect on far-field concentrations. Given the relatively small lateral diffusivity, initial plume variations are maintained for old plume ages.

Parameter	**Influence on young dredge plume**	**Influence on old dredge plume**
Computational approach	Flux & Concentration	Flux & Concentration
Computational grid size	Concentration	Flux & Concentration
Lateral distr. source	Concentration	Concentration
Vertical distr. source	Flux	-
Moving source term	Flux & Concentration	Flux & Concentration
Diffusivity	Concentration	Concentration

Table 1: Overview of effects of influencing parameters on far-field results for both young as well as old dredge plumes

The conclusions drawn in the experiment were further tested by comparison with measured field data. The comparison gave rise to similar conclusions and demonstrates acceptable performance of the model. Calibration of the model by adjusting the settling velocity and diffusivity lead to reasonable settling velocities for the plume's sediment. However, the velocities are considered too high for fine sediment, indicating that floc formation or dynamic processes are still taking place in the measured far-field plumes.

Results on the influence of parameters, requested output and comparison with the measured data finally lead to recommendations on effective modelling techniques regarding forecast modelling of dredge plumes. In general a horizontally and vertically fine gridded 3D model would lead to the most accurate results. However, determined by the requested output, less computationally demanding approaches can serve as alternative. The alternatives were based on research conclusions on the computational approach, computational grid size and variation in source term input.

Contents

Nomenclature

B	Initial buoyancy flux through overflow pipe	m^4/s^2
C	Suspended sediment mass concentration	kg/m^3
$\overline{C}$	Time averaged suspended sediment mass concentration	kg/m^3
C'	Fluctuating component of suspended sediment mass concentration	kg/m^3
C_{2D}	2D Chézy coefficient	$m^{1/2}/s$
C_{chezy}	Chézy coefficient	$m^{1/2}/s$
C_b	Near bed suspended sediment concentration	kg/m^3
C_d	Wind drag coefficient	–
C_M	Suspended sediment concentration of dry bed	kg/m^3
D	Deposition rate	kg/sm^2
D_l	Plume width (defined by top hat profile)	m
D_m	Molecular diffusion coefficient	m^2/s
D_p	Diameter of primary mud particles	m
D_{pipe}	Diameter of overflow pipe	m
$D_t(x,y,z)$	Turbulent diffusion coefficient in x,y or z direction	m^2/s
E	Evaporation in Equation C.2	m/s
E	Erosion rate	kg/sm^2
$E1$	Coefficient in Equation 2.19	–
$E2$	Coefficient in Equation 2.19	–
F_D	Drag force	N
F_g	Gravity force	N
F_η	Turbulent momentum flux in η-direction	m/s^2
F_ξ	Turbulent momentum flux in ξ-direction	m/s^2
$\sqrt{G_{\eta\eta}}$	Coefficient used to transform curvilinear to rectangular coordinates	m
$\sqrt{G_{\xi\xi}}$	Coefficient used to transform curvilinear to rectangular coordinates	m
H	Total water depth ($H = d + \zeta$)	m
K	Dispersion coefficient	m^2/s
L	Characteristic length scale of turbulent eddies	m
M	Initial momentum flux through overflow pipe	m^4/s^2
M	Erosion parameters	–
M_s	Sediment flux	kg/s
M_η	Source or sink in η-direction	m/s^2
M_ξ	Source or sink in ξ-direction	m/s^2
P	Precipitation	m/s
P	Hydrostatic water pressure	kg/ms^2
P_η	Gradient hydrostatic pressure in η-direction	kg/m^2s^2

P_ξ	Gradient hydrostatic pressure in ξ-direction	kg/m^2s^2
Q	Initial volume flux through overflow pipe	m^3/s
R_L	Auto correlation function	–
Re	Reynolds number	–
Re_p	Particle Reynolds number	–
Ri	Richardson number	–
Ri_f	Flux Richardson number	–
Ri_l	Local plume Richardson number	–
S	Erosion/Deposition step function	–
Sc	Schmidt number	–
T_L	Lagrangian time scale	s
U	Depth averaged flow velocity in x-direction	m/s
U_{10}	Average wind speed at 10 m above free surface	m/s
U_a	Flow velocity of ambient water	m/s
ΔU_g	The centreline excess velocity in a buoyant jet	m/s
V	Depth averaged flow velocity in y-direction	m/s
W	Outflow velocity of overflow plume	m/s
W_0	Initial velocity of overflow plume uniform across the jet	m/s
b	Half the width of the plume in the ZEF	m
d	Depth below some horizontal plane of reference	m
d_g	Equivalent grain diameter	m
d_{50}	Median equivalent grain diameter	m
f	Coriolis parameters	$1/s$
g	Gravitational acceleration	m/s^2
g'	Reduced gravitational acceleration	m/s^2
h	Water depth	m
i	Channel slope	–
k	Probability of transfer of solute	–
l_Q	Characteristic length scale of buoyant jet	m
l_t	Lagrangian length scale	m
m	Mass	kg
m_e	Erosion constant	–
nf	Fractal dimensions of mud flocs	–
q	Solute mass flux	kg/s
$q_{in/out}$	Discharge	m^3/s
t	Time	s
u	Flow velocity in x direction	m/s
$\overline{u}$	Time averaged flow velocity in x direction	m/s
u'	Fluctuating component of flow velocity in x direction	m/s
u_*	Shear velocity	m/s
u_L	Lagrangian velocity scale	m/s
v	Flow velocity in y direction	m/s
$\overline{v}$	Time averaged flow velocity in y direction	m/s
v'	Fluctuating component of flow velocity in y direction	m/s
w	Vertical flow velocity	m/s
$\overline{w}$	Time averaged vertical flow velocity	m/s

w'	Fluctuating component of vertical flow velocity	m/s
w_s	Settling velocity	m/s
z_M	Jet to crossflow vertical length scale	m
z_B	Plume to crossflow vertical length scale	m
Θ_{cr}	Shields critical mobility factor	–
α	Sediment shape factor	–
β	Sediment shape factor	–
ε_s	Eddy diffusivities of sediment fraction	m^2/s
μ	Dynamic viscosity	Ns/m^2
ν	Kinematic viscosity	m^2/s
ν_t	Turbulent viscosity	m^2/s
ν_V	Vertical eddy viscosity	m^2/s
ν_H	Horizontal eddy viscosity	m^2/s
ρ_0	Reference density of water	kg/m^3
ρ_a	Density of air	kg/m^3
ρ_s	Density of grains	kg/m^3
ρ_w	Density of water	kg/m^3
$\Delta\rho$	Density difference between jet and ambient fluid	kg/m^3
σ^2	Variance of a distribution	–
ω	Velocity in the σ-direction in the σ-coordinate system	m/s
τ	Time interval	s
$\tau_{b,cr}$	Shields critical bed shear stress	N/m^2
τ_{cw}	Mean bed shear stress due to current and waves	N/m^2
τ_d	Critical bed shear stress for deposition	N/m^2
τ_e	Critical bed shear stress for erosion	N/m^2
τ_s	Shear stress at surface	N/m^2
τ_t	Turbulent (Reynold) shear stress	N/m^2
ζ	Water level above some horizontal plane of reference	m

Acronyms

ADCP	Acoustic doppler current profiler
ADI	Alternating direction implicit
CFD	Computational fluid dynamics
CFL	Courant-Friedrichs-Lewy number
CVP	Counter-rotating vortex pair
EIA	Environmental impact assessment
HLES	Horizontal large eddy simulation
LES	Large eddy simulation
LMOB	Lean mixture overboard system
OBS	Optical backscatter
SSC	Suspended sediment concentration
TSHD	Trailing suction hopper dredger
ZEF	Zone of established flow
ZFE	Zone of flow establishment

Chapter 1

Introduction

Dredging consists of the excavation of material from a sea, river or lake bed and the relocation of this excavated material. It is by this very nature that dredging activities are an environmental impact (Bray, 2008). The excavation and relocation of material can have direct consequences on habitats living in the vicinity of the works, but also on habitats living many kilometres away.

One of the environmental effects related to dredging is the (re)suspension of fine sediment, leading to increased turbidity. Turbidity is a description of how clear the water is; an optical measure for cloudiness of the water column due to the presence of undissolved matter. The term suspended sediment concentration (SSC) is also used in literature. SSC is the measurement of the dry -weight mass of sediment that is suspended in the water. SSC is a more exact measure than turbidity, however turbidity is commonly used due to the simplicity of measurements. SSC and turbidity are two different approaches for the same phenomenon.

Suspended sediment originating from dredging activities are called dredge plumes. Dredge plumes have become an environmental issue in the 1970's (VBKO, 2003). It should be noted that dredging is not the only source for plumes of sediment. High river peak discharges, storms and ship-manoeuvrings are also associated with sediment plumes (Aarninkhof et al., 2007).

This research focuses on the dispersion of dredge plumes. In this introductory chapter the environmental impact of increased SSC levels is explained. Also, the sources and classifications of dredge plumes are introduced and modelling and measuring methods available are outlined. Following this introduction the research objectives and research questions are formulated. The chapter is concluded with the research approach and structure of the report.

1.1 Environmental impact of dredge plumes

The environmental impact of a dredging activity depends on the existing environment, the sensitive receptors present and their sensitivity to the activity. Sensitive receptors are flora or fauna to which ecological risks are posed (Bray, 2008). The degree of environmental impact of dredging activities is therefore highly site specific. Cases are reported with only impact close to the work area, while in other cases impact may occur more than 70 km away from the source, governed by the prevailing current (PIANC, 2010). Other site specific conditions (background SSC levels, water depth, hydrodynamic conditions) as well as the type and duration of dredging further determine the level and location of impact (Figure 1.1). Furthermore, it is possible for some ecosystems to adapt to the increase in SSC levels, which may decrease environmental impact. It should also be

mentioned that dredging activities do not necessarily have a negative influence on the environment, and can in some cases even have a positive effect. For instance, through resuspension organic matter can be released in the water column and provide a food source for fish.

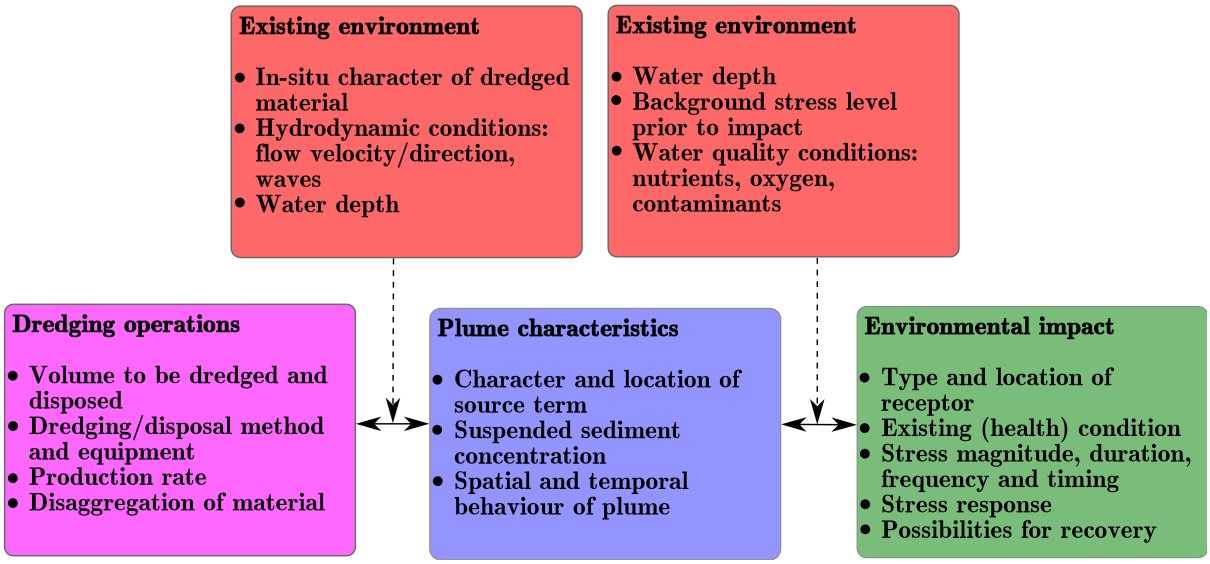

Figure 1.1: Overview of plume characteristics and potential environmental impact (free after: Jacobs et al. (2013)).

An Environmental Impact Assessment (EIA) is a standard procedure to identity and assess potential environmental impact of a proposed project. Nowadays, even in projects where local or national legislation do not require an EIA, some form of environmental assessment is conducted (PIANC, 2010). These assessments require thorough insight in presence and dispersion of SSC and the corresponding impact on environment.

This study will merely focus on the spreading of the SSC, not on impact to environmental receptors. Possible negative impacts of dredging induced SSC are listed below:

1. Turbid water absorbs more heat from the sunlight. Warmer water will lead to a lower concentration of oxygen in the water (oxygen dissolves better in colder water). This can be harmful to organisms.

2. The suspended particles affect the transmittance of the light of the water, decreasing the photosynthetic activity of plants and algae. Coral reefs or sea grasses are vulnerable to this shading.

3. As a consequence of the particles settling to the bottom, flora and fauna living on the sea bed can get covered by sediment.

4. Increasing SSC levels have an aesthetic effect; water looks dirty. This can, for instance, have a negative effect on recreational activity in the area.

5. If water is used for drinking purposes high SSC levels can be a threat.

6. The suspended particles help the attachment of heavy metals and other toxic organic compounds and pesticides.

1.2 Dredge plumes

1.2.1 Sediment sources

Sediment can be released from dredging activity by a wide range of mechanisms and at different levels in the water column. Bray (2008) describes four stages of the dredging process in which sediment can be released, regardless the type of dredging equipment used; being dislodging, vertical transport, horizontal transport and placement. The type of equipment and corresponding release mechanisms influence the impact of the dredge plume. Sediment released close to the bed will settle quickly, reducing the impact to the environment. The main causes of sediment release, sorted by type of equipment, are (VBKO, 2003):

- *Grab Dredger*
  Sediment release mechanisms are: the impact of the grab on the bed, disturbance of the bed during closing, spillage from the grab during hoisting, material washed from outer surface of grab during hoisting, leakage during slewing to the barge, washing of residual adhering material during lowering and splashing and leakage from transport barge.

- *Bucket Ladder Dredger*
  Sediment release mechanisms are: disturbance around buckets, sediment spilling and being eroded from the buckets as they ascend, leakage from the discharge chutes, release of air trapped in the descending buckets and dragging the bucket chain over the bed.

- *Cutter Suction Dredger*
  Sediment release mechanisms are: action of the cutterhead, ladder being dragged over the bed (in shallow water), leakage during loading into barges or during transport through pipelines.

- *Backhoe Dredger*
  Sediment release mechanisms are fairly similar to those from the Grab Dredger. From the primary mechanisms three kind of plumes are generated: a near-bed cloud of sediment generated by grab impact, a columnar plume due to hoisting of the barge and a near-surface plume representing material escaping the barge during slewing. Each mechanism of each grabbing cycle will be characterized by different rates of sediment release and will occur sequentially. Therefore, released sediment observed at a point downstream of the dredger will vary continuously.

- *Trailing Suction Hopper Dredger*
  Sediment release mechanisms are: overflow from the hopper, release through the Lean Mixture OverBoard (LMOB) system, disturbance of the bed by the draghead, scour of the bed caused by the dredger propellers and disturbance of gas in the sediment.
  Figure 1.2 gives an overview of the different mechanisms. Two groups can be identified; release from within the vessel and release due to disturbance of the bed. Release from within the vessel can be explained as a sediment-water mixture spilled through the overflow. During the dredging process the vessel is filled with a mixture of sediment and water. When dredging sands, stiff clays or gravels the overflow is used to discharge excess water from this dredging process. Most of the sediment will remain in the vessel as it has settled. However, fine sediment may leave the vessel along with this excess water acting as sediment source to the dredge plume. In case of dredging with overflow, this mechanism is the dominant source

of sediment. Therefore, in this research dredge plumes originating from the overflow of a Trailing Suction Hopper Dredger (TSHD) are evaluated. Overflow dredge plumes are a major contributor to environmental impact of dredging activities. Also, much data is available for overflow dredge plumes, which could be used for comparison with model simulation results.

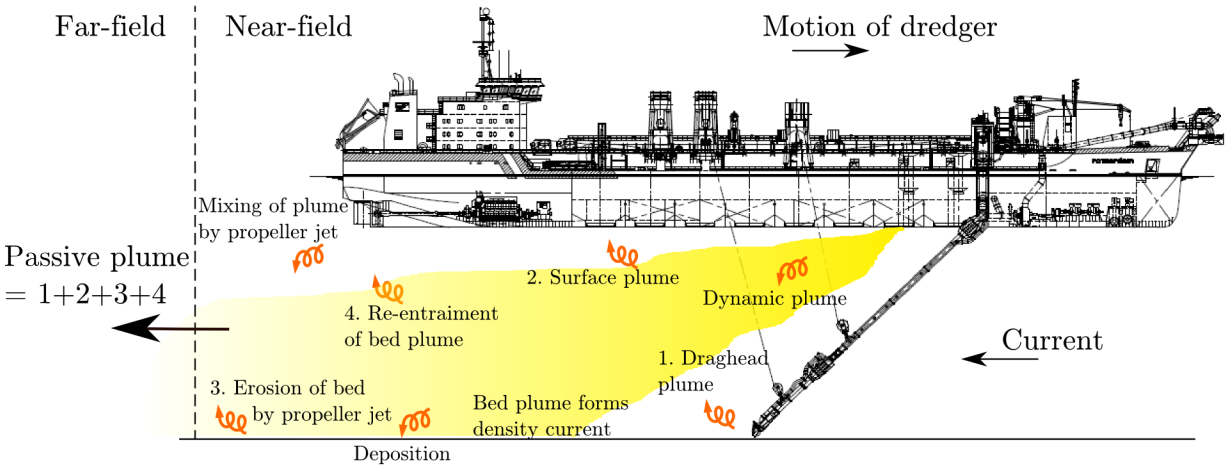

Figure 1.2: Mechanisms for release of sediment from TSHD dredging (free after: Becker et al. (2014) and Spearman et al. (2011)).

1.2.2 Dredge plume behaviour

The released sediment forms plumes, which Lee and Chu (2003) characterize as "flows produced by continuous sources of buoyancy". When an initial momentum is present, plumes are forced. In that case we speak of a buoyant jet (Lee and Chu, 2003). Sediment plumes originating from dredging, both forced and unforced, are referred to as dredge plumes. The distinction between jet and plume is often not made. In this report the term dredge plume is used for all jets or plumes originating from dredging activity.

In evaluation of dredge plumes two types can be classified; dyanimc and passive plumes. Dynamic plumes descend rapidly to, or remain on, the seabed since the sediment-water mixture is denser than the ambient water. Over time the plume will slow down due to friction. The bulk behaviour, rather than the settling velocity of individual sediment grains, is important in a dynamic plume (Dankers, 2002). The zone of impact is small, since the settling velocity of the bulk is relatively high (Winterwerp, 2002).

Passive plumes arise due to mixing of the dredge plume with ambient water. Mixing will occur when the current velocities of the ambient water are strong enough, transporting particles through the whole water column. In passive plumes the settling velocity of individual particles is low, so passive plumes can be present on long time and spatial scales. Winterwerp (2002) states that the behaviour of dredge plumes closely resembles the behaviour of buoyant gas plumes released in the atmosphere and buoyant plumes of waste and cooling water in open water. Fischer et al. (1979) describe the behaviour of the buoyant gas plumes and waste water plumes using the Richardson number Ri and a velocity ratio ζ.

$$Ri = \frac{g' D_{pipe}}{W^2}, \tag{1.1}$$

$$\zeta = \frac{U_a}{W}, \tag{1.2}$$

where g' is the reduced gravitational constant, D_{pipe} is the diameter of the overflow pipe (initial diameter of the plume), U_a is the velocity of the ambient water relative to the sailing vessel and W is the outflow velocity of the plume.

Winterwerp (2002) shows experimentally the behaviour of dredge plumes in terms of the Richardson number and the velocity ratio. The Richardson number expresses the ratio of potential to kinetic energy. A large Richardson number indicates that buoyancy is important in the flow and the kinetic energy is insufficient to end the dynamic behaviour of the plume. The velocity ratio is a measure for the ambient current velocity in relation to the velocity of the plume. Figure 1.3 shows a diagram in which the velocity ratio and the Richardson number are related. For high velocity ratios and low Richardson numbers the plume is passive (mixing zone), while for higher Richardson numbers and low velocity ratios a density current is present (dynamic plume). In between there is a transition zone in which both dynamic and passive processes are important.

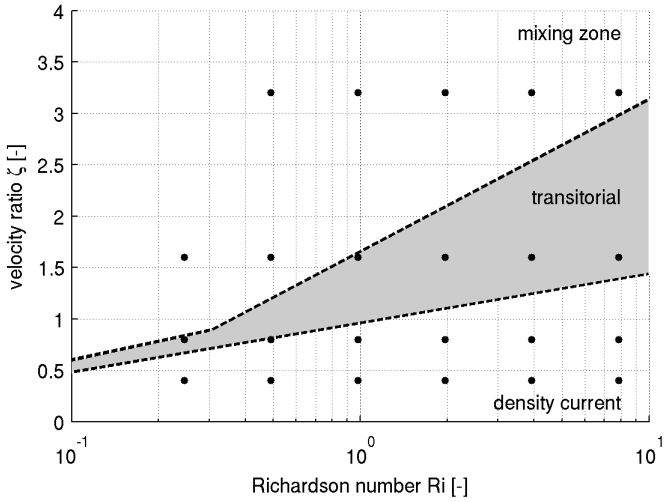

Figure 1.3: Ri, ζ diagram determining classification of dredge plume (Winterwerp, 2002).

In reality a dredge plume is often not solely dynamic or passive, but a dynamic and a passive phase can be determined. Depending on the source and ambient current properties, released sediment leaving the source will first travel as an dynamic plume, where the behaviour is determined by material concentration and properties. Due to interaction with the ambient water a dynamic plume will eventually transform to a passive plume. The area around the dredging operation where a dynamic plume exists is called the near-field, while the transition to a passive phase marks the start of the far-field. In reality it is hard to mark the separation between the near- and far-field as a clear location, therefore a transition zone (the mid-field) can be identified. Figure 1.2 showed a overview of the the fields and contributing mechanims in case of dreding with overflow.

1.2.3 Source term definitions

The source terms for dredge plumes describe the sediment fluxes released into the water column during dredging operations. The sources are hard to determine due to the presence of turbulent processes and difficulties in measuring. The Protocol for the Field Measurement of Sediment Release from Dredgers (VBKO, 2003) defines three different source terms: the true source, the practical source and the virtual source. Figure 1.4 shows a graphical overview of the different stages of plume development and corresponding source terms, including time and spatial scales.

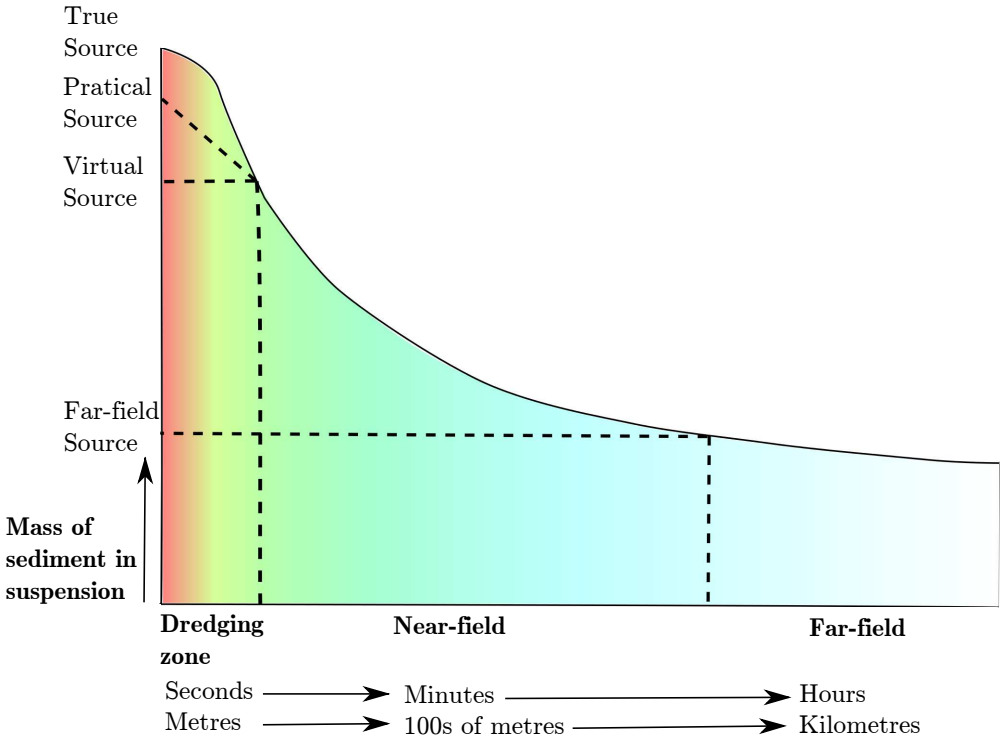

Figure 1.4: Development of dredge plumes and corresponding source terms (free after: VBKO (2003)).

The *true source* is the actual source of sediment at the location where sediment becomes detached from the dredging equipment. In this area the water is highly turbulent and it is dominated by large lumps of sediment and a sediment-water mixture of high concentration. This highly turbulent area is called the dredging zone (direct vicinity of dredging equipment). As the sediment moves out of this dredging zone it reaches the near-field. The amount of sediment reaching the near-field is called the *practical source*. This practical source is the sediment released to the water column excluding the large lumps which have settled at the sea bed immediately. The practical source is defined as the first location moving away from the dredging equipment where measuring sediment concentration is possible. Using this measured data a third source term can be defined: *the virtual source*. The virtual source is a computed release rate at the location of the dredging activity using the data measured in the near field. The protocol suggests the virtual source as the input parameter for numerical modelling, stating it is has mathematical relevance, without describing in detail what is happening at that location.

However, in current projects and research another source term for numerical modelling is often

used: the amount of suspended sediment entering the far-field (see for instance Becker et al. (2014) and De Wit et al. (2014c)). The transition from near- tot far-field gives this fourth source term, based on the fact that different processes are involved in plume dispersion in the two fields. The *far-field source* defines the amount of suspended sediment leaving the near-field. This source term accounts for actual amount of sediment released to areas further away from the dredging works, responsible for far-field environmental impact. In this report the far-field source term is often referred to as source term.

1.2.4 Source term determination

In order to estimate or calculate the far-field source term, the near- and far-field need to be addressed separately. Processes dominating plume behaviour are significantly different in the near- and far-field. Furthermore, the temporal and spatial scales of the plume behaviour are also different. These large differences in scales and processes ask for different modelling approaches for the two regions of interest.

When investigating far-field dredge plume impact, near-field information is needed to determine far-field source terms. Several empirical model packages are available to model the near-field behaviour of dredge plumes. Another way to simulate dredge plumes in the near-field is through process based numerical modelling. Besides modelling, more and more extensive monitoring campaigns are required during execution of dredging works. In these campaigns, among other things, SSC levels are monitored in the near- and far-field. This data can be used to verify that source terms remain below certain approved levels.

Modelling and measurement campaigns might result in different levels of detail of the far-field source term. The complexity of the processes involved and the status of the project can give rise to large uncertainties. Due to these uncertainties all methods have their advantages and drawbacks.

To simulate far-field dredge plume dispersion often hydrodynamic engines as Delft3D-FLOW or MIKE are used, simulating the spreading of the plume by the ambient fluid. The far-field source term serves as input to the far-field model. Regardless of the method used to determine the source term, an important aspect of simulating dredge plumes is the coupling between the near-field output and the far-field model.

1.3 Research Objective

Forecast modelling of dredge plumes is often applied prior to dredging activities, to study environmental impact. An important parameter for the far-field models is the source term. The estimated and calculated source terms do often not match and validation of the numerical model and its input is often not performed.

Research has been conducted on the dispersion of dredge plumes, both in the near-field as well as in the far-field. Research dealt with both environmental impact and modelling implications, see for instance: Nichols et al. (1990), Winterwerp (2002), Aarninkhof and Luijendijk (2010), Spearman et al. (2011) and De Wit et al. (2014b). Due to the difference in dispersion processes and scales in the two fields, an important aspect is how to couple the near- and far-field. Extensive near-field modelling may result in detailed knowledge on characteristics of the plume and the corresponding far-field source term. However, depending on the far-field model and required output, detailed knowledge might not necessarily result in more accurate results.

The characteristics of the plume at the transition are determined by the near-field spreading processes, which in term are driven by the plume characteristics. The ambient conditions in the far-field govern the further spreading of the plume. Together with model parameters and assumptions, these processes determine the capability of predicting environmental impact. Gaining more insight in these topics requires research in all stages of dredge plume development. Existing models and data from several monitoring campaigns can be used to do so. The main research objective of the master's thesis is formulated as follows:

To obtain more insight into the most important parameters, and their influence, in modelling dredge plume dispersion, in order to support more informed selection of modelling techniques and model input regarding forecast modelling spread of SSC in the far-field.

The research objective will be achieved by addressing the following research questions:

I What are the dominant dredge plume dispersion processes in the near-field, far-field and transition zone and what are the corresponding model schematisations?

II What is the influence of model, input and ambient parameters on modelling far-field dredge plume dispersion?

The first question focuses on the near- and far-field plume behaviour. The theory will give insight in the dominant near-field processes, describing things as interaction with cross flow and entrainment. The far-field dredge plume spreading is driven by the ambient flow. The location of the transition, the amount of sediment leaving the near-field and the characteristics of the plume at this location are plume characteristics at the transition from near- to far-field. Subsequently, research on modelling and measuring techniques aims to identify influencing parameters and investigate implementation of near-field output on far-field models.

Knowledge on important model, input and ambient parameters is used to set-up a modelling framework for dispersion of dredge plumes. The second research questions focuses on the influence of the different parameters on modelling far-field dredge plume dispersion.

1.4 Research approach

A literature review is performed to describe all relevant processes involved in dredge plume dispersion, both in the near- as well as in the far-field. Next to a complete process description, the modelling approaches and measuring strategies for the different plume stages will be investigated. Based on both the plume spreading processes and the modelling implications, governing dispersion processes and model and input parameters are identified. The influence of the set of parameters will be tested in an experimental set-up by means of a numerical model. This numerical model represents a relatively simple case, which makes it possible to carefully test the parameters' influence. Results of the experiments are compared with field data. Conclusions are drawn on the modelling performance of this relatively simple experimental situation, which ultimately leads to recommendations on modelling techniques for modelling dredge plumes in the far-field in a broader sense. See Figure 1.5 for a graphical overview of the scope of the processes involved in the different research stages.

1.5 Report structure

The report is structured in such a way that it serves the research approach and objective best. In Chapter 2 the theoretical framework is explained, including a description of involved processes and corresponding modelling approaches.

Chapter 3 includes the model set-up of the numerical model experiment. Furthermore, the most important far-field dispersion parameters are depicted and explained in more detail. The chapter is finished with the outline of the experiment in terms of experimental scenarios and an explanation of the presentation of results.

In Chapter 4 the results to the scenarios are presented. Subsequently, in Chapter 5, model results are compared with field measurements. Results from both chapters are discussed in Chapter 6.

In Chapter 7 conclusions regarding the research questions and objective are outlined. Furthermore, recommendations are given, both for engineering practice as well as for further research.

In the Appendices a more detailed description is given to some of the theory. Appendix A discusses turbulent transport. In Appendix B a definition of fine sediment and some of its characteristics is given. Appendix C shows an overview of the hydrodynamic and sediment transport equations solved in Delft3D-FLOW.

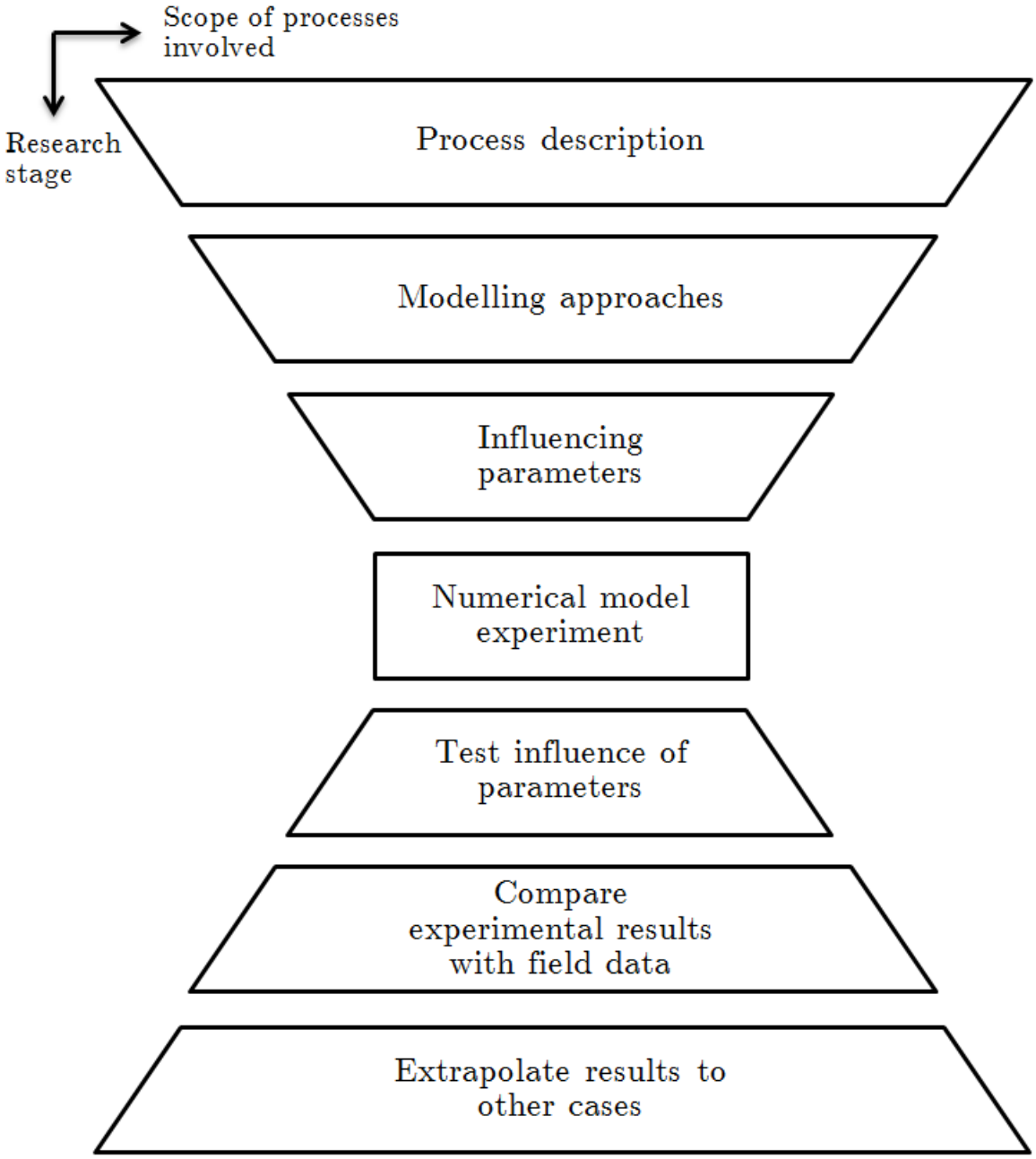

Figure 1.5: Order of research stages showing the scope of processes involved in every stage.

Chapter 2

Theoretical Framework

This chapter discusses the theoretical framework to the subject of dredge plume dispersion. At first all relevant processes in the near- and far-field are explained. Also, the modelling and monitoring methods are considered, in order to complete the theory on dredge plumes.

2.1 Description of processes

A literature study was performed to acquire more insight in the processes involved in plume dispersion. The three regions, near-field, far-field and the transition, are handled separately in this description. First the near-field processes and plume behaviour are explained, describing the main characteristics of a plume and the important plume processes in the near-field. Then, the far-field processes are outlined, including the advection-diffusion equation, turbulent diffusion, shear flow dispersion and settling and suspension of sediment. Finally the transition from near- to far-field is discussed.

2.1.1 Near-field

The introduction stated that the dispersion of a dredge plume in the near-field is comparable to the spreading of buoyant gas plumes released in the atmosphere and buoyant plumes of waste and cooling water in open water. The discussion of near-field dredge plume behaviour will therefore start with a description of buoyant jets and plumes in general. Further, other processes influencing near-field dredge plume spreading in particular are described. The type of dredging equipment used (type of source) determines in what way and at what rate sediment is released in the ambient water. For the description of the near-field processes in this study overflow from a TSHD is considered as source. The processes involved in spreading other sources of sediment are similar, though due to different release rates and locations the description might slightly change (see Section 1.2.1).

Buoyant jets and plumes

When released into ambient water, the velocity difference between a buoyant jet and the ambient water gives rise to a velocity gradient and turbulence (in case of a sufficiently high Reynolds number). This results in a large transport of momentum. Eddies are created at the boundary of the ambient and the jet fluid, over which this transport takes place. In a fully developed flow eddies

are present over the whole width of the jet. However, knowledge on the exact behaviour of buoyant jets and plumes is still limited and most is based on empirical data.

An integral jet model is a way to analyse a buoyant jet released in ambient water. It is studied extensively by, for instance, Fischer et al. (1979) and Brooks (1972). In such models the governing equations for continuity, momentum and tracer mass conservation are written in a coordinate system *s,r*. Here s is the stream wise coordinate along the jet centre line and r the radial coordinate away from the centre line. Important assumptions in such a model are the velocity and concentration profile being considered self-similar along the jet trajectory. This implies that the profiles remain the same shape along the trajectory, whilst maximum concentration and velocity can vary. By integrating the governing equations across the buoyant jet a set of differential equations remains, giving a prediction of the jet trajectory, width, velocity and tracer concentration (dilution) (Lee and Chu, 2003). Fischer et al. (1979) divide the parameters involved in describing buoyant jets into three categories: jet parameters, environmental parameters and geometrical factors. Jet parameters include all initial conditions of the fluid released in the jet, environmental parameters include all ambient factors as stratification and crossflow current velocity and geometry factors are the jet shape, its orientation and, if present, adjacent solid boundaries or a free surface.

Close to the source, flow of a buoyant jet is governed by its initial conditions, including geometry of the jet, initial fluxes and density difference between the jet fluid and the ambient water. The initial volume flux (Q), initial momentum flux (M) and initial buoyancy flux (B) for a round pipe can be calculated as follows:

$$Q = \frac{1}{4}\pi {D_{pipe}}^2 W_0, \tag{2.1}$$

$$M = \frac{1}{4}\pi {D_{pipe}}^2 {W_0}^2, \tag{2.2}$$

$$B = g\frac{\Delta\rho}{\rho_w}Q, \tag{2.3}$$

where D_{pipe} is the pipe diameter, W_0 is the outflow velocity uniform across the jet, ρ_w is the density of the ambient fluid and $\Delta\rho$ is the density difference between the jet and the ambient fluid.

When released in ambient water two zones can be identified: the zone of flow establishment (ZFE) and the zone of established flow (ZEF). After released from the pipe the buoyant jet enters the ZFE. Here the velocity profile is transformed from the pipe velocity distribution to a jet velocity distribution at the end of the ZFE. Between the jet fluid and the ambient water a shear (or mixing) layer is created in which ambient water is entrained into the jet. The core of the jet is not mixed yet. As moving away from the pipe the mixing layer is widened until the potential core is completely 'eaten' by the mixing layer and the flow distribution is fully developed. In an integral jet model the transition to a self-similar velocity profile marks the end of the ZFE and the start of the ZEF (see Figure 2.1).

When a jet is released in still ambient water, Fischer et al. (1979) state that the length of the ZFE is about 7 times the diameter of the pipe. For a simple turbulent round jet Fischer et al. (1979) define a length scale in terms of volume flux (Q) and momentum flux (M), which defines the initial jet geometry:

$$l_Q = \frac{Q}{\sqrt{M}}, \tag{2.4}$$

Let z be the distance along the trajectory of the jet. In case $z >> l_Q$ the properties of the jet are solely defined by the distance from the jet orifice and the flow is fully developed. While for $z \approx l_Q$ the flow is still influenced by the jet geometry.

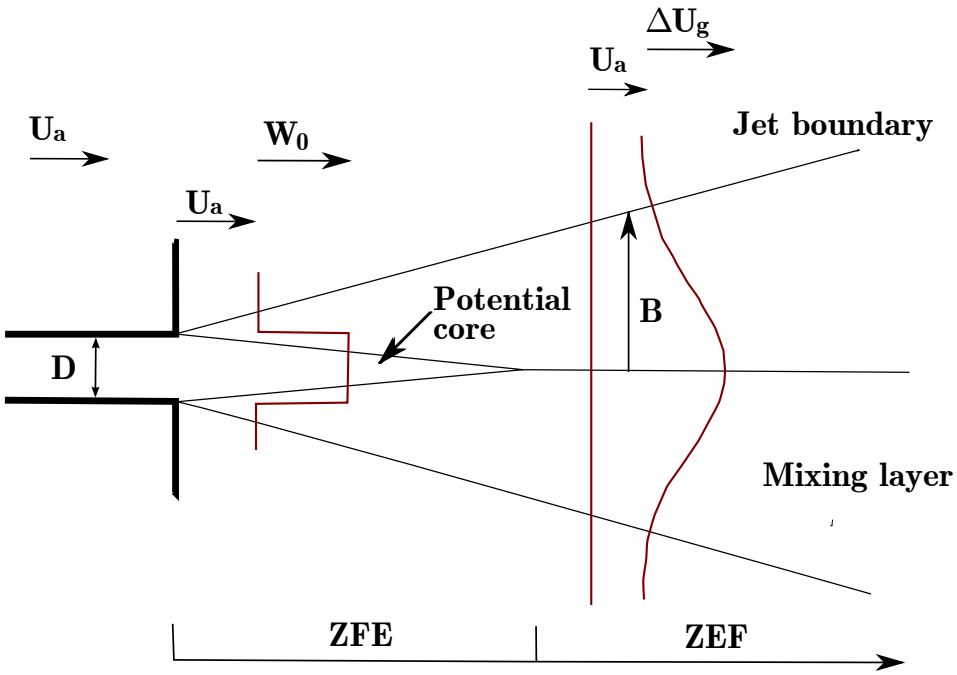

Figure 2.1: Schematic overview of a round jet in crossflow in which b is half the width of the plume, U_a is the ambient flow velocity, W_0 the initial jet velocity and ΔU_g the centre line excess velocity in the ZEF (free after: Lee and Chu (2003)).

In the ZEF the mean velocity and concentration profile can be taken self-similar, implying that the time averaged velocity/concentration can be described in terms of the mean value and a measure of the width in the cross section. In the ZEF the buoyant jet can be plumelike or jetlike, depending on the initial volume and momentum fluxes and the momentum created by buoyancy effects. If the momentum due to buoyancy is greater than the initial momentum, the flow is characterized as plume, otherwise it behaves like a jet. Moving away from the source, every flow will eventually turn to a plumelike character, since buoyancy will be transferred to momentum.

The presence of an ambient current affects the flow trajectory of the buoyant jet leaving the vessel. Ambient water is an environmental factor which tends to bend the buoyant jet in the direction of the crossflow. A buoyant jet leaving the overflow will always start as a vertical jet into the ambient water. The crossflow velocity, momentum flux and buoyancy flux determine the development of the buoyant jet. Eventually the flow will be bend and plumelike. Two characteristic length scales can be used to determine whether a flow is bent by the crossflow and behaves plume or jet like (Fischer et al., 1979) (Lee and Chu, 2003) (Rodi, 1982):

$$z_M = \frac{\sqrt{M}}{U_a}, \tag{2.5}$$

$$z_B = \frac{B}{{U_a}^3}, \tag{2.6}$$

where U_a is the velocity of the ambient crossflow. In case $z_M > z_B$ the buoyant jet will first behave jetlike and then become plumelike, almost like the case without ambient crossflow. If $z_B > z_M$ the

crossflow is the dominant feature and the buoyant jet will first bend over and then behaves as a bend over jet (Rodi, 1982).

In the ZEF the buoyant jet can be estimated by just a few parameters. Due to the self-similarity assumption the buoyant jet can be defined in between two outer boundaries. At these boundaries a turbulent mixing layer is present, over which water is entrained. The jet development can be described by a measure for the vertical jet velocity, the centre line trajectory and a combination of width and a concentration or dilution at each point of the centre line.

Fischer et al. (1979) and Rodi (1982) use conservation of momentum and the self-similarity assumption to derive equations for the jet trajectory, velocity and dilution rate depending on the type of plume. With these equations it is possible to describe the jet trajectory of the dredge plume and cross sectional variations. However, through the self-similarity assumption several processes are only represented through approximations or not taken into account at all.

Entrainment, stratification, waves, vortex pair creation and other dredge plume specific phenomena, as stripping, vessel interaction and influence of the propellers on the buoyant jet, are important for spreading of a dynamic dredge plume. The combination of these processes determine the actual end of the near-field and corresponding plume characteristics at the transition from near- to far-field.

Entrainment

Entrainment is the process of ambient water getting enclosed by the jet fluid at the boundaries of the jet. Hereby dispersion takes place which widens the jet as it spreads. The entrainment of ambient water contributes to a higher total mass of the buoyant jet. To ensure a constant momentum flux through every cross section the jet velocity decreases. Dredge plumes consist of a certain concentration of fines. Due to entrainment of ambient water this concentration is lowered, as the ambient water generally has a lower (or zero) fine concentration.

Two types of entrainment processes can occur. Shear entrainment is entrainment because of turbulent eddies created on the boundary of two adjacent layers of fluid with different velocities. In case of a dredge plume leaving an overflow with a sufficiently high Reynolds number ($Re >> 1000$) the flow can be classified as turbulent. The turbulent fluctuations present in the mixing layer, in combination with the velocity gradient between the two fluids, create a turbulent shear. Eddies (or vortices) are created as consequence of this turbulent shear, ultimately leading to entrainment of ambient water. The mechanisms of shear entrainment can be divided into three phases (Sreenivas and Prasad, 2000). In the first phase, known as the induction phase, eddies are formed and entrap ambient fluid as rolling around. Dimotakis (1986) describes two following stages. In the second phase (diastrophy) turbulent straining of the fluid reduces its spatial scales until viscous diffusion dominates. In the last phase (infusion) the ambient fluid is mixed at molecular level with the jet fluid. See Figure 2.2.

Shear entrainment is caused by a velocity difference in the axial direction. If entrainment is caused by a velocity difference in the normal direction it is called forced entrainment. Forced entrainment is generated by the interaction with the crossflow. When a buoyant jet is released in a crossflow the time-averaged cross profile and the jet trajectory are influenced. This is comparable to flow around are rigid structure, however, in this particular case entrainment is enhanced.

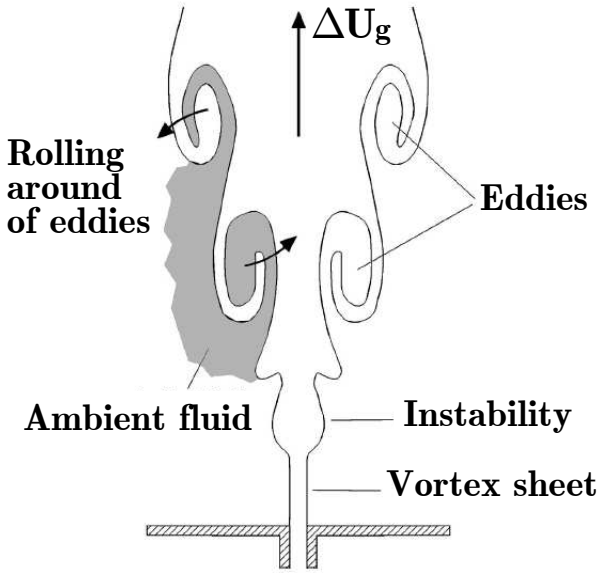

Figure 2.2: Process of shear entrainment of ambient fluid due to rolling around of eddies (Sreenivas and Prasad, 2000).

Vortex pair creation

For a buoyant jet interacting with a crossflow current, the time-averaged cross profile of momentum in the ZEF has transformed to a vortex pair shape. These counter-rotating vortex pairs (CVP) are constantly diverging and in some cases bifurcation can even take place.

Van Eekelen (2007) describes the cause of the creation of CVP in buoyant jets by a sort of shear stress exerted by the ambient crossflow on the jet. More shear stress is exerted on the edge of the jet than on the centre, causing a torque which makes rotation around two axis possible. A similar process is described by Jirka (2004), stating that the rotation is caused by a azimuthal shear stress. Others have discussed that the source of CVP is the boundary layer vorticity generated from the jet nozzle (Fric, 1990). However, the exact reason for this vorticity movement is not described in detail in literature.

The creation of CVP in the near-field influences the jet's cross sectional velocity and concentration profiles. The two vortices can divert, resulting in a kidney shaped concentration profile instead of the often assumed Gaussian profile. Vortex divergence is investigated by, for example, Fischer et al. (1979), determining a near constant angle of $8 - 10°$. Whether vortex diversion takes place strongly depends on the local conditions. Strong turbulent diffusion will hold the CVP together, while in low turbulent diffusion regimes diversion can take place.

Two diverting vortices can eventually bifurcate, which means that ambient fluid enters the centre line and two separate elements can be identified. In general bifurcation can only take place at boundaries, since diversion rates increase and turbulent diffusion can no longer retain ambient water from the centre line of the jet.

Stratification

Due to, for example, depth varying salinity levels ocean waters can be stratified. This results in an increasing density in depth of the ambient water. The velocity of the dredge plume is directly linked to the density difference between the ambient water and the plume fluid. The increasing ambient density, in case of stratification, will result in a lower dredge plume velocity as the plume travels down the water column. Depending on the initial momentum flux, the density difference between the ambient water and the sediment mixture, stratification can even cause the plume to stop sinking when a level of natural buoyancy is reached. At this height, called the terminal height of rise, the plume reaches zero vertical velocity and will start to travel horizontally (see Section 2.1.3). In this case the plume is prevented from reaching the bottom.

Stripping

Several definitions of stripping can be found in literature. Stripping is the removal of material from the dynamic plume into the ambient fluid caused by the interaction between the plume and the crossflow. Van Eekelen (2008) did experimental research on the influence of stripping on behaviour of dredge plumes, based on this description.

The amount of material stripped from the plume is important as it results in suspended sediment being present in the upper part of the water column. In this way it is a source of sediment for the far-field. Research by Boot (2000) resulted in estimates of the amount of sediment loss by stripping of $3 - 5\%$ of the total amount of sediment. However, experiments by Van Eekelen (2008) do not show significant influence of stripping on overflow plumes in the near-field. Moreover, Van Eekelen (2008) couples the loss of some plume content to other processes as air entrainment in the overflow, irregular discharge through the overflow and dynamic plume irregularities due to plume/vessel interaction. These are all vessel related phenomena.

Vessel movement and propeller interaction

Vessel related phenomena may influence the near-field behaviour of overflow plumes to a large extent. Vessel motion can cause waves inside the hopper affecting the outflow of the overflow mixture. Furthermore, flow round the hull of the vessel can influence the mixture after released in the water. At last, the wake produced by the vessel's propeller can enhance mixing of the jet behind the vessel.

Due to waves, wind and currents a vessel will move, both rotating and translating in its six degrees of freedom. This movement can cause waves inside the hopper which can lead to a time varying direction and magnitude of the overflow discharge. This phenomenon is known as a pulsed plume (De Wit et al., 2014a).

When the water level in the overflow shaft becomes much lower than the water level in the hopper, air can be entrained in the overflow plume. The entrainment of air results in lower excess density of the overflow mixture and the discharge is no longer continuous. This can result in clouds of sediment, water and air bubbles moving across the near-field, instead of a continuous overflow plume traveling to the bottom (Dankers, 2002). Air entrainment can cause the sediment to rise to the free surface instead of sinking to the bottom. The effects can be reduced by applying a so called 'green valve system', which increases the flow velocity through the overflow shaft, reducing the amount of air entrained (Bray, 2008).

The degree of influence of the several vessel induced phenomena on the behaviour of overflow plumes depends on water depth, ambient conditions, specifications of the vessel and its site specific features (vessel speed, draft etc.). De Wit et al. (2014c) investigate the influence of pulsing, flow around the hull and the propeller on the plume, through numerical modelling. They states that the dredging speed is an important parameter in combination with above mentioned effects. With high dredging speeds the overflow plume will stay close to the keel of the vessel, which enhances propeller effects and influence of the aft of the vessel. The flow around the hull of the vessels tends to lift the plume upward. Propeller effects can be found in a lifted plume due to the higher mixing and entrainment into the propeller jet. This enhances the formation of a surface plume. A surface plume is sediment separated from the dredge plume, which ends up near the free surface. The propeller also elongates the plume in vertical direction (De Wit et al., 2014a). Pulsing is responsible for larger vertical spreading of the dredge plume. Furthermore, it causes a deeper plume path. Depending on the dredging speed it enhanced or reduces the presence of a surface plume (together with propeller effects). For normal dredging speeds the surface plume is enhanced while for high dredging speeds the surface plume is reduced.

2.1.2 Far-field

In the far-field the dredge plume is classified as a passive plume. The passive dredge plume disperses with the mixing effects of currents and waves. The plume transports suspended sediment away from the disposal area through advection with (tidal) currents and diffusion processes. The three main mechanisms whereby dispersion of the plume occurs are:

- *Turbulent diffusion* is the diffusion process with similar effect as molecular diffusion, though on larger length scales.
- *Shear flow dispersion* is generated by gradients in the mean flow, referred to as a shear flow. Spreading in the direction of these flows is caused by the velocity profile in the cross section.
- The *settling and (re)suspension* of sediment particles to/from the bed. Erosion and settling effects the amount of sediment suspended in the water column.

Advection diffusion equation

Transport in fluids occurs through a combination of advection and diffusion. The transport by the mean motion of the fluid is called advection, while diffusion is transport associated with the random motions within the fluid. The advective mass flux through the unit area in the yz plane by the velocity component in the x direction is given by the quantity (uC). Here u x *unit area* is the volume per unit time and C is the concentration of mass in that volume. Multiplication gives the quantity uC, which is the rate at which fluid volume passes through the unit area.

Fick (1855) was one of the first to study diffusion. He describes how Fourier's heat flow leads to a hypothesis to describe the molecular diffusion process. By following the same mathematical formalism as Fourier's law for heat conduction, Fick's law was derived. The law states that the mass flux of the solute through a unit area per unit time in x direction is proportional to the gradient of the solute concentration in the same direction.

$$q = -D_m \frac{\delta C}{\delta x}, \tag{2.7}$$

where q is the solute mass flux, C is the mass concentration of the solute and D_m is the coefficient of proportionality. D_m has the dimension ($length^2/time$) and is also called diffusion coefficient or molecular diffusivity. D_m is a property of both the fluid and the diffusing solute. The minus sign indicates transport from high to low concentrations.

Combining Fick's law with conservation of mass gives an equation describing the diffusion process. Conservation of mass leads to a relationship which is true regarding the type of transport process, relating the mass flux ($q(x,t)$) and concentration ($C(x,t)$). Combining the two relationships gives the diffusion equation extended to all three dimensions (x y z, respective coordinates in parallel, lateral and vertical direction), describing mass transfer by Fickian diffusion processes:

$$\frac{\delta C}{\delta t} = D_m(\frac{\delta^2 C}{\delta x^2} + \frac{\delta^2 C}{\delta y^2} + \frac{\delta^2 C}{\delta z^2}), \tag{2.8}$$

In this equation the diffusion coefficient (D_m) is assumed to be a constant. Adding the advective flux to equation of the solute mass flux results in an equation describing the total mass transports, reffered to as the advection diffusion equation:

$$\frac{\delta C}{\delta t} + u\frac{\delta C}{\delta x} + v\frac{\delta C}{\delta y} + w\frac{\delta C}{\delta z} = D_m(\frac{\delta^2 C}{\delta x^2} + \frac{\delta^2 C}{\delta y^2} + \frac{\delta^2 C}{\delta z^2}), \tag{2.9}$$

The description of Fick's law accounts for mass transport by molecular diffusion in laminar flow only. The molecular diffusion coefficient in water is typically small, around 10^{-9} m^2/s. The time (t) needed to spread a solute over a distance (L) depends on this coefficient, and can be estimated with (through scaling):

$$t \approx \frac{L^2}{D_m}, \tag{2.10}$$

Given the small diffusion coefficient, this equation holds very long durations for spreading of a solute. In most fluid motions in the environment spreading of a solute is much faster than calculated from molecular diffusion only. Clearly, other diffusion processes must be involved in these fluid motions. Since most fluid motions in nature are turbulent, turbulent diffusion can be accounted to the rapid mixing.

Turbulent diffusion is the diffusion of a solute produced by the turbulent motion of the flow. A turbulent motion is characterized by vortices (or eddy's) in the flow, with length scales (or eddy sizes) ranging from the smallest Kolmogorov scale up to to the largest integral scale. The effects of turbulent diffusion are the same as for the random molecular motions, though acting on a larger scale.

The advective diffusion equation (Equation 2.9) can be extended for turbulent flows by decomposing the velocity and concentration terms into a mean and a fluctuation component:

$$C = \overline{C} + C', \qquad u = \overline{u} + u', \qquad v = \overline{v} + v', \qquad w = \overline{w} + w', \tag{2.11}$$

where the overlined components are the time averaged and the primed are the fluctuating components. Filling in the components into Equation 2.9 and taking the time average (such that $\overline{\overline{C} + C'} = \overline{C}$) results in:

$$\frac{\delta \overline{C}}{\delta t} + \overline{u}\frac{\delta \overline{C}}{\delta x} + \overline{v}\frac{\delta \overline{C}}{\delta y} + \overline{w}\frac{\delta \overline{C}}{\delta z} = D_m(\frac{\delta^2 \overline{C}}{\delta x^2} + \frac{\delta^2 \overline{C}}{\delta y^2} + \frac{\delta^2 \overline{C}}{\delta z^2}) - \overline{u'C'}\frac{\delta}{\delta x} - \overline{v'C'}\frac{\delta}{\delta y} - \overline{w'C'}\frac{\delta}{\delta z}, \tag{2.12}$$

The new three terms appearing in Equation 2.12 represent the diffusion by turbulent motion (due to the correlation between fluctuation velocity and concentration components). The molecular transport term is generally much smaller than the turbulent flux and is therefore neglected in most cases. This does not mean that molecular diffusion is not important in mixing of a solute. Momentum or matter is transported from the largest to the smallest length scales (down the energy cascade). The actual energy dissipation is taken care of by the molecular diffusion on the smallest length scales.

The turbulent fluxes can be written as a gradient type transport using an eddy diffusion coefficient (D_t):

$$\overline{u'C'} = -D_{t(x)}\frac{\delta C}{\delta x}, \qquad \overline{v'C'} = -D_{t(y)}\frac{\delta C}{\delta y}, \qquad \overline{w'C'} = -D_{t(z)}\frac{\delta C}{\delta z}, \tag{2.13}$$

where, $D_{t(x)}$, $D_{t(y)}$ and $D_{t(z)}$ are the turbulent equivalents of the molecular diffusion coefficient, often referred to as "Fickian turbulent diffusion coefficients", turbulent diffusion coefficients or eddy diffusivities (Fischer et al., 1979). Using the eddy diffusivities, the assumption that turbulent transport is much greater than molecular transport and ignoring the overline for average concentration and velocity, Equation 2.12 becomes:

$$\frac{\delta \overline{C}}{\delta t} + \overline{u}\frac{\delta \overline{C}}{\delta x} + \overline{v}\frac{\delta \overline{C}}{\delta y} + \overline{w}\frac{\delta \overline{C}}{\delta z} = \frac{\delta}{\delta x}(D_{t(x)}\frac{\delta C}{\delta x}) + \frac{\delta}{\delta y}(D_{t(y)}\frac{\delta C}{\delta y}) + \frac{\delta}{\delta z}(D_{t(z)}\frac{\delta C}{\delta z}), \tag{2.14}$$

For time scales larger than the Lagrangian time scale the above equations can be applied in combination with constant diffusion coefficients. This means that after some start up time mixing in a stationary homogenous turbulent flow can be considered as a diffusion process with a constant diffusion coefficient. For a more extended description of turbulence and the derivation of the advection diffusion equation see Appendix A.

Shear flow dispersion

Advection by a constant velocity is not very effective in mixing a solute as it only carries material, without changing its distribution. Non-constant advective flows, shear flows, are able to stretch and distort the distribution of a material. The lateral velocity gradient results in certain parts of the material being carried faster than other parts, which causes intensification of concentration gradients and therefore dispersion. Dispersion is used to describe diffusion caused by a shear flow.

An example of shear flow dispersion is the combination of a velocity profile over the vertical of a cross section and diffusion in the direction transverse to the flow direction. A patch of a solute is released in a shear flow (see Figure 2.3). The initial patch is transported downstream and distorted by the non-constant advective flow. Transverse diffusion then smears out the material over the vertical resulting in a wider patch of solute downstream, hence the two phenomena have resulted in longitudinal dispersion of the solute.

Taylor (1953, 1954) describe the spread of a solute in laminar pipe flow. This theory is extended over the years to all other kinds of flows to describe dispersion in rivers or estuaries. Taylor (1953) considers dispersion of a solute in laminar flow in a tube. Fischer et al. (1979) applies this concepts to a two-dimensional flow in between two walls, to show that Taylor's theory is applicable to other types of flow.

Appendix A.4 shows the derivation of the diffusion equation for a shear flow case. Generally the longitudinal diffusion term can be neglected, since the dispersion due to the velocity profile

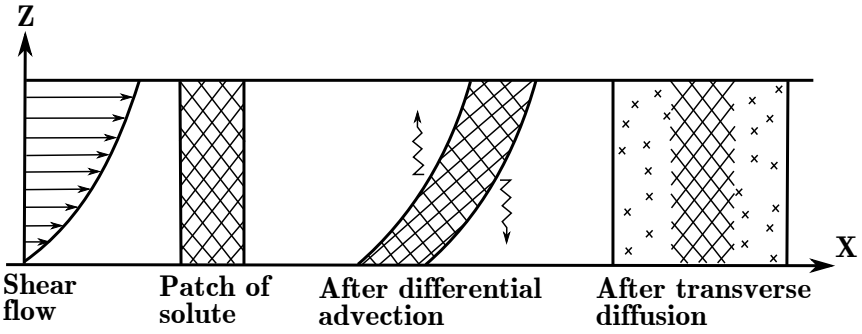

Figure 2.3: The dispersion of a patch of solute by a combination of shear flow and transverse diffusion.

is much larger than due to molecular diffusion in longitudinal direction. The one-dimensional diffusion equation can be rewritten for cross sectional averages in the fixed coordinate system (*x,y*), by reintroducing the mean advective velocity to give the one-dimensional dispersion equation:

$$\frac{\delta \overline{C}}{\delta t} + \overline{u}\frac{\delta \overline{C}}{\delta x} = K\frac{\delta^2 \overline{C}}{\delta x^2}, \tag{2.15}$$

where K is the so called (longitudinal) dispersion coefficient. K plays the same role for the whole cross section as the diffusion coefficient D_m does on microscopic scale.

$$K = \frac{-1}{hD_m}\int_0^h u' \int_0^y \int_0^y u' dydydy, \tag{2.16}$$

In this equation the longitudinal advective transport is balanced by the cross sectional diffusive transport. This balance can only occur when the mean concentration ($\overline{C}$) varies slowly and mean concentration gradient ($\frac{\delta \overline{C}}{\delta x}$) is nearly constant over a long period of time. In that case the concentration fluctuations (C') become small, since cross sectional concentration differences are smoothed by the cross-sectional concentration gradient. These required circumstance take some time to establish. Once established the further spreading can be calculated using Equation 2.15.

The dispersion equation as presented above concerns laminar flow only. It can be extended for turbulent flow, taking into account two main differences; the velocity profile in turbulent flow differs from laminar flow and the molecular diffusion coefficient should be replaced by the turbulent diffusion coefficient. Taylor (1954) extents the theory on dispersion in laminar flow to turbulent flow in a pipe. For the case described above the dispersion coefficient in turbulent flow becomes:

$$K = \frac{-1}{hD_t}\int_0^h u' \int_0^y \int_0^y u' dydydy, \tag{2.17}$$

Sediment settling and (re)suspension

Passive dredge plumes consist of fine sediment suspended in water, being transported by the ambient current. The largest sand particles will have settled in the dredge vessel or in the near-field. When reaching the far-field the plume merely consists of silt and clay. Water samples taken in several dredge plumes by Smith and Friedrichs (2011) strengthen this suggestion. The suspended sediments in the sampled plumes consisted of 1 % sand, 46 % silt and 53 % clay.

Fine sediment is defined as all particles having a diameter smaller than 63 μm. Fine sediment can be classified as silt or as clay. Silt and clay particles are different in size and behave differently. Properties of clay are plasticity and cohesion. A mixture of silt and clay is often referred to as mud. Sediment mixtures containing a significant proportion of clays are known as cohesive sediments. For more information on the classification of fine sediment and its characteristics see Appendix B.

Sediment is different from other constituents transported by water (e.g. salt or heat), since exchange takes place between the water column and the bed. Sediment is eroded from the bed, being a source of sediment to the water column. While sedimentation of sediment may reduce SSC. For a dredge plume transported away from its source this implies that sediment eventually will settle on the bed. Also, if bed shear stresses exceed certain values, it is possible for plume sediment to get eroded from the bed again. Much research has been done on the erosion and sedimentation of sand and mud, see for instance Van Rijn (1993), Partheniades (1980) and Soulsby (1997). Mixtures of sand and mud require a different approach and can not be treated as either sand or mud (Whitehouse et al., 2000).

One of the important properties of cohesive sediments is the ability to form flocs. This process, called flocculation, originates from the fact that particles can aggregate and break up again. Flocs are formed by attractive forces, governed by collision and cohesion. Flocs can be formed within the hopper and are often present in overflow dredge plumes Smith and Friedrichs (2011). However, flocs can also be formed in the water column as the plume is transported. High SSC levels coupled with low turbulence regimes are favourable for the flocculation process (Winterwerp and Van Kesteren, 2004). Results of the field experiment conducted by Smith and Friedrichs (2011) on overflow dredge plumes give rise to similar conclusions. A measured increase of settling velocities and floc sizes within the dredge plume suggested the importance of floc formation.

Movement of sand particles will occur if the load on sand particles is larger than the strength. The load is given by the fluid force acting on the particle, while the strength is the resisting force related to submerged weight and friction force of the particles. The shields diagram is often used as a measure for threshold of motion. In this diagram motion of particles starts when the particle mobility factor (Θ) exceeds a critical particle mobility factor (Θ_{cr}). Shields critical mobility factor is given by:

$$\Theta_{cr} = \frac{\tau_{b,cr}}{(\rho_s - \rho_w) g d_{50}}, \tag{2.18}$$

where $\tau_{b,cr}$ is the Shields critical bed shear stress, ρ_s and ρ_w are the density of the grains and water and D_{50} is the median of the grains size distribution. Van Rijn (1993) extends the shields diagram for movement in situations of currents and waves present and studies influence of e.g. bed slope and bed forms. Deposition of sand occurs when the settling velocity of the grains is larger than the lift velocity. The settling velocity for sand can be calculated using stokes law.

For cohesive sediments the presented formula for settling velocity in a Stokes' regime can not be used, since they are not spherical and their density is not known. Due to the high water content in flocs the density (ρ_f) decreases compared to the particle density, resulting in a decrease of the settling velocity. The aggregation of particles to form flocs results in larger particle diameters, which increases the settling velocity. See Appendix B for more information on the properties of fine sediment.

Partheniades (1980) identifies several types of erosion for cohesive sediments. If individual clay particles are eroded, this is called surface erosion. Mass erosion occurs due to large internal stresses generated by flow or waves, eroding larger lumps of cohesive sediment. The critical erosion shear-stress (τ_e) is defined as the shear stress from which erosion of flocs starts. The erosion shear-stress

can be calculated using the Thorn and Parsons empirical relation:

$$\tau_e = E1{C_M}^{E2}, \tag{2.19}$$

where *E1* and *E2* are dimensional coefficients and C_M is the dry density of the bed. Whitehouse et al. (2000) state that values $E1 = 0.0012$ and $E2 = 1.2$ give the best fit. When the bed shear-stress (τ_0) exerts the critical shear stress ((τ_e)), cohesive sediment is eroded. The rate of erosion (E), defined as the dry mass of mud eroded per unit area per unit time ($\mathrm{kgm^{-2}s^{-1}}$), can be calculated using an empirical equation by Partheniades:

$$E = \begin{cases} m_e(\frac{\tau_{cw}}{\tau_e} - 1), & \text{for } \tau_{cw} > \tau_e \\ 0, & \text{for } \tau_{cw} \leq \tau_e \end{cases} \tag{2.20}$$

where τ_{cw} is the maximum bed shear stress due to currents and waves, τ_e and m_e the erosion coefficient.

Deposition of cohesive sediment depends on the near bed concentration (C_b), the settling velocity (w_s) and a critical bed shear stress for deposition (τ_d). An empirical relation can be used to calculate the rate of deposition (Whitehouse et al., 2000) :

$$D = \begin{cases} -(1 - \frac{\tau_{cw}}{\tau_d})C_b w_s, & \text{for } \tau_{cw} < \tau_d \\ 0, & \text{for } \tau_{cw} \geq \tau_d \end{cases} \tag{2.21}$$

This is a approximation of the deposition rate, since in reality mud flocs have wide distribution in sizes, densities, strengths and settling velocities. Applying a median settling velocity, single shear stress for deposition and near bed concentration therefore calculates an approximation for the actual deposition of cohesive sediments.

Mixtures of mud and sand can behave as non-cohesive or cohesive, which has large influence on deposition and erosion rates. Whether a sediment bed is classified as cohesive or not, depends on the clay content. Van Ledden and Van Kesteren (2004) validated experimental research to show that the transition of a bed from non-cohesive to cohesive occurs at a clay content of 5-10 %. Besides the clay content the network structure is an important feature for erosion behaviour. Based on the clay content and network structure six bed types can be distinguished (Dankers, 2002) (Van Ledden and Van Kesteren, 2004).

Turbulent dispersion and diffusion coefficients

It is often hard to determine diffusion and dispersion coefficients for a real flow case. Through tracer studies it is, for example, possible to determine dispersion coefficients. However, these studies are rather costly and impractical. In engineering practice the coefficients are often estimated or used as calibration parameter. Depending on the (vertical and lateral) characteristics of the plume, (hydrodynamic) conditions in the river, estuary or ocean and the degree of calculation detail used, the turbulent diffusion and dispersion coefficients can be calculated. At first, estimations for the vertical, lateral and longitudinal diffusion and dispersion coefficients for a uniform, straight, infinitely wide channel of constant depth will be given (steady, uniform flow). After which influence of several other processes on these coefficients is discussed.

Steady flow in a uniform channel

A cloud of tracer, in this case suspended sediment, deposited in a uniform channel with steady flow will grow in time in the vertical, lateral and longitudinal direction. Mixing over the depth of the channel happens at a faster rate than lateral mixing. The turbulent diffusion coefficient can be taken constant when the Lagrangian length scale is larger than several times the depth (as the depth is approximately the size of the largest eddies). Also, the turbulent diffusion coefficient can be written as a product of a velocity (turbulence intensity) and the Lagrangian length scale ($D_t = l_T\sqrt{\overline{U}^2}$) (see Appendix A.4). In open channel flow the turbulence intensity is proportional to the shear stress on the wall (bed shear stress). The bed shear stress can be expressed as a shear velocity, which is often used instead of the stress itself. The shear velocity in uniform flow is defined as:

$$u_* = \sqrt{\frac{\tau_0}{\rho}} = \sqrt{ghi}, \tag{2.22}$$

where τ_0 is the bed shear stress, h is the water depth and i is the slope of the channel.

The vertical turbulent diffusion coefficient for a logarithmic velocity profile is determined following the same analogy as for the turbulent viscosity, which is a measure for the transport of momentum (Appendix A.4). The Schmidt number gives the ratio of the turbulent viscosity (ν_t over turbulent diffusivity ($D_t(z)$). A Schmidt number of 1 results in a vertical diffusion coefficient equal to to the vertical mixing coefficient for transport of momentum:

$$\nu_t = D_t(z) = \kappa h u_*(z/h)[1 - (z/h)], \tag{2.23}$$

Averaging over depth and taking $\kappa = 0.4$ (Von Kármán constant) results in:

$$D_t(z) = 0.067 h u_*, \tag{2.24}$$

where z is the level above the bed. Lower Schmidt numbers (0.5 - 1) are common to be found, resulting in slightly higher vertical diffusion coefficients, due to the fact that transport of a tracer is more efficient than transport of momentum.

When looking at an infinitely wide uniform channel no velocity profile exists in transverse direction. Therefore it is impossible to establish a lateral diffusion coefficient following the same analogy as for the vertical direction. Fischer et al. (1979) summerises a large set of separate measurement results in straight rectangular channels determining the lateral diffusion coefficient. These measurements indicate that a good approximation for the lateral diffusion coefficient is given by $\frac{D_t(y)}{hu_*} = 0.1 - 0.2$, resulting on average in:

$$D_t(y) = 0.15 h u_*, \tag{2.25}$$

In real streams lateral mixing coefficients will show much variation, due to channel curvature, depth variations and sidewall irregularities. None of these variations influence the rate of vertical mixing substantially, since the scale of the vertical motions is limited by the local depth. The factors do cause transverse flows which affect lateral mixing. Based on experimental studies approximations can be made for the lateral diffusion coefficient in case of one of the factors present. In a channel bend, for instance, the coefficient can increase to $D_t(y) \approx 0.8 d u_*$, due to secondary circulation (Fischer et al., 1979).

Longitudinal diffusion coefficients are of the same order of magnitude as the lateral coefficients, however, longitudinal mixing is generally much higher. Along a channel, mixing by turbulent eddies (diffusion) is unimportant compared to shear flow dispersion, as was shown in Section 2.1.2.

The longitudinal dispersion coefficient depends on the vertical (or lateral) diffusion coefficients and the velocity profile. For a logarithmic velocity profile, established in steady uniform flow, Elder derived the longitudinal dispersion coefficient from a vertically parabolic distributed vertical diffusion coefficient (Elder, 1959):

$$K(x) = 5.93hu_*, \tag{2.26}$$

As for the lateral diffusion coefficient, the longitudinal dispersion coefficient is highly site specific and depends on many factors. The coefficients highly depends on the variations in flow geometry. Experimental study has shown that taking into account all these effect may result in lateral dispersion coefficients of $(100 - 500)hu_*$.

Other mixing processes

The dispersion parameters derived were a measure for spreading of a solute in a uniform stationary flow case. Mixing resulted from a combination of small scale turbulent diffusion and a larger scale variation of the advective mean velocities. In channel flow the combination of those two is fairly simple. However, in reality other processes effect the velocity components in a channel or estuary. Processes as the tide, Coriolis, stratification or wind may influence the direction and magnitude of the velocity components. Hereby, mixing of a sediment plume is enhanced or suppressed.

The presence of tidal flow influences mixing in two ways (Fischer et al., 1979). Firstly, a tidal flow generates shear flow dispersion, similar to the dispersion found in channel flow. It is different from river flow because the direction and magnitude of the mean velocity component are not constant in time and space, due to the oscillating character of the flow. The varying velocity components will have its effects on the direction and magnitude of the spreading. The second contribution of the tide is generated by friction of the tidal flow running over the channel bottom. The vertical mixing coefficients as derived for uniform channel flow could be applied in a tidal situation. The only complication is the fact that the shear velocity (u_*) varies with varying velocity. A minimum value (nearly zero) is found around slack tide, while the shear velocity is maximum at time of highest velocities.

Another contribution of the tide is the effect on settling and erosion of sediment. The oscillating velocity components will result in varying bed shear stresses. Depending on the velocities, water depth, sediment and bed properties, this influences erosion and sedimentation patterns.

Wind effects on mixing in a channel, lake or estuary are found when a current is induced. Effects are highly dependent on the local ambient and plume conditions. Wind induced phenomena are, for example, breaking waves, surface currents induced by drag on a water surface, up- and downwelling and circulating flow in a basin with varying depth. Whether these phenomena can occur depend on local conditions. For instance, for circulation to occur a (semi) closed basin is required, making it impossible to experience in channel flow.

Stratification of ocean, estuary, lake or river water may also influence mixing of sediment. The formation of vertical stratification in the water column is a consequence of water masses with different densities. In between these separate water layers interfaces exist. Density differences in stratified flows tend to restore stratification. Turbulent eddies are damped at the interface of two layers, counteracting the tendency of turbulence to mix the fluids. This is known as turbulence damping. The mixing length of the turbulent eddies are bounded by stratification. Empirically determined damping functions exits, relating the mixing length to the Richardson Number (a measure for stratification). Part of the mixing of sediment is governed by the turbulent eddies. Hereby, the damping of this turbulence can have a large effect on the sediment distribution in a stratified environment.

As an example a salt wedge is considered. A salt wedge can occur in a river discharging in the ocean. The density differences at the river mouth between the ocean and river water drives the salt water to travel upstream the river. The salt water will travel in the lower half of the water column as fresh water is discharged to the sea in the upper part. Imagine suspended sediment is present in this stratified environment. The damping of turbulence at the interface results in turbulent motions in the upper layer to be weaker. Turbulence generated at the bottom can not penetrate the interface in between the layers. If not enough turbulence is present to keep the sediment in suspension, the sediment will settle. Furthermore, once sediment has reached the lower layer it can not be transported back in the upper part of the water column. In this way, the presence of stratification (the salt wedge) will have have large effects on the sedimentation patterns and distribution of the suspended sediment in the estuary.

2.1.3 Transition from near- to far-field

It has been shown that an overflow dredge plume released from a TSHD behaves as a negative buoyant jet in crossflow in the near-field. The sediment-water mixture is generally denser than the ambient water and will descend to the bed while mixing with the ambient water. The ambient conditions, initial conditions and interaction with the vessel have proven to be important parameters for the actual behaviour of a dredge plume in the near-field. Furthermore, the mechanisms by which far-field dispersion takes place were outlined. To define the transition from near- to far-field, first the end of the descend of the plume is determined, after which a definition for the actual transition is given.

Bed/Dynamic collapse

The termination of a plume's descend is either caused by a collapse on the bed or when the vertical velocity become zero. The first is called bed collapse while the second is called dynamic collapse. After collapsing on the bed the plume can be approximated as a density current traveling over the bed. For thin density currents on a horizontal bed, the propagation velocity of the front is related to the thickness of the current and the gravitational acceleration corrected for buoyancy (Spearman et al., 2011) (Hallworth et al., 1998). Here the height of the density current is assumed constant over the length of the current.

In case of stratified ambient water the plume can reach a level of neutral buoyancy, as was already mentioned in Section 2.1.1. In this case horizontal traveling starts at the level of neutral buoyancy, before the plume has reached the bed. The traveling of a dynamic collapsed plume is similar to the movement of a density current on the bed. The only differences is the presence of a density gradient from the neutral buoyancy position throughout the thickness of the plume (Baird, 2004).

Termination of collapse phase/transition

Transition from the near- to far-field, or the transition from dynamic to passive plume behaviour, is governed by buoyancy effects and the ambient current. At the transition the buoyancy effects diminish and mixing is taken over by turbulence generated by the ambient water. A measure for the importance of buoyancy over kinetic energy is given by the Richardson number. De Wit (2010)

uses a local Richardson number:

$$Ri_l = \frac{g' D_l}{{U_a}^2}, \tag{2.27}$$

D_l is the local plume width defined by a top hat profile, U_a is the ambient crossflow velocity and g' is the reduced gravity term given by $\frac{\Delta\rho}{\rho_a}$. Here, $\Delta\rho$ is the density difference between the plume and the ambient water and ρ_a is the density of the ambient water. Akar and Jirka (1994) use the flux Richard number to describe the interaction between buoyancy and ambient turbulence for a plume traveling as a density current over a bed:

$$Ri_f = \kappa^2 \frac{g' h}{{u_*}^2}, \tag{2.28}$$

where h is the local thickness of the density current and u_* is the critical velocity of the crossflow. Akar and Jirka (1994) cite earlier research by, amongst others, Turner (1973) and Prych (1970), to conclude that the transition from the dynamic to the passive phase happens when the flux Richardson number lies between 0.1 and 0.2. Akar and Jirka (1994) use an average value of 0.15. De Wit (2010) uses an average value of 0.15 for the local Richardson number as transition criterion. Generally speaking, when the Richardson number is below 0.15, buoyancy effects have diminished and mixing is taken over by the ambient current.

2.2 Modelling approaches

Given the large differences in scales and processes, separate modelling approaches are applied for the near- and far-field. In theory existing models are capable of covering the entire range of spatial and temporal scales in one integral model, but these (unsteady, baroclinic, non-hydrostatic) models are very computationally expensive and not yet usable for engineering practice (Morelissen et al., 2013). Figure 2.4 shows an overview of the various stages of dredge plume dispersion and the available model approaches and their applicability. When simulating dredge plumes the coupling of the near-field to the far-field is an crucial step. At first understanding of the methods to simulate near-field dredge plume behaviour is discussed. Subsequently, modelling approaches for the far-field are addressed. Finally, the possible coupling methods are mentioned.

2.2.1 Near-field

Near-field models or near-field data analysis are used to determine the actual amount of sediment entering the far-field. In engineering practice the amount of detail in simulating near-field dredge plume dispersion depends on the purpose of the study and the availability of input data. In the initial project stage the type of equipment and amount of material to be dredged might not be known, which makes extensive near-field modelling difficult. When more information is available field data can be analysed or near-field models are applied to determine the far-field source term. All methods have their drawbacks in terms of assumptions made on the near-field plume behaviour. The models and data, corresponding assumptions and the implications for the output (far-field source term) are discussed in this section.

Models

To model near-field plume development three modelling approaches can be distinguished; jet-integral models, length scale models and (3D) numerical models. Jet-integral and length scale

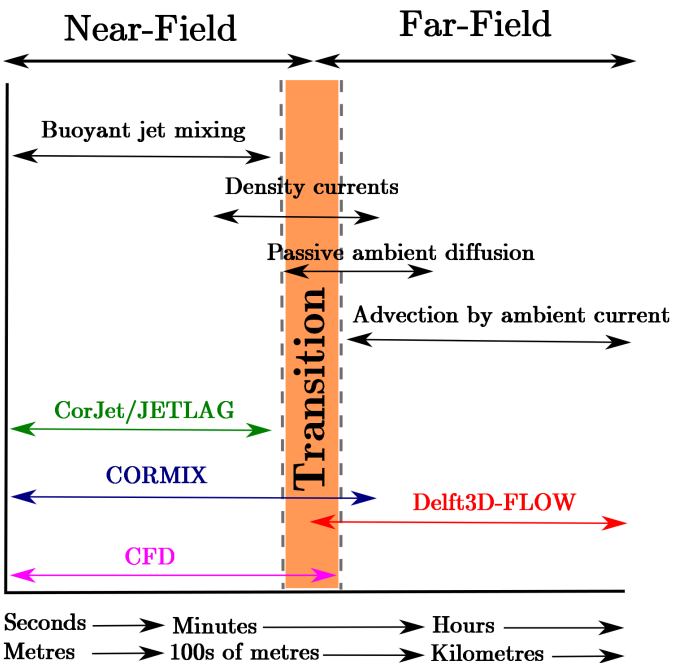

Figure 2.4: Application areas of available dredge plume models (colored arrows) and spreading processes (black arrows). The horizontal axis shows time and spatial scale (free after: Doneker (2008)).

models are empirical models, whereas numerical models are process based.

Examples of jet-integral models are CorJet, VISJET or JETLAG (Jirka, 2004) (Lee and Chu, 2003). Jet-integral models simulate the plume as a whole, taking the cross-profile distribution of the velocity and concentration self-similar along the jet trajectory. The models are based on conservation of mass, momentum and buoyancy. Predictions of these integral models show good comparison to laboratory experimental data, predicting the asymptotic behaviour of pure jets and plumes correctly (Zhoa et al., 2011). Several mechanisms involved in buoyant jet development in the near-field are taken into account; e.g. interaction with the cross flow and entrainment. Jet models use different empirical relations to account for these processes. Other influencing phenomena as plume-vessel interaction, are not accounted for in these models. Furthermore, jet models can not take into account any boundaries interaction, since they make use of unlimited ambient water.

CORMIX is a length scale model (or flow class model) which is similar to the jet-integral models (Jirka et al., 1996). The main difference is that it can deal with boundary interaction. Length scale models divide the buoyant jet into compartments, chosen on characteristic length scales. For each compartment a flow class is identified on which formulations for development of the jet in that particular compartment are based. As for jet integral models processes as entrainment are included by means of approximations.

A third near-field modelling approach is 3D Computation Fluid Dynamics (CFD) modelling. De Wit (2010) presents a 3D CFD model for overflow dredge plumes. The model is based on the non hydrostatic Navier Stokes equations and initial momentum, and density differences of the plume are fully taken into account. The model results are validated against plume experimental data, showing accurate reproduction of the data.

In the numerical model all important whirls of the overflow dredge plume are modelled, and processes are not based on empirical relations. For turbulence modelling a LES approach is applied in the CFD model. All turbulent fluctuations smaller than the grid size are filtered away and replaced by a sub-grid-scale shear tress. Turbulent eddies larger than the grid size are resolved on the grid. By applying a rather small grid size the most important large eddies will be modelled, resulting in a detailed description of the near-field dredge plume behaviour. In this model factors as vessel and propeller interaction can be taken into account.

Near-field model output results in plume data on the transition from near- to far-field. From jet-integral models and length scale models a lateral and vertical distribution of the plume concentration and details on the transition location can be determined. CFD modelling will give similar results. However, depending on the grid size, more detail can be accounted for.

Monitoring data

More and more, extensive monitoring campaigns are conducted around dredging works. At many project sites the contractor, or a third party, is required to monitor plume parameters in the near- and/or far-field during execution of the work. The data is used to confirm that impact of the dredging works are limited below acceptable levels. Furthermore, the data can be used for model validation.

Characterisation monitoring is carried out during execution of the work. In characterisation monitoring production parameters (on-board data) are monitored. In case of a TSHD this is data about the overflow mixture; overflow time, overflown volume, the total volume of material in the hopper and average density. Simultaneously near-field, mid-field and far-field data is gathered which characterises the plume parameters. Near- and mid-field data can be gathered through a combination of Acoustic Doppler Current Profiler (ADCP), turbidity sensors and water quality measurements. ADCP measurements are used to gather flow velocities on transects behind the dredging activity. At the same time turbidity is measured along the transect (both optical and acoustic). The systems are calibrated against water samples collected in the area. These calibrated measurements are used to determine sediment fluxes through the measured transects. For more information on characterisation monitoring see Chapter 5.

Apart from these measurements turbidity can be measured using real-time turbidity monitoring buoys at several locations around the area of interest. Generally the buoy locations will be at the transition from near- to far-field. Furthermore far-field survey is conducted at locations further away from the works. Accretion levels can be measured at locations where forecast modelling predicted high sedimentation rates. Also, satellite images can be used to study plume sizes in the far-field.

Analysis of a large number of transect data can result in far-field source terms. In such an analysis sediment fluxes measured in the mid-field are related to production parameters. The amount of fines produced (true sediment source flux) can be determined through measuring overflow discharges and concentrations. From the transect turbidity and velocity measurements sediment fluxes through the transects can be calculated. Relating a whole set of transects to an overflow discharge (knowing the distance between vessel and transects) results in a sediment source term for the far-field. Measurement campaigns are also used during the execution phase to verify that SSC or accretion levels stay within certain limits.

Besides the use of monitoring data during the execution phase, data obtained at many dredging works can also be used prior to a project. During the initial project stage not much is known about

execution (duration, production, ambient conditions etc.). Becker et al. (2014) describe a procedure to quickly estimate source terms based on equipment used and type and rate of material to be dredged. Equations are derived for several types of equipment using plume specific empirical plume factors, which resulted from earlier measurement campaigns. In this way a far-field source term (flux) can be estimated. A high degree of uncertainty remains, though Becker et al. (2014) state that the transparency, simpleness and rigorousness are benefits of this approach. Furthermore, estimations of these plume factors can be improved by combining knowledge from more measurement campaigns.

Major issue of both source term determination methods is the fact that only a source term flux is calculated. Both methods provide no data on the actual transition from near- to far-field, nor on the distribution of the plume at that point. Although, it is of course possible to analyse the measured transects to determine sediment distributions.

2.2.2 Far-field

Hydrodynamical engines like Mike or Delft3D-FLOW can be used to model spreading of dredge plumes in the far-field. The horizontal equations of motion and the continuity equation are solved by the engine to simulate the hydrodynamics, forced by the boundary conditions. Furthermore, the advection diffusion equation is included, describing the transport of substances (SSC in this case). Through the hydrodynamic pressure assumption these software engines do not account for vertical accelerations. Since buoyancy difference in the near-field cause vertical accelerations, these models can not calculate plume behaviour in this region correctly. Modeling far-field dispersion of dredge plumes is possible since spreading is governed by the ambient flow.

The far-field spreading processes as described in the process description should be included in the far-field model. Besides the physical processes, several model parameters or assumptions may influence results. Careful choices should be made on things as; the number of dimensions used, grid sizes, time step, diffusion coefficients etc. The most important model parameters involved in dredge plume dispersion will be explained in Section 3.2. Appendix C elaborates on the formulations for flow and sediment transport modelling used in Delft3D-FLOW.

2.2.3 Model coupling

In theory existing models are capable of covering both the near- and far-field in one integral model, however, for engineering practice these models are less usefull. Therefore separate handling of the fields is applied, making the correct coupling between the near-field output and the far-field essential for optimal simulation of the whole system. Despite the procedure of far-field source term determination, through modelling or monitoring data, incorrect representation of the source term should be avoided. Figure 2.5 shows an top view of a possible dredge plume modelling sceanrio.

One possible coupling method is dynamic coupling of a near-field model to a far-field model. Examples of such coupling between a length-scale model (CORMIX) or jet-integral model and a far-field model (Delft3D-FLOW) are found in Morelissen et al. (2013) and Choi and Lee (2005). By dynamic coupling near-field results are transferred to the far-field simulation with a sufficiently small time interval to account for changes in ambient conditions. Furthermore, the coupling can be considered online. Which means that during a far-field simulation the computational results are used to define the input for the near-field simulation and vice verse. Constant updating of the boundary conditions and near-field output implies that detailed knowledge is available on ambient conditions, equipment used (true sediment source term), near-field mixing processes and

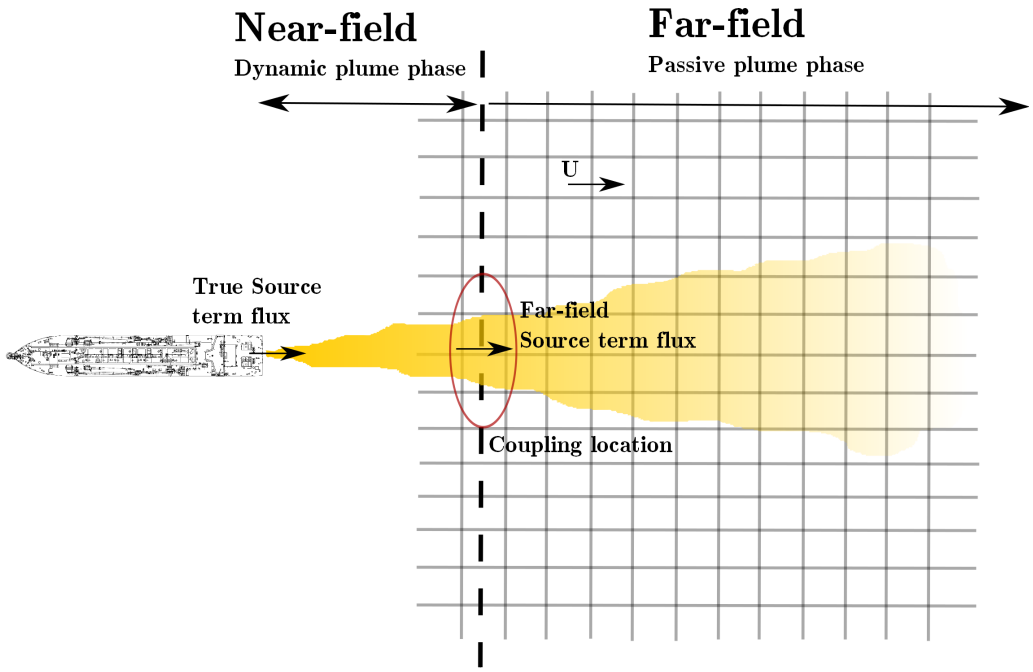

Figure 2.5: Top view of a dredge plume modelling scenario indicating the near-field, far-field and coupling location.

other parameters. In forecast modelling of dredge plumes, much of these parameters are still unknown and even in further project stages these parameters are uncertain. It could be argued whether dynamic coupling results in more accurate results taking the unknowns and uncertainties into account. Furthermore, if the interest of the far-field model results are accretion levels many kilometers away from the dredging activity, the amount of detail applied in this early stage could be of less importance.

If dynamic coupling is not used, still models or data are used as far-field model input. 'One way' coupling considers the near-field results as source information for the far-field models by introducing the scalar concentration predicted at the end of the near-field (Zhoa et al., 2011). In dredging application the near-field models or monitoring data analysis are used to determine far-field source terms. In this way no feedback from the far-field to the near-field model and vice verse is possible. Only changes in source term magnitude, location or distribution can be accounted for. Due to the many unknowns and uncertainties (project stage, equipment, overflow rates, ambient conditions and approximations in near-field processes) this representation of reality is usually sufficient. Again, the amount of detail applied to the far-field source term depends on the project stage and area of interest. The effects of source term detail applied is part of the experiment conducted in this research.

Another way to deal with the uncertainties involved in simulating dredge plumes is by applying a probabilistic approach. Becker (2011) describes a risk-based approach to assess the impact of dredge plumes on sensitive receivers. In such an approach uncertainties in source input, ambient parameters and environmental effects can be taken into account to evaluate environmental impact of dredging activities.

Chapter 3

Numerical model experiment

In the theoretical framework the important processes and corresponding modelling approaches were outlined. An experiment is set up following this analysis. The experiment is conducted using a numerical model set-up simulating a simplified flow case. The goal of the experiment is to verify the influence of several model, input and ambient parameters. First the model set-up is outlined, after which the most important parameters are further explained. Subsequently a modelling framework is established. Finally, the choices on parameters result in a number of modelling scenarios.

3.1 Model set-up

For experimental research on far-field dredge plume dispersion a uniform, straight, infinitely wide channel of constant depth is simulated. By applying proper boundary conditions, flow in such a channel can be regarded stationary and uniform. This implies that flow conditions do not show variation in time and space. Such flow is rarely found in reality, but serves as an useful schematisation for testing model and input parameters.

For the 2D and 3D computational approaches the software engine Delft3D-FLOW is used. Dredge plume dispersion is evaluated on a numerical domain of 35 kilometers long and 3.5 km wide, with a constant water depth of 10 m and a slope of 10^{-5}. For the horizontal computational grid four different grid sizes are applied ($\Delta x, \Delta y$): 50 m, 100 m, 250 m and 500 m. For the 3D simulations 20 layers (Δz), each of 0.5 m, are implemented in vertical direction. An overview of the numerical domain is shown in Figure 3.1.

3.1.1 Delft3D-FLOW

The equilibrium water depth for steady uniform flow conditions can be determined using the Chézy formula, relating the flow velocity to the slope, hydraulic radius and roughness of the channel.

$$u = C_{chezy}\sqrt{Ri}, \tag{3.1}$$

where u is the mean flow velocity, C_{chezy} is the Chézy coefficient, R is the hydraulic radius ($\approx$ water depth) and i is the bottom slope. Given a Chézy coefficient of 65, results in a mean flow velocity of 0.65 m/s. The flow velocity is established using a constant discharge as upstream boundary, while at the downstream boundary the water depth is kept constant. Turbulent transport of momentum and sediment is accounted for by horizontal (2D and 3D) and vertical (3D) eddy viscosities and

Parameter	**Value**
Calculation time	1 day
Time step	60 seconds
Slope	10^{-5}
Water depth	10 m
Bed roughness	65 $m^{1/2}/s$
Horizontal eddy viscosity	0.021 m^2/s
Horizontal eddy diffusivity	0.05 m^2/s
Vertical eddy viscosity	k-ϵ model
Vertical eddy diffusivity	k-ϵ model
Upstream boundary	22750 m^3/s
Downstream boundary	10 m

Table 3.1: Ambient and model parameters used in the experiment.

	Sediment 1
Sediment type	Cohesive
Specific density	2600 kg/m^3
Dry bed density	500 kg/m^3
Settling velocity	2.57 mm/s
Deposition bed shear stress	1000 N/m^2
Erosion bed shear stress	4 N/m^2
Erosion parameter	0.002 kg/sm^2
Source term flux	100 kg/s
Source term input duration	90 minutes
Source term (plume) width	500 m

Table 3.2: Sediment and source term input parameters used in the experiment.

diffusivities. More model parameters are presented in Table 3.1. A further description on choices made regarding the model and ambient parameters can be found in Sections 3.2.1 and 3.2.3

The input location of the sediment source is chosen in the middle of the channel, 3750 m from the upstream boundary. The experiment is conducted using one dredge plume, which is implemented on the grid in several different manners. The width of the plume at the transition from near- to far-field is set to 500 m (the size of the largest grid cell) and only consists of sediment of one grain size. The start time of input of the source is twelve hours after the start of the calculation. Any fluctuations of the depth averaged velocity due to initial effects have disappeared by this time. The source term flux is 100 kg/s for a total duration of 90 minutes. All source term and sediment related parameters are mentioned in Table 3.2.

Variation in lateral direction is added by applying three different kind of source terms: a point source, a line source and laterally distributed line source. In vertical direction also three different plumes are implemented, this is elaborated on in Section 3.2.2.

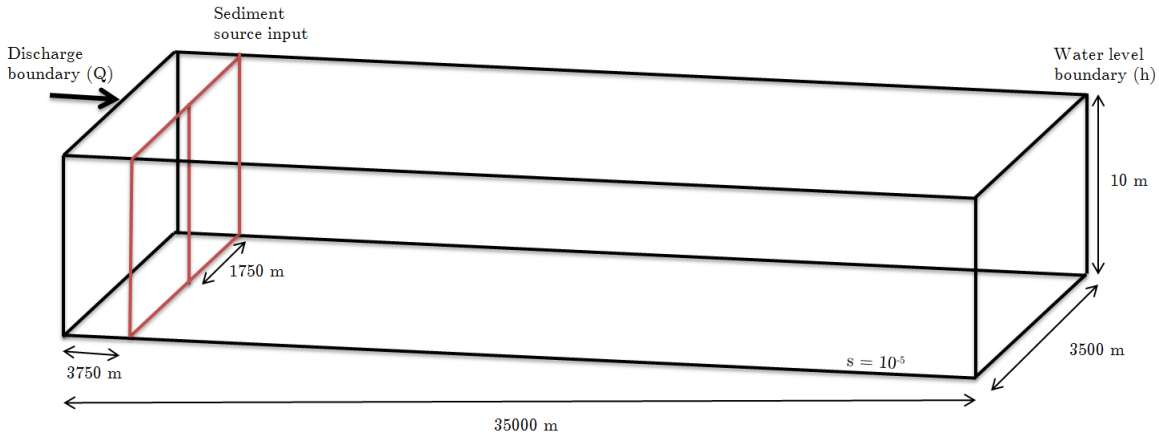

Figure 3.1: Overview of the numerical model domain.

3.1.2 One dimensional analysis

Besides an 2D and 3D computational approach the solution to the one dimensional dispersion equations can be used to calculate far-field dispersion of dredge plumes. In some specific cases this gives a reasonable representation of the concentration increase due to sediment plumes. Given the input rate (source term flux), flow velocity in the channel, settling velocity of the sediment particles, dispersion coefficient and water depth, the sediment flux at a distance x from the input location can be calculated. This sediment flux (M_s) is used to calculate the concentration in the centre line of the plume at this distance *C(x)*. The centre line concentration can be used to calculate the concentration perpendicular to the centre line. A solution to the one dimensional dispersion equation has the form of a Gaussian distributed concentration profile. The plumes moves away from the source with the mean flow velocity while the concentration profile is broadened:

$$C(x,y) = \frac{M_s}{hu\sqrt{4\pi K\frac{x}{u}}} exp^{-(\frac{y^2}{4K\frac{x}{u}})}, \tag{3.2}$$

where *C(x,y)* is the concentration at distance x along the centre line of the plume and distance y perpendicular to the centre line of the plume, h is the water depth, K is the dispersion coefficient and u is the depth averaged velocity in the channel. The solution to this equation gives a measure of the lateral distribution of the plume at a distance x from the source.

The channel dimensions, depth averaged velocity, dispersion coefficients and sediment properties will be kept constant. The source term is implemented as point source. To compare the one dimensional solutions to the Delft3D-FLOW simulations the width of the point source is related to the horizontal grid sizes used in 2D and 3D.

3.2 Far-field dispersion parameters

3.2.1 Modelling parameters

Computational approach (1D/2D/3D)
Far-field dredge plume dispersion can be simulated either using the one, two or three dimensional equations. Choices made regarding the computational approach depend on the available time and

wanted degree of detail. The quickest way to simulate a dredge plume is by applying the analytical solution to the 1D diffusion equation. An 1D analysis might give a reasonable preliminary view of the dispersion of a plume.

For a 2DH flow simulation the depth averaged shallow water equations are solved on a grid with one vertical computational layer. For vertically homogenous flows a depth averaged approach is sufficient. In a 3D simulation a vertical grid is applied, which is of interest if the horizontal flow field shows vertical variation. In case of far-field dredge plume modelling, vertical variation is often present at the transition from near- to far-field. Using 3D modelling makes it possible to implement this vertical variation properly. Furthermore, phenomena as turbulent diffusion, the sediment concentration distribution and the vertical velocity distribution are modelled more accurately in 3D. However, further away from the source the vertical variation might diminish and 2D simulation can be sufficient as well. The degree of detail in a 3D computation should be weighted against the computational efficiency of a 2D simulation.

Besides the difference in source term input detail, the erosion and deposition rates are to be considered in deciding the computational approach. The erosion and deposition rates in Delft3D-FLOW are calculated using the Partheniades-Krone formulation (Section 2.1.2 and Appendix C.2). Deposition rates depend on the settling velocity of the sediment, the near bed concentration and the maximum and critical bed shear stress. In Delft3D-FLOW the near bed concentration is taken as the average of the near bottom computational layer. When modelling in 3D this is the concentration in the cell closest to the bottom. In case a sediment concentration profile is present this may result in higher concentrations near the bed than at the free surface. For a 2D case only one 'cell' is available in vertical direction. The average concentration in this cell will generally be lower than the average concentration in the near bottom computational layer when modelling 3D. Comparing a 2D and 3D case, with equal settling velocity, erosion and deposition parameters, will thus result in higher deposition rates in 3D.

Grid size

The model area should be covered by a curvilinear grid, to discretise the shallow water equations in space (see Appendix C.1). The grid sizes ($\Delta x, \Delta y, \Delta z$) determine the degree of detail of the source term input, degree of detail of results and computational efficiency. The grid sizes and time step (Δt) together give certain limitations due to stability and accuracy of the integration methods used.

The amount of lateral and vertical variation applied on the source term depends on the grid size. For instance, a plume width of 500 meters can be implemented in only one grid cell using an horizontal grid of 500x500 m. No lateral variations can not be accounted for. With a 50x50 m grid lateral variation of the plume can be applied. In the experiment several grid sizes are chosen in order to test the effects of added variation to the source term on far-field dispersion.

Another issue might arise for large grid cells in combination with small source term fluxes. Sediment can dilute immediately due to numerical diffusion. Absolute effects are largest when overall concentrations are low. The amount of numerical diffusion depends on the numerical scheme used for discretisation of the advection terms. Delft3D-FLOW presents two possible advection schemes to approximate scalar transport: the Cyclic method or Van Leer-2 method. Higher order advective difference methods, like the Cyclic scheme, can introduces non-physical oscillations on coarse grids near locations of steep concentration gradients. Due to the fact that the difference operators do not guarantee positive result, physically incorrect negative concentrations can occur. A Forester filter can be applied in Delft3D-FLOW. This is a filtering technique to remove this

computational noise. The Van Leer-2 scheme is strictly positive for 2DH simulations. However, due to the large amount of damping (numerical diffusion) the results are less accurate than for the Cyclic method.

The presence of these wiggles thus depend on the grid size and the concentration gradient. Therefore, possible wiggles are expected only to be found close to the source, where concentration gradients are highest.

Time step
To guarantee stability and accuracy of the time integration of the shallow water equations certain time step limitations need to be taken into account. The accuracy of the model depends on the Courant-Friedrichs-Lewy number (CFL), which generally should be smaller than 10. However, in case time and spatial variations are small, which is the case in this experiment, the Courant number can be even higher. The Courant number is given by:

$$CFL = \frac{\Delta t \sqrt{gh}}{\Delta x}, \tag{3.3}$$

where g is the gravitational acceleration, h is the water depth, Δt is the time step and Δx the horizontal grid size. In the experiment a time step of 60 seconds is chosen. This guarantees sufficiently low Courant numbers for all grid sizes. The timeste also meets other time step limitations, which are mentioned in Appendix C.1.

Turbulent viscosity and diffusivity
To account for turbulent transport of momentum and matter a turbulent viscosity and diffusivity have to be specified. For 2DH modelling only one horizontal viscosity and diffusivity are needed to account for horizontal turbulent transport. It is also possible to input spatial varying values for viscosity and diffusivity. In this experimental situation no time and spatial velocity variations are present (steady uniform flow) . This implies that there are no velocity gradient present in horizontal direction, resulting in no horizontal turbulent transport of momentum. Therefore, the horizontal viscosity is not of importance. The diffusivity, taking care of the mixing of matter needs to be specified, since horizontal concentration gradients will occur when modelling dredge plumes. An alternative for the determining the horizontal eddy diffusivity could be the application of a Horizontal Large Eddy Simulation (HLES), which is also supported by Delft3D-FLOW. The model is not tested in this research, but it could serve as an alternative for the uniform values.

In Section 2.1.2 the diffusion coefficient for both longitudinal and lateral direction were defined. The turbulent diffusion coefficient for the lateral direction is several orders of magnitude smaller than the longitudinal coefficient. However, in Deflt3D-FLOW no separation can be made between horizontal turbulent transport in x (longitudinal) and y (lateral) direction. In situations where turbulent transport (turbulent fluctuations) are of the same order in both directions this is not an issue. Though, in the experimental situation a logarithmic velocity profile is established in longitudinal direction, while in lateral direction no velocity profile is present. This implies that lateral mixing of the plume happens at a far longer time scale than longitudinal mixing.

For a 3D modelling approach a vertical viscosity and diffusivity have to be specified next to the horizontal equivalents. Several models are implemented in Delft3D-FLOW to calculate the vertical eddy viscosity and diffusivity; Constant, Algebraic, $k - L$ and $k - \epsilon$. The turbulent closure models serve to close the Reynolds averaged equations and the advection diffusion equation (see Appendix A).

Erosion and deposition parameters
For calculation of erosion and deposition rates in Delft3D-FLOW the Partheniades-Krone formulations are used. Critical values for deposition and erosion and an erosion parameter have to be specified. Together with a current and waves related maximum bed shear stress, erosion and deposition rates are determined. When selecting these input parameters, the scope of the project and available data are determining factors. In case extensive data sets on the bed and suspended sediments are available, characteristic parameters can be calculated accordingly. When data is available on erosion and deposition rates, the parameters can be used to calibrate the model to that data. In case no data is available the erosion and deposition parameters should be estimated or based on expert judgment.

For this experimental set-up obviously no data is available on sedimentation or erosion rates. Still, the erosion and deposition parameters are important for sediment transport, since these determine the exchange of sediment between the water column and the bed. In the stationary uniform flow case considered in this study the erosion and deposition rates determine the shape of the vertical sediment concentration profile. The sediment concentration profile can take any possible shape, depending on the settling velocity, flow velocity and surface and bed boundary condition. The sediment profile can be determined by the upward sediment flux by turbulent diffusion and erosion and the downward flux through settling and deposition. The exchange of sediment between the suspension and the bed is given by the bed boundary condition:

$$w_s C_b + D_t(z)\frac{\delta C}{\delta z} = D - E, \tag{3.4}$$

where w_s is the settling velocity, C_b is the concentration of the bottom computational layer (lowest cell), D is the deposition rate and E is the erosion rate. In case deposition and erosion rates are zero or equal to each other, integrating Equation 3.4 over depth results in the well-known Rouse profile (given a parabolic distributed diffusion coefficient). In case the left hand side of the equation is nonzero, the concentration profile will adapt to the erosion or sedimentation flux at the bottom.

Input parameters determining erosion/deposition are the critical bed shear stress for erosion, the critical bed shear stress for deposition, the erosion parameter and the settling velocity of the plume's sediment particles. Due to the lack of data, a possible way to estimate these parameters is by looking at 'extreme' cases. A case with maximum deposition rates and no erosion will give maximum deposition rates, while the other extreme is a situation with with no sedimentation or erosion at all.

3.2.2 Source term input parameters

Source term magnitude
The source term magnitude is the amount of suspended sediment (or spill rate) entering the far-field, and is expressed as a fines flux (kg/s). The spatial and temporal variation should be accounted for through correct implementation on the computational grid. As only the far-field is modelled, the dredge plume is dispersed by the ambient flow only. Therefore, implementing the source should not add initial momentum to the ambient flow. The source flux should directly be 'taken' by the ambient flow.

In Delft3D-FLOW the source term is implemented as a discharge of water and sediment. For each input cell a discharge (m^3/s) and a concentration (kg/m^3) have to be specified. The source

term flux is a multiplication of the input discharge and the input concentration. Any combination of those two parameters could lead to the same flux, however, the notion of minimizing the additional momentum limits the number of choices. The discharge (and thus the velocity) should be sufficiently small. The maximum allowed discharge depends on the flow velocity of the ambient fluid and the size of the computational grid.

Input location
The input location of the source term depends on the grid size, location of transition from near- to far-field, the source term dimensions and the type of source. The transition location from near- to far-field can be defined as the input location of the source term on the computational grid. When, for instance, the length of the near-field is smaller than the grid size, the input cell for the source term can be the same as the cell where the dredging activity is performed. The actual input location does therefore also depend on the grid size and dimensions of the plume at the transition.

Another aspect to take into account is the fact that dredging activities, and thus corresponding far-field source terms, can be either stationary or non-stationary (referred to as a moving source). Dredging with a back-hoe at one location can be interpreted as a stationary source. However, when dredging with a TSHD, the vessel (and thus the true source term) is generally moving. The degree of movement during operations can be important for temporal and spatial variation of the source. A stationary source can be allocated to one or several grid cells, with no spatial variation in time. While moving sources require varying source input in space and time. The correct suspended sediment flux should be accounted to the correct grid cell. This depends on the degree of movement of the source (length of the dredge track and dredge speed) and sediment flux at that point in time. Whether to apply a moving source in the model is further dependent on the model's time step and the computational grid dimensions. Thus, the degree of movement of the true source in combination with ambient conditions and model parameters will determine whether movement of the source term should be modelled at all.

Lateral and vertical source term distribution
The theoretical framework showed that the near-field behaviour of dredge plumes depends on a large number of factors, related to the ambient conditions, sediment characteristics and equipment used. A denser plume will settle more quickly and may result in much higher sediment concentrations in the lower water column. Besides the actual near-field processes the near-field modelling approach determines to a large extent the knowledge of the far-field source term. Furthermore, the computational approach and grid size (in relation to plume dimensions) determine to what extent lateral and vertical variations can be included.

To test the effects of all these factors several variations of the 500 m wide, 100 kg/s, source term have been developed. In lateral direction a point, line and distributed line source are used in the experiment. The line sources are all 500 m wide, while the point source width depends on the grid size. In vertical direction three different distributions are implemented; a uniform distribution, a distribution with all sediment in the lower half of water depth and one distribution with varying concentration over depth (see Figure 3.2). Table 3.3 gives an overview of the source terms used for each grid size and computational approach. The vertically distributed line source are only distributed over the vertical, so no lateral distribution is applied in these cases.

Sediment grain size
The sediment characteristics of the sediments present in the dredge plume are an important para-

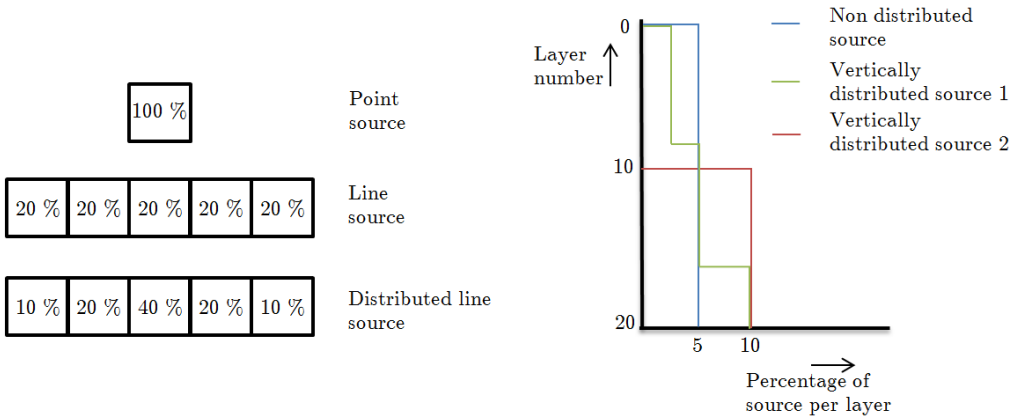

Figure 3.2: Lateral source term distributions (left figure) and vertical source term distributions (right figure), showing percentage of source term flux per cell or layer.

Type of source	**Approach**	**50x50**	**100x100**	**250x250**	**500x500**
Point	1D/2D/3D	x	x	x	x
Line source	2D/3D	x	x	x	
Distributed line source	2D/3D	x	x		
Vertically distr point source 1	3D	x	x	x	x
Vertically distr point source 2	3D	x	x	x	x
Vertically distr line source 1	3D	x	x	x	
Vertically distr line source 2	3D	x	x	x	

Table 3.3: Source terms used in the experiment sorted by grid size and computational approach.

meter in both near- and far-field dredge plume dispersion. The settling velocity determines (among other parameters) the deposition and erosion rates, sediment concentration profile and consequently the far-field dispersion of the plume. Sediment with a higher settling velocity will settle faster, resulting in the plume remaining closer to the source than for finer particles.

In reality more than one particle size is present in a dredge plume. In far-field models it is possible to add several sediments and calculate the transport of each sediment. However, it is common practice to schematise the plume's sediments as only one or just a few particle classes.

As the largest particles (sand) will have settled in the dredge vessel or in the near-field, the dredge plume merely consists of silt and clay. Therefore, the plume's sediment is modelled as a cohesive sediment in Delft3D-FLOW.

In the theoretical framework (Section 2.1.2) the properties of plume's sediment were outlined. Flocculation is an important property of cohesive sediment. By the application of several sediment classes in the model it is possible to account for the flocculation process. One of the particle classes would represent the flocs. However, since the flocculation process is not time invariant, this would require implementation of a time variant settling velocity and floc size. As investigation on the influence of flocculation is not a goal of this research, flocculation is not taken into account in the experiment. Modelling with one sediment particle class is therefore sufficient.

In the first stage of this experiment one cohesive sediment is implemented with a settling velocity

of 2.57 mm/s, corresponding to a particle diameter of 63 μm. In a later stage the actual influence of the settling velocity on plume dispersion and sedimentation is tested.

3.2.3 Ambient parameters

In the experiment a simplified flow case is modelled. Processes as wind or stratification of the water column are not taken into account. The flow conditions in the channel determine to a large extent the dispersion of dredge plumes. The magnitude and direction of the mean flow velocity will have a large effect on the longitudinal transport of the plume. Furthermore, ambient parameters as water depth will determine settling of particles and thus dispersion of dredge plumes. In deeper water it will take longer for particles to reach the bed.

In the first stage the water depth and flow velocity are not varied, as in a later stage the actual influence of these parameters on plume dispersion is investigated.

3.3 Modelling framework and scenarios

All influencing parameters for modelling far-field dredge plume dispersion have been identified. The effects on the model output will be tested in the experiment. Figure 3.3 shows a modelling framework illustrating all stages involved in far-field dredge plume dispersion, including the influencing parameters. Two ambient groups have been identified; the ambient conditions and the dredge source. The model stages start with the requested output, which is the goal of the simulation. A model simulation finally results in model output. In case of successful modelling, the model output meets the requested output.

For the requested output, distinction is made between a young and an old plume and between the output parameters flux and concentration. The plume age is a measure for both the location of the plume and elapsed time at that location. The distinction between young and old is made to identify the influence of the age of the plume on far-field plume results. In Section 3.4 the definition of plume age and interpretation of young and old are further elaborated on. The distinction in parameters is made because high levels of SSC are related to both sediment fluxes and peak concentrations. However, importance depends on the local conditions and requirements. Peak concentrations are related to the highest concentrations present, while the sediment flux is related to the total amount of sediment moving through the considered (cross) section. Together with the peak concentration (maximum concentration) also the lateral distribution of the concentration is considered. Sediment concentrations could be important in the vicinity of, for example, a drinking water intake. High sediment concentrations make use for drinking purposes impossible. Whereas, if sedimentation is important the total sediment flux can be the governing parameter.

In most studies ambient conditions serve as starting point, since they are a consequence of the investigated area. Of course, varying ambient conditions will have influence on model results, through the model parameters. However, no choices can be made as data often follows from measurements. In the experiment, the sediment type, water depth and flow velocity are considered. These ambient parameters determine the model parameters, with special focus on the diffusivity and the erosion and deposition parameters.

Next to the ambient conditions, the dredge source is also an invariable and follows from the type of equipment used and the project stage. Hereby, the source term is determined by the (knowledge on) the actual dredge source. Influence of detail in source term parameters will be investigated in the experiment. Also, the importance of a moving source on computational results will be included.

The requested output, ambient conditions (through the corresponding model parameters) and dredge source together determine the computational requirements. In the computational requirements stage, choices are made regarding the computational approach, grid size and source term input. Within the computational requirements all of the above parameters are linked. In the experiment the parameters are varied in order to test their influence on the model output. This is done in other to identify efficient 'paths' for given ambient or input situations. Also, the experiment will give an impression on the most important parameters while following a certain path. This can help to identify which parameters to focus on, given some requested output.

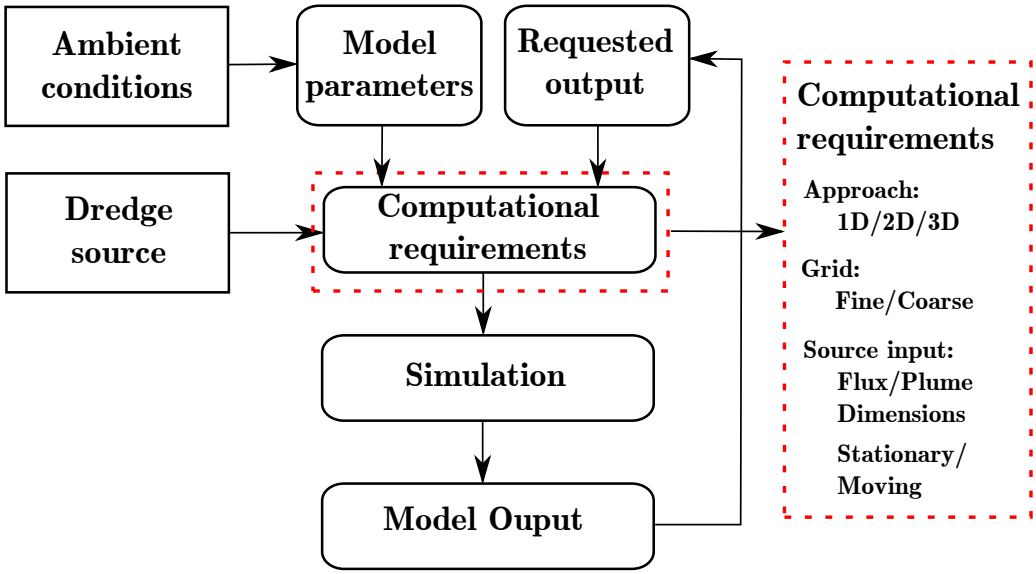

Figure 3.3: Framework for far-field dredge plume modelling, indicating model stages and influencing parameters.

To test the effects of the ambient, model and input parameters on far-field dredge plume dispersion several scenarios are developed. The experiment is divided into three stages:

1. In the **reference cases** first the overall performance of the model is tested by comparing model results to *the analytical solution*. Further, values for *turbulent diffusivity*, *erosion and deposition parameters* and *source term magnitude* are determined. Through several reference model runs the influence of these parameters is tested. From these results values are determined to be used in the other two stages.

2. In the **first stage** of the experiment the influence of *computational approach*, *grid size* and *source term distribution* on far-field plume dispersion is investigated. The scenarios used correspond to the cases listed in Table 3.3.

3. In the **second stage** the experiment is further extended to test the influence of a *moving source term*, *settling velocity* and *ambient flow parameters* (flow velocity).

3.4 Presentation of results

The results of the model runs for the different scenarios are compared for both sediment fluxes and peak concentrations. Fluxes and concentrations are compared in longitudinal and lateral sections at different times. Figure 3.4 shows an overview of the computational grid, indicating the source term location and possible output locations. The longitudinal results are given at three time steps (30, 80 and 230 min after the start of the source input). The figure shows an example of such a plot, in which the total flux (over the cross section) is drawn for each plume age observed at a certain time. The plume age is both a measure for the traveled time and the traveled distance of the plume. It can be calculated by dividing the distance traveled from the source by the ambient flow velocity.

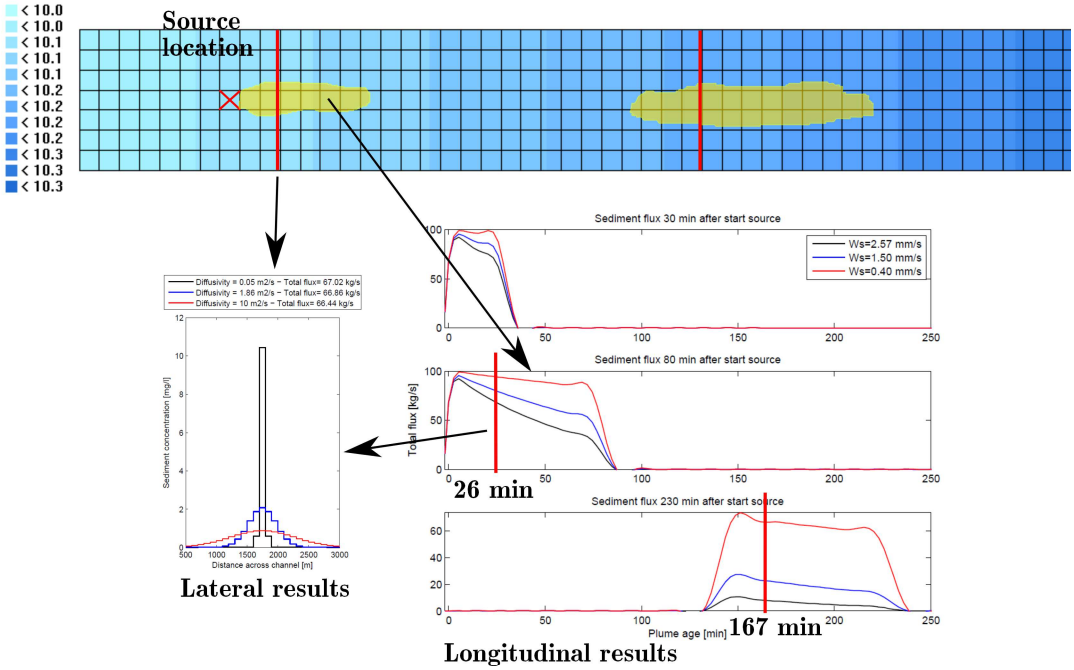

Figure 3.4: Top view of numerical grid indicating input location of source term and output locations, including examples of possible result graphs.

Lateral results are compared at two times, 80 and 230 min after start of source input. After 80 min the concentration distribution is drawn for a plume age of 26 min. This is considered to be a young dredge plume. The far-field source is still continuous, as it has not stopped yet. After 230 min the source input has stopped and the plume has been 'released'. It has traveled further in the far-field. A concentration distribution is taken for a plume age of 167 min, which is classified as an old plume. An example of such a graph is added in Figure 3.4. The figure shows the distribution of the concentration in lateral direction, while in the legend the total longitudinal sediment flux through the considered section is given. The angular shape of the graphs results from the use of a numerical grid with a certain size. The concentrations are accounted to a whole grid cell. A coarse grid and/or sharp concentration gradients will therefore result in more jagged shaped concentration profiles. A combination of both lateral and longitudinal figures will give an impression of the dimensions of the plume at a certain point in time in both longitudinal and lateral

direction.

Most figures in this report show peak concentrations and sediment fluxes. Some analysis may ask for different representation of results or comparison of other parameters. In these cases this will be clearly indicated.

Chapter 4

Results

4.1 Reference cases

4.1.1 Validation to analytical solution

The results of the 2D and 3D simulations are compared to results of the analytical equation, in order to prove that the numerical model is capable of predicting dispersion of sediment plumes. For the uniform stationary channel flow considered in the experiment the dispersion along the direction of the flow can be calculated using the formula of Elder (Elder, 1959), as described by Fischer et al. (1979). A similar equation as Equation 3.2 is used to determine the analytical result for an instantaneous release of a patch of sediment into the channel. This sediment disperses along the channel as it is advected by the mean flow and slowly broadened. The dispersion coefficient equation as formulated by Elder is used for the analytical solution:

$$K(x) = 5.93hu_*, \tag{4.1}$$

where the water depth (h) is 10 m and the critical velocity (u_*) is 0.03 m/s. This results in a dispersion coefficient (K) of 1.86 m^2/s. For the 2D simulations the eddy diffusivity is also set to 1.86 m^2/s.

Figure 4.1 shows results at three times after release of the patch. The plume age is a measure for the longitudinal distribution of the plume. The figure displays the total flux along the plume for simulations with several grid sizes. The 2D results show close resemblance with the analytical solution. For all grid sizes the location of the sediment flux peak corresponds to the location of the the analytical solution. The flux peaks are lower than the analytical solution, due to the fact that the patch of sediment is more spread in all model simulations. A smaller grid size leads to a sharper profile with a higher flux peak, as can be concluded from the results.

The 3D simulation results show a similar shaped flux profile as for the 1D and 2D simulations. The only difference can be found in the location (and thus plume age) of the flux peak. The patch of sediment is lagging behind the other patches. This is a result of differences in vertical sediment profile. For the 2D and 3D simulations a constant (over depth) sediment profile is assumed. In the 3D simulation the profile will adapt to the flow conditions. As sedimentation and erosion are zero in the simulation, the vertical sediment profile will establish into the Rouse profile, with higher concentrations at the bottom than at the top of the water column. Consequently, at the location of highest sediment concentration the velocity is at its minimum (logarithmic velocity profile). On average this results is slower movement of mass centre of the sediment patch.

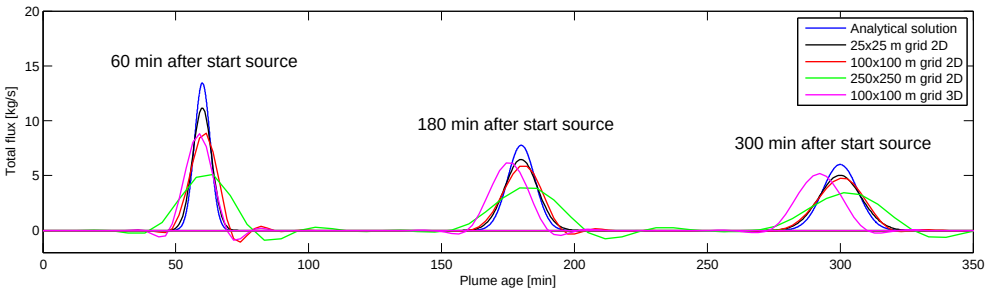

Figure 4.1: Sediment flux distribution as function of the plume age at three different times for both several 2D/3D simulations and the analytical solution.

The negative concentrations present in Figure 4.1 originate from choice on the discretisation scheme for the advection diffusion equation. As was stated in Section 3.2.1, the Cyclic scheme may results in non-physical oscillations in areas of sharp concentration gradients on coarse grids. This is nicely demonstrated by the results presented in Figure 4.1. Sharp gradients (shortly after sediment release) and larger grid sizes result in wiggles at the back and front of the sediment plume. Further away from the source concentration gradients tend to decrease, resulting in smaller, or disappearance of, negative concentrations. Therefore, possible wiggles are expected only to be found shortly after release of the plume, where concentration gradients are highest. It should be noted that a Forester filter is applied in the simulations, but this did not solve the issue.

The Van Leer-2 scheme was also tested, as this scheme guarantees strictly positive concentrations. However, the scheme enhances numerical damping, leading to lower plume fluxes. Furthermore, 3D simulations on relatively fine grids (50x50 m) were not possible for the Van Leer-2 scheme. Therefore, the Cyclic method is further applied in the experiment.

4.1.2 Source term magnitude

The increase of momentum at the input location of the source term should be minimal. The added source term, together with the flow velocity and grid size determine the actual momentum increase. A model run with a 500x500 m grid was used to test the influence of several source term magnitudes. The discharge through the input grid cell in case of no source is 3250 m^3/s. Figure 4.2 shows the depth averaged velocity just downstream of the input location for a case with no source term, a 1 % discharge increase and a 10 % discharge increase. With a discharge increase of 10 % the depth averaged velocity is increased significantly. Even for the 1 % higher discharge there is a slight increase. From these results can be concluded to keep discharge increase in the input cell well below 1 % throughout the whole experiment.

4.1.3 Eddy viscosity and diffusivity

In the horizontal plane the viscosity does not play a role, so only the diffusivity is evaluated here. From the theoretical framework and parameter description can be concluded that different diffusivities should be applied for the lateral and longitudinal direction. However, a choice should be made, since only one horizontal eddy diffusivity can be defined in Delft3D-FLOW.

Figures 4.3 and Figure 4.4 show lateral concentration profiles and longitudinal flux results for model runs with three different eddy diffusivities. The longitudinal diffusivity can be approximated

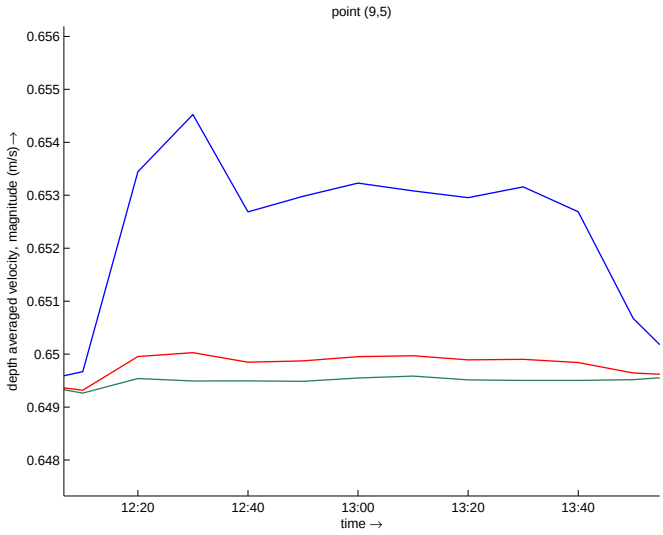

Figure 4.2: Depth averaged velocity at input location after adding 1) no source term (green line), 2) source term with 1 % discharge increase (red line) and 3) source term with 10 % discharge increase (blue line).

using the Elder formula. This results in an eddy diffusivity of 1.86 m^2/s, as was calculated earlier. The lateral diffusivity can be approximated by a similar equation (see Section 2.1.2):

$$D_t(y) = 0.15hu_*, \tag{4.2}$$

in which the water depth (h) is 10 m and the critical velocity (u_*) is 0.03 m/s. For the experimental situation this results in a lateral eddy diffusivity of 0.05 m^2/s. A third diffusivity tested; the Delft3D-FLOW default value, 10 m^2/s

The concentration results in lateral direction show the differences in mixing for the three diffusivities at two time steps and plume ages (for a young and an old plume). Clearly, a higher horizontal eddy diffusivity leads to more lateral spreading, while the total fluxes through these cross sections are similar. For a young dredge plume (left figure) a diffusivity of 1.86 m^2/s results in a peak concentration which is 50 % of the concentration for a diffusivity of 0.05 m^2/s. After 230 min, for a plume age of 167 min, this difference has become even larger. Here the peak concentration for a diffusivity of 1.86 m^2/s is approximately 20 % of the concentration for a diffusivity of 0.05 m^2/s. The peak concentration for 10 m^2/s are about 50 % of the 1.86 m^2/s concentration results, and more or less stable for both the young and old plume.

Figure 4.4 shows the flux variation along the plume. A higher eddy diffusivity gives rise to more longitudinal spreading, and therefore a lower maximum flux and wider plume. Though, the differences in flux results are much smaller than the differences for the concentration in lateral direction. Thus, the diffusivity has large effects on the distribution of the concentration, while effects on longitudinal flux results are limited. Furthermore, in Figure 4.4 the physically incorrect negative concentrations are clearly visible in the longitudinal results for model runs with a diffusivity of 1.86 m^2/s and 0.05 m^2/s. For a simulation of 10 m^2/s these oscillations have disappeared due to the fact that concentration gradients are lower. This is also an effect of the larger lateral spreading of the plume.

Since the experiment considers a uniform stationary flow case, eddy diffusivities of 1.86 m^2/s or 10 m^2/s lead to overestimation of lateral spreading. Although it is not known what the 'real' diffusivity coefficient should be, it is clear that in the experimental case no lateral velocity profile is present. Therefore only little lateral mixing would take place. Since only one horizontal value can be specified, the lowest value is chosen; the eddy diffusivity for lateral mixing.

The vertical eddy viscosity and diffusivity need to be defined for the 3D simulations. The vertical viscosity takes care of vertical momentum exchange and can be related to the velocity profile. In Delft3D-FLOW several models are available, but it is also possible to apply a constant value. Figure 4.5 shows vertical viscosity/diffusivity profiles and corresponding velocity profiles. A constant viscosity leads to a parabolic velocity profile, while the for the k-l and k-ϵ models the well known logarithmic velocity profile is established. Also lateral concentration profiles for model runs with different vertical diffusivities were compared. The k-ϵ and k-l model show similar results, while for a constant diffusivity the peak concentration is slightly higher. This can be explained by the fact that the vertical concentration for a constant diffusivity case shows less depth variation. This leads to a lower near bed concentration, resulting in less sedimentation. Also the surface concentration is higher than the $k-\epsilon$ and k-l cases. For the 3D model simulations in this experiment the k-ϵ is used for both eddy viscosity and diffusivity.

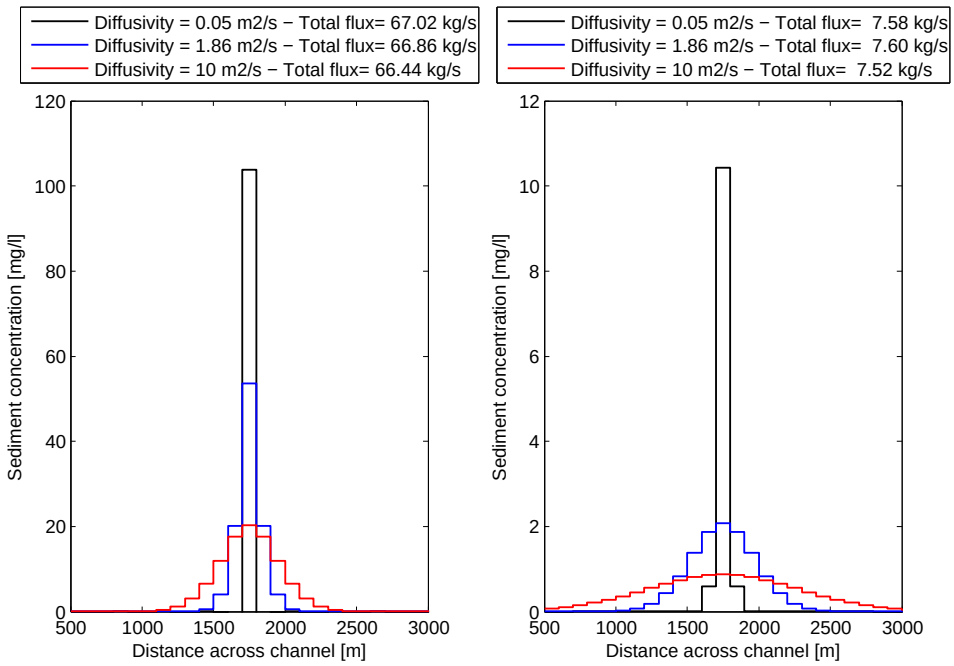

Figure 4.3: Lateral concentration profiles and sediment fluxes observed 80 min after start source, for a plume age of 26 min (left figure) and observed 230 min after start source for a plume age of 167 min (right figure), for simulations with three different eddy diffusivities.

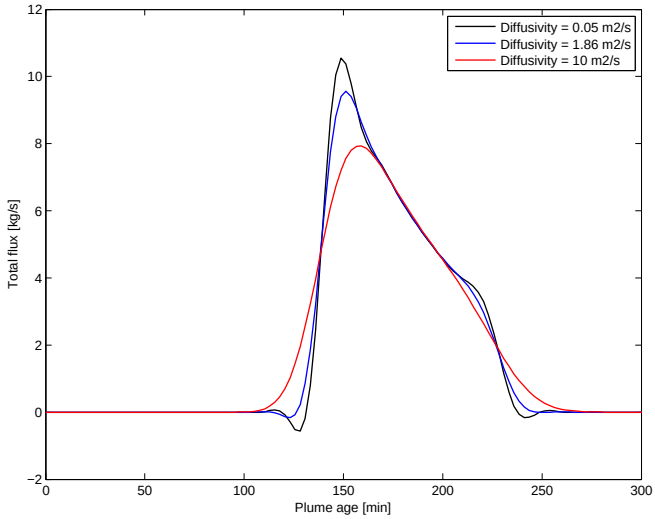

Figure 4.4: Total flux as function of the plume age for simulations with three different eddy diffusivities, 230 min after start source.

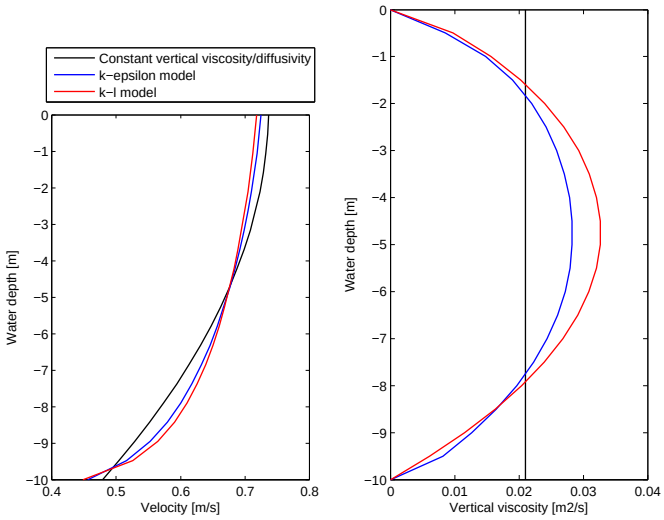

Figure 4.5: Vertical velocity profiles (left figure) and viscosity/diffusivity profiles (right figure) for different vertical viscosity and diffusivity models, at a distance 4250 m downstream of the boundary.

4.1.4 Sediment settling and erosion

The erosion and deposition parameters determine the deposition and erosion rates. Moreover, these parameters influence the vertical concentration profile in the channel through the bed boundary condition. As this is an experimental situation, no data is available on deposition or erosion rates. Therefore, as a reference, several combinations of erosion and deposition parameters are tested in both 2D and 3D simulations.

Figure 4.6 shows the cumulative sedimentation/erosion across the channel at the end of the simulation for several cases. In the lower figure vertical concentration profiles are plotted, 500 m

downstream of the source (80 min after start source). In the simulations the settling velocity, ambient velocity and source term are taken constant. Results are presented for a case with maximum deposition and no erosion (assuming the critical stress for deposition is always higher than bed shear stress), a case with both deposition and erosion and a case with no deposition and no erosion. These three cases can be considered as extreme situations.

Highest deposition rates occur for a case with maximum deposition rates (blue and black lines). Most sediment is deposited near the source, while reducing concentrations gradually lower the deposition rates traveling downstream. The gradient of the vertical concentration profile is, as expected (Section 3.2.1), zero at the bed. This results in the plotted vertical concentration profile (lower figure, dark blue line). In case both erosion and deposition are applied, the deposition of sediment shows larger spreading over the channel length (green and red line). This can be explained by the fact that some settled sediment may be eroded again. The actual shape of the sedimentation profile along the channel depends on the choices on critical bed shear stresses. The vertical sediment profile will adapt at the bed to the bed boundary condition. In case no erosion and deposition are applied, the vertical concentration profile will establish to the well known Rouse distribution (light blue line). This case shows highest concentrations over the vertical, as no sediment is deposited. The concentration profile is time invariant, as no erosion nor sedimentation takes place.

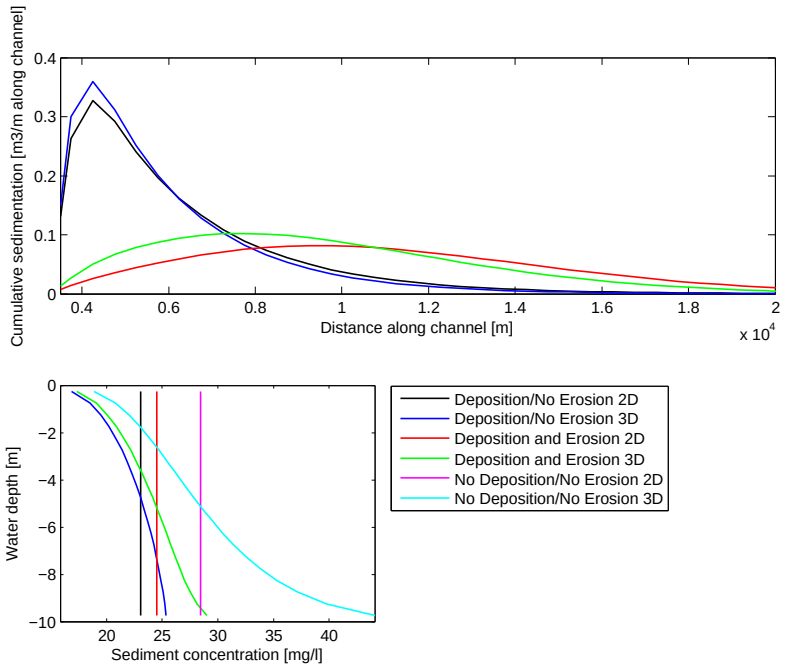

Figure 4.6: Vertical sediment concentration profiles in the middle of the channel 500 m downstream of the source input location (bottom figure) and the cumulative sedimentation/erosion across channel (top figure) for different erosion/deposition cases, all with the same settling velocity (2.57 mm/s).

The 2D and 3D simulation results indicate significant differences in deposition rates. These are caused by the differences in near bed concentrations for the 2D and 3D simulation (see lower figure). These result in higher deposition rates near the source in 3D. Further downstream the larger deposition rates give rise to decreasing near bed concentrations for the 3D cases.

The sedimentation is a major interest in assessing environmental impact of dredge plumes. Sedimentation is a property of both the flow and the sediment characteristics (plume's material). Erosion of sediment is rather a characteristic of the bed, hence it is hard to define in an experimental situation. In this experiment only sedimentation is taken into account, by means of a maximum critical bed shear stress for deposition. In this way the difference in deposition rates of the various simulations can be compared. When looking at other flows, a tidal case for instance, erosion effects might be interesting to take into account.

4.2 Experiment stage one

In the first stage the influences of computational approach, grid size and source term input on sediment concentration and fluxes are investigated. Lateral concentration results for all 2D simulations are plotted in Figures 4.7 and 4.8. The figures include both the fluxes through the cross section as well as the concentration distributions. The peak concentration represents the highest concentration present in lateral direction.

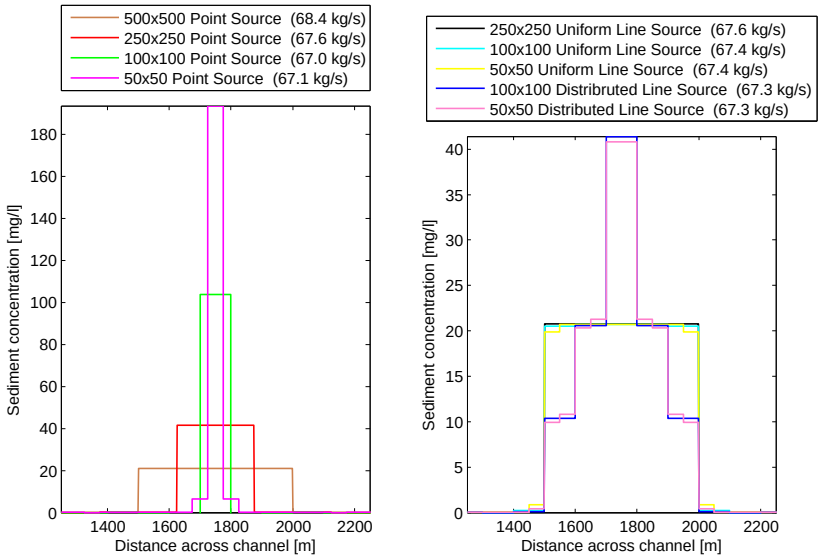

Figure 4.7: Lateral concentration profiles and sediment fluxes observed 80 min after start source for a plume age of 26 min for several 2D simulations.

The total fluxes for a young plume (plume age: 26 min) observed after 80 min are similar for all 2D simulations. The small differences that occur can be accounted to the fact that the results for the coarser grids (500x500 m and 250x250 m) are less accurate. Less grid cells are present to capture the plume than for smaller grid sizes. These very small concentration difference (0.3 mg/l) may lead to a noticeable flux difference (about 1 kg/s). Results for the old plume (plume age: 167 min) observed after 230 min show that this concentration difference, and corresponding flux difference, is still present (about 1 kg/s). However, since absolute flux values have dropped, the relative influence is much bigger here. The relative flux error for the simulation results for the 500x500 m grid after 80 min is about 1.5 %, while after 230 min the error has increased to 13.5 %. Both after 80 min and 230 min, concentration results show large variation. After 80 min peak concentrations range from 20 to almost 200 mg/l (factor 10 difference). After 230 min this has

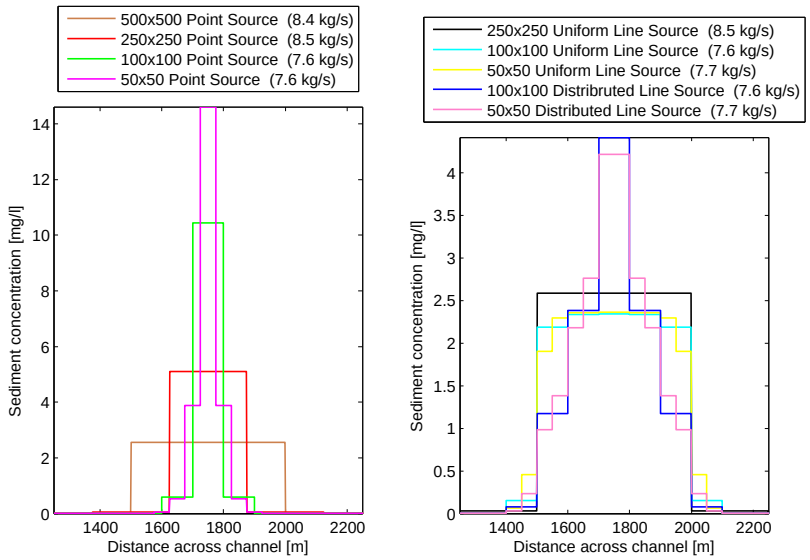

Figure 4.8: Lateral concentration profiles and sediment fluxes observed 230 min after start source for a plume age of 167 min for several 2D simulations.

dropped to a factor 6 difference (about 2.5 to 14.5 mg/l), but this is still significant. Besides peak concentration, lateral distribution of the concentration illulstrate large differences. The differences are induced by the variations in grid size, relatively low diffusivity and the lateral variation of the source term.

The source term plume width was 500 m. Implementing this plume as a point source on a 50x50 m grid, results in overestimation of the peak concentration for the young dredge plume by a factor 10, which can be approximated by taking the plume width divided by the grid size. This can be counter-acted by application of a line source (500 m wide). This results in a peak concentration close to the simulated concentration on a 500x500 m grid (point source).

If a distribution is present at the transition from near- to far-field, this can not be included for a grid size similar to the plume's width. For the chosen distribution, peak concentrations are twice as high as for the point source on a 500x500 m grid (after 80 min). Again, the results for the old dredge plume show that this difference is decreasing, but remain significant (factor 1.5).

The concentration results are closely related to the diffusivity applied in the simulations. Following the conclusions in the reference test; a higher diffusivity leads to faster lateral spreading of the plume. This also implies the effect of the source term input variations will decrease. A diffusivity of 1.86 m^2/s, for instance, showed significant influence of source term distribution for the young dredge plume (after 80 min). However, after 230 min peak concentrations are similar, regardless the type of source input.

Comparing the young dredge plume to the old dredge plume illustrates that overall concentrations have dropped significantly. This is due to the fact that much sediment has settled to the bed. The amount of sedimentation depends on the concentration as well as on the width of the plume. In case of lower peak concentrations (suppressing sedimentation), the plume is wider (enhancing sedimentation). The combination of the two resulted in comparable amounts of sedimentation for all different source term configurations.

Comparing the results of the one dimensional solution to Delft3D-FLOW output is only possible

in lateral direction, for a young dredge plume, because the one dimensional analysis requires a constant inflow of sediment. After 230 min the source input is not continuous anymore, and the plume has been 'released'. The lateral concentration profiles for 1D and 2D point source simulations are shown in appendix Figure D.1. The peak concentrations for the 1D results are lower than corresponding peak concentrations for 2D simulations. The differences are getting smaller for the larger grid sizes. On a 50x50 m grid the concentration in 2D is 1.5 times higher than in 1D. The peak concentration results on a 500x500 m grid are fairly similar to the 1D results, but the plume is wider when calculated in 1D.

The calculated fluxes in 1D are about 10 % lower than calculated in 2D. The solution used to determine the sediment concentration in 1D is accounting for more sedimentation than calculated in the 2D model.

The same model runs as performed in a 2D computational approach were done in 3D. Figure 4.9 shows the lateral concentration profiles for simulations on a computational grid of 100x100 m. In Appendix D the results for the other grid sizes are included. In these simulations the distributed source terms refer to vertically distributed sources. The lateral distributed line sources are excluded from these plots.

The results indicate clear differences between the 2D and 3D results in both peak concentration and fluxes, both for the young as well as for the old dredge plume. These are induced by the before mentioned differences in deposition rates. Hereby an error is generated in the 2D simulations on both flux and concentrations. For the young dredge plume the peak concentration is about 5 % higher than calculated in 3D, while the flux is overestimated with about 6 %, regardless the type of source term or grid size applied. For the old dredge plume these relative differences further increase. Figure D.7 in Appendix D shows total cumulative sedimentation along the channel at the end of the simulation. In the first 1000-2000 m downstream of the source, amounts of sedimentation for the 3D simulations are much higher than for the 2D equivalents. After some time the deposition rates for the 2D simulations take over the 3D deposition rates. However, the differences remain small since the overall concentrations have dropped. Looking at the old plume, the concentration error has risen to 40-45 %, and the flux is overestimated with approximately 40 %. The flux results along the plume, drawn in Figure D.6 in Appendix D, support these findings.

The relative differences clearly illustrate the large errors made when simulating in 2D. In the next stage a possible solution to this issue is discussed and tested.

A final remark is made on the relative influences discussed in this first stage. In some situations one might only be interested in absolute concentration differences, instead of relative errors. If, for instance, a maximum allowable peak concentration is defined, the relative error might not be governing, but the absolute simulated peak concentration is. The absolute concentration error for a point source simulation is much larger than for the line source, as the peak concentration is much higher.

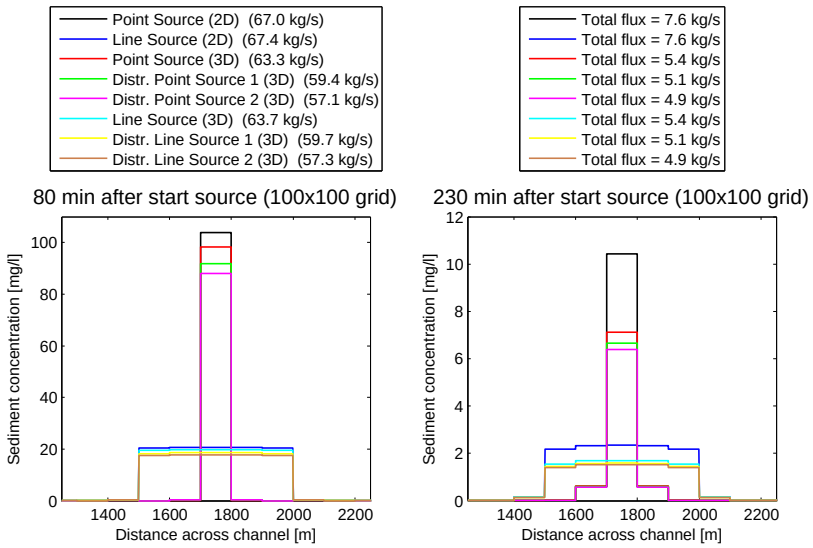

Figure 4.9: Lateral concentration profiles and sediment fluxes observed 80 min after start source for a plume age of 26 min (left figure) and observed 230 min after start source for a plume age of 167 min (right figure) for several 2D and 3D simulations.

The 3D computational approach was also used to test the influence of the vertical distribution of the source term on far-field fluxes and concentrations. Three different distributions, both for point and line sources, were implemented. From Figure 4.9 can be concluded that both the flux and peak concentration are lowest for a source with all sediment in lower half of the water level (Distr. source 2). Both the flux and the concentration are 10 % lower than a uniformly distributed source in 3D. The relative difference is the same for the young and the old dredge plume. Vertically distributed source 1 results in fluxes and concentrations which are 6 % lower than its uniformly distributed equivalent.

Estimations based on the dispersion coefficient state that vertical mixing in a river takes approximately 50-100 times the water depth, which in this case would be 500-1000 m downstream of the source. Investigation of the sediment profiles shows that indeed after 600 m the vertical sediment profile has the same shape as for the uniform source, indicating that vertical mixing of the sediment has taken place. The higher concentrations at the bottom in the first 600 m do cause higher deposition rates. Whereas these higher deposition rates cause smaller peak concentrations and fluxes. As transported downstream the relative flux and concentration differences remain stable, but absolute differences become smaller. In the Appendix (Figure D.6) total fluxes along the plumes for different plume ages are plotted, confirming these findings. Simulations on other grid sizes support the results discussed above. Relative differences in sediment flux and peak concentrations are approximately the same.

Figures 4.11 and 4.12 again show the sediment concentrations for the 2D and 3D simulations observed 230 minutes after source start. In Appendix D the same plots are added from other viewing angles. The plots illustrate the concentration in the channel (depth averaged in case of 3D simulation). These plots make it possible to compare the shape of the concentration profiles. The results of the simulations on the 500x500 m grid show a different shape than the other model runs. The grid cells are too big to cover the concentration profile correctly. The other simulations show more or less the same shape.

Figure 4.12 illustrates the concentration differences between the different source terms for the same grid size (100x100 m). A point source (2D) results in peak concentrations nearly ten times higher than the peak concentration simulated for a uniform line source in 3D.

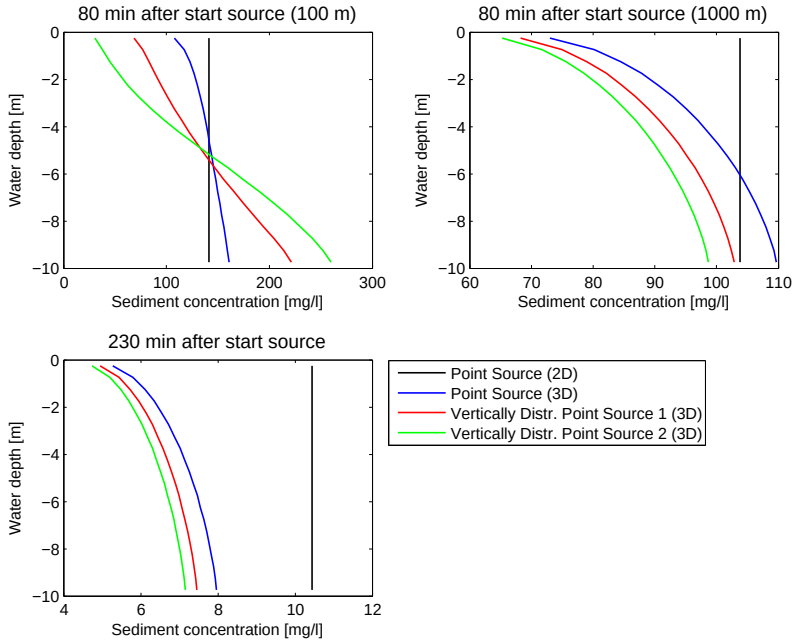

Figure 4.10: Vertical sediment concentration profiles within the dredge plume observed 80 min after start source (100 m and 1000 m downstream of source) and observed 230 min after start source (6500 m downstream of the source).

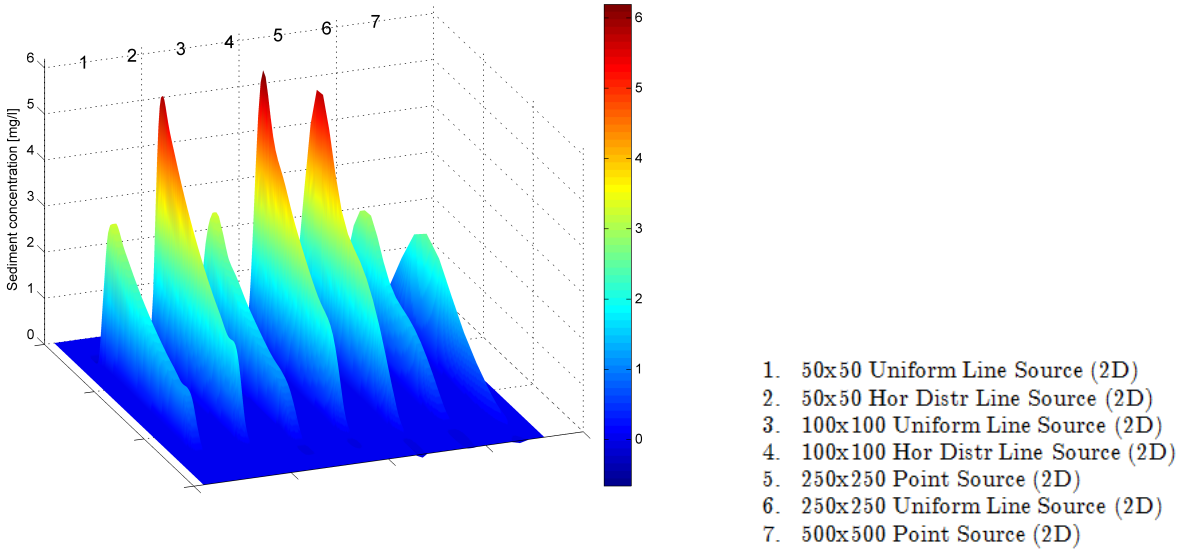

Figure 4.11: Sediment concentration profiles observed 230 minutes after start source for different grid sizes and sources (2D and 3D).

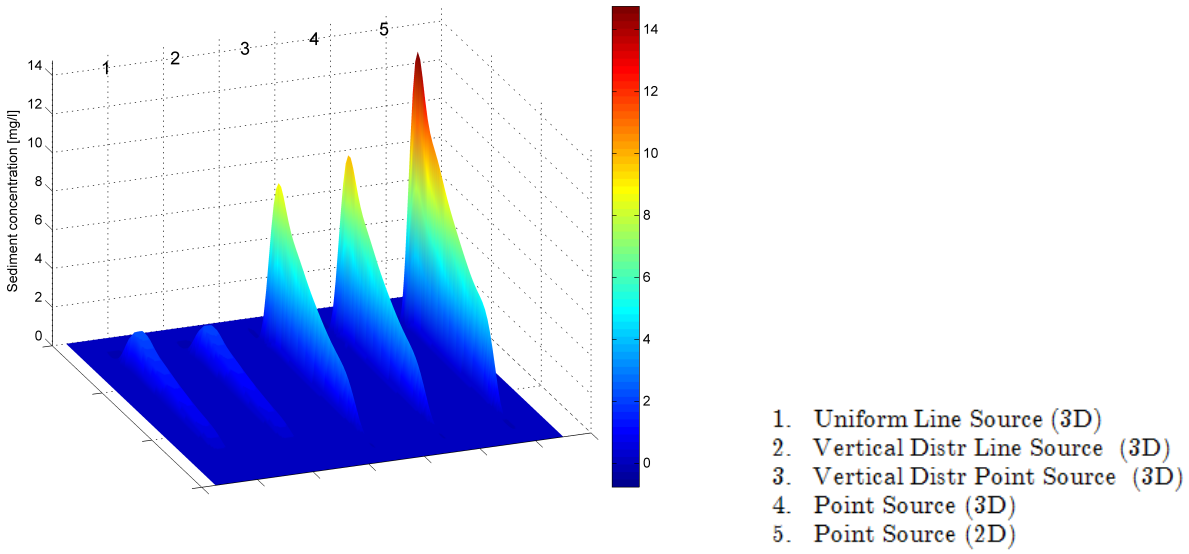

Figure 4.12: Sediment concentration profiles observed 230 minutes after start source for different sources on a 100x100 grid.

4.3 Experiment stage two

4.3.1 Deposition of sediment

Differences in deposition rates for 2D and 3D simulations were observed in experiment stage one. The cause was already mentioned, being the differences in concentrations above the bed. The near bed concentration (concentration in lowest cell) is used in the Partheniades-Krone formulations to determine the deposition rate. The deposition rate further depends on the settling velocity of the sediment particles. Since only one vertical cell is present in a 2D simulation, no vertical concentration variations can be accounted for. In reality the vertical concentration profile will adapt to the flow conditions. This will generally result in higher sediment concentrations near the bed than at the surface. In a 3D simulation the vertical sediment profile does adapt to the flow, resulting in a depth varying sediment concentration profile. Therefore, the 2D near bed concentration is lower than the concentration for an identical 3D case (same flow conditions and settling velocity).

The sediment concentration profile calculated in 3D more realistic than for a identical 2D case, causing underestimation of deposition rates in 2D. The bottom figure of Figure 4.13 shows sediment concentration profiles for some 2D and 3D case. In the upper figure the difference between the 2D and 3D sedimentation along the channel is plotted (3D minus 2D sedimentation results).

Erosion is not accounted for in the experimental situation. Therefore only the deposition rate needs to be considered when describing cumulative sedimentation/erosion along the channel. The Partheniades-Krone formulations for cohesive sediment fractions give the following equation for the sedimentation flux (for more information on the Partheniades-Krone formulations see Appendix C.2 and Section 2.1.2):

$$D = w_s C_b S(\tau_{cw}, \tau_d), \tag{4.3}$$

$$S(\tau_{cw}, \tau_d) = \begin{cases} (1 - \frac{\tau_{cw}}{\tau_d}), & \text{when } \tau_{cw} < \tau_d \\ 0, & \text{when } \tau_{cw} \geq \tau_d \end{cases} \tag{4.4}$$

where w_s is the settling velocity, C_b is the near bed concentration (concentration of lowest cell), τ_{cw} is the maximum bed shear stress and τ_d is the critical shear stress for deposition.

In the experiment a maximum critical bed shear stress for deposition is applied. This results in $S \approx 1$. Moreover, the deposition flux is then given by $w_s * C_b$. Here we see the strong dependency of the deposition flux on the near bed concentration. The near bed concentration itself depends on the settling velocity, deposition rates and flow parameters, all given through the bed boundary conditions (see Equation 3.4.

The black line in Figure 4.13 illustrates the difference between the 2D and 3D calculation for a settling velocity of 2.57 mm/s. Close to the source the sedimentation in 3D is higher than in 2D. After approximately 2000 meter the black line becomes negative, indicating that more sediment is deposited here for the 2D case than for the 3D case. This can be explained by the fact that the higher deposition has resulted in lower concentrations in 3D.

The settling velocity can be adjusted in order to guarantee equal deposition rates. A higher settling velocity will result in higher deposition rates, but will also introduce lower concentrations. For the case shown in Figure 4.13 the deposition rate close to the source in 3D is $6.5 * 10^{-5}$ kg/sm^2, while for the 2D case this is $5.9 * 10^{-5}$ kg/sm^2. This is 9 % lower. Increasing the settling velocity for the 2D simulation from 2.57 mm/s to 2.90 mm/s (11.5 % increase) results in a reduction of the concentration of about 2.5 %. Together, this results in a deposition rate for the 2D case which is comparable to the 3D simulation, hence the blue line in Figure 4.13 is approximately zero.

The adjustments on settling velocity are based on the parameters for erosion and deposition as applied in the experiment. Other configurations of these parameters result in different near bed concentrations for the 2D and 3D cases, hence the difference between the two is also influenced (see Figure 4.6).

4.3.2 Settling velocity, flow velocity and water depth

The influence of the settling velocity, flow velocity and water depth is investigated by varying one of the parameters at a time. The same model and source term configuration as in stage one are used. The numerical grid size is 100 m. The figures show the sediment fluxes as function of plume age at three different times.

Figure 4.14 presents the results of several different flow velocities. The plumes have similar shapes for all flow velocities. A higher flow velocity will cause faster advection of the plume, however plume ages are equal. The plume age is coupled to both the flow velocity and the location of the plume; plume age [s] = Location [m] / Velocity [m/s], which is more or less constant for each flow velocity. The main differences between the plumes can be found at the back and front of each plume. A higher flow velocity results in sharper gradients at the back and front of the plume. For lower flow velocities these gradients are more gentle, and the plume is broader. This difference increases further downstream of the source. This also explains the difference in flux peaks after 230 min.

Another consequence of higher velocity might be a higher erosion rate, due to an increasing bed shear stress. However, as erosion is not taken into account in the experiment, this is not noticeable in the results.

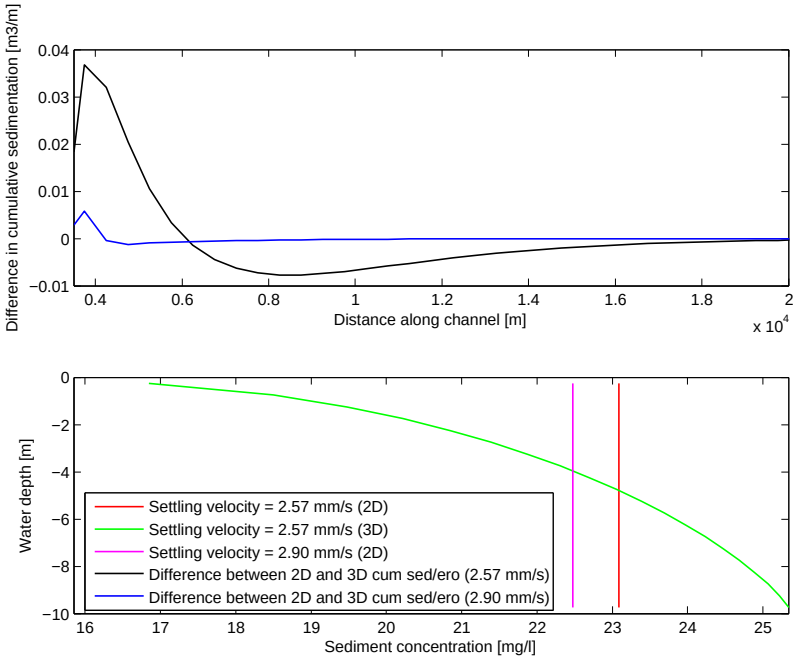

Figure 4.13: Sediment concentration profiles (bottom figure) for a case without erosion taken 1000 m downstream of the source. Top figure shows the difference between the 2D and 3D cumulative sedimentation/erosion across channel (3D results minus 2D results) for different settling velocities.

Figure 4.15 shows the flux results for simulations with varying water depth. The water depth is of big influence on the total sediment flux within the plume. After 230 min the plume has nearly disappeared in a channel with a water depth of 5 m. This is caused by faster sediment settling in lower water depths. Due to a constant sediment flux at the input location, the the difference in sediment flux is smallest here. Further downstream differences between the different water depths increase.

Figure 4.16 shows the results for varying settling velocities. Obviously, the settling velocity is of influence on the settling of sediment particles. A higher settling velocity will result in sedimentation rates near the source, hence lower sediment fluxes. This is indicated by the quick drop of the flux lines for settling velocities of 1.5 and 2.57 mm/s (black and blue lines), compared to 0.4 mm/s (red line).

For the upper two figures the source plume shapes show difference for each settling velocity. Due to the fact that the source is still active here, a constant flux is added, while deposition rates are different for each settling velocity. This results in a steeper plume profile for higher settling velocities. When the source has stopped and the plume is 'released' (lower figure), the plume shapes are equal. This indicates that after 'release' of the plume, scaling could be used to calculate plume fluxes for different settling velocities.

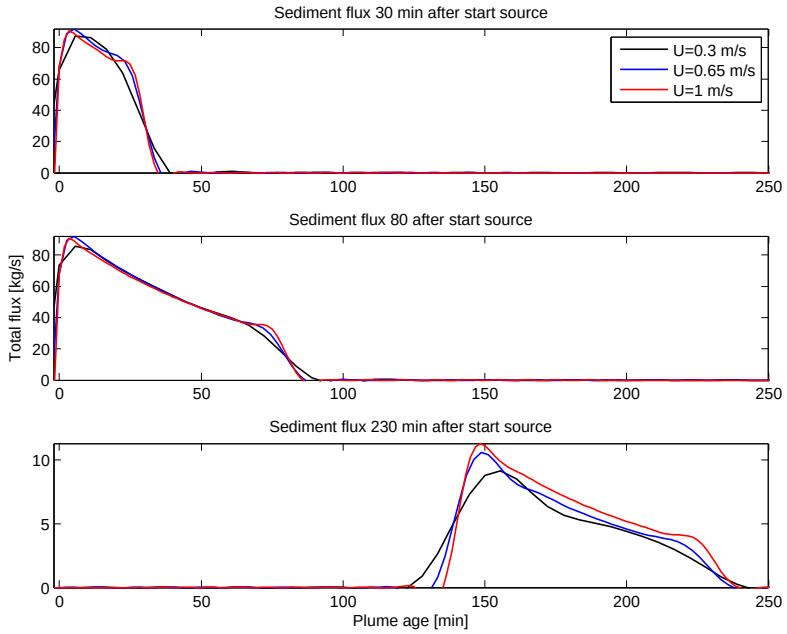

Figure 4.14: Total flux as function of plume age observed 30, 80 and 230 min after start source for four different flow velocities.

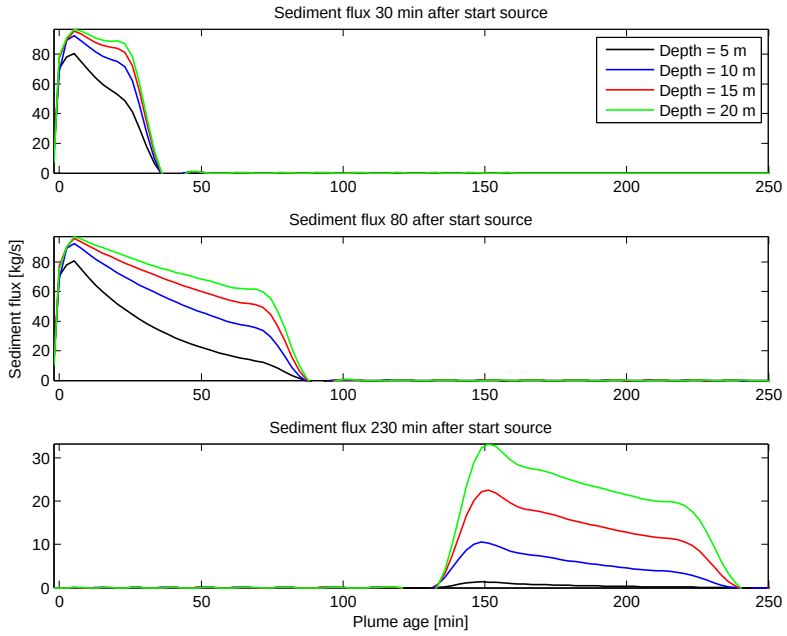

Figure 4.15: Total flux as function of plume age observed 30, 80 and 230 min after start source for four different water depths.

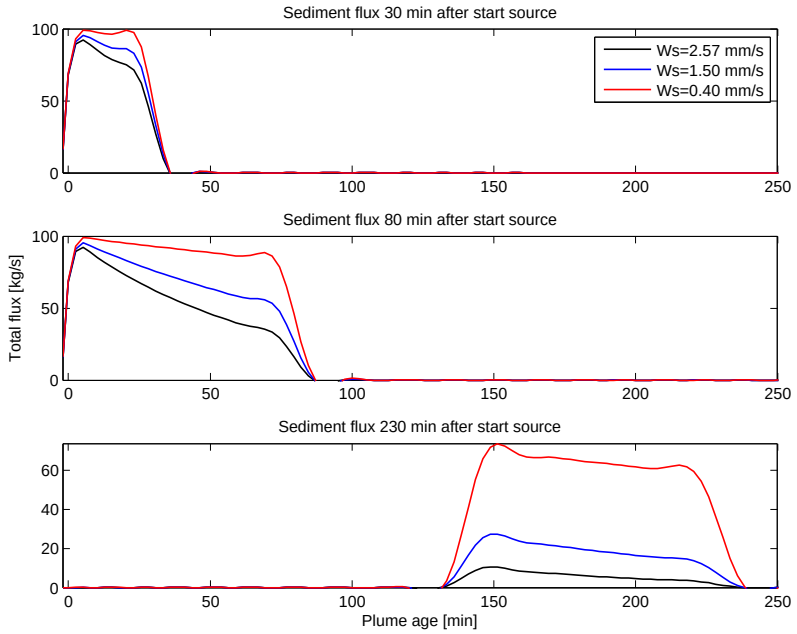

Figure 4.16: Total flux as function of plume age observed 30, 80 and 230 min after start source for three different settling velocities.

4.3.3 Moving sources

When dredging with overflow, the vessel is often dredging tracks and consequently the (true) source of sediment is moving. The movement of the vessel will result in a far-field source term which is not stationary in time. The experiment is extended for several non-stationary sources, to investigate the effects on sediment fluxes in the far-field.

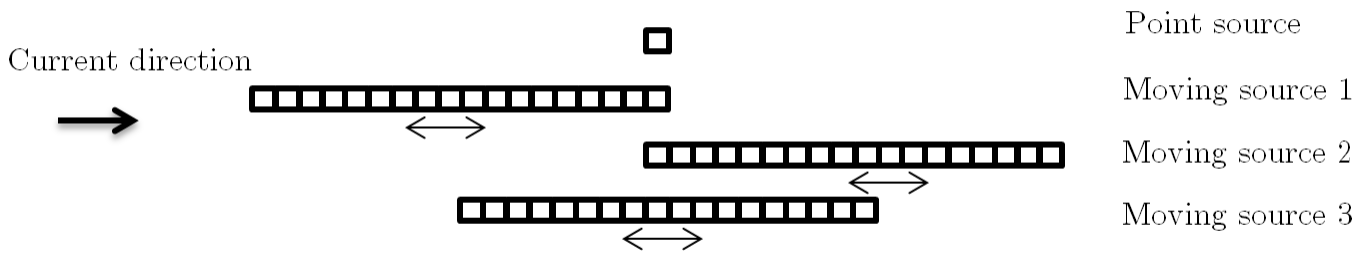

Figure 4.17: Overview of implementation of moving source terms.

Figure 4.17 shows an overview of the moving sources applied. A dredge track of 1800 m, parallel to the current direction, is simulated. Dredging is often performed in this direction, because it is hard for the vessel to keep track when dredging in any other than the current direction. The results

are compared to a stationary situation (point source). The three moving situations drawn in Figure 4.17 make comparison possible for a situation where the point source is placed at the beginning (Moving source 2), end (Moving source 1) or middle (Moving source 3) of the track. Three different dredging speeds have been applied: 0.55 m/s (comparable to the flow velocity), 1.33 m/s (twice the flow velocity) and 1.67 m/s (more than twice the flow velocity). These are typical dredging speeds in engineering practice. The current flow velocity remains constant for all situations; 0.67 m/s.

Figures 4.18, 4.19 and 4.20 show the sediment flux results for the three dredging speeds for moving source 3 compared to a stationary point source. For the other two situations, moving source 1 and 2, the plume fluxes were not comparable to the stationary results. Therefore, these are not included in the report. A stationary point source should thus be situated in the middle of the dredged track.

The non-stationary plume results are related to a one way dredge track, either moving upstream or downstream. The stationary source is a point source with a duration equal to dredging duration in case of moving sources. Also, for all simulations the total mass of sediment input is equal. This implies that a higher dredging velocity requires a larger sediment source input flux, as the total dredging time is shorter. In this way the flux results for each of the simulations can be compared. It should be noted that for the results after 30 min this is not possible, since the source input has not stopped yet. This results in different sediment volumes being present for each of the situations at this point in time.

The results are compared both on the width of the plume as well as on plume peak fluxes, for the three times plotted (30, 80 and 230 min after start source). The results for all the upstream moving sources (red lines) show much difference with the stationary point sources (black lines), regardless which dredging speed is considered. The calculated fluxes are more than half the fluxes calculated for the stationary sources. While the plume width is approximately twice the width of a stationary source plume.

When looking at the downstream moving sources (blue lines), the results show differences for each dredging speed. For a dredging speed of 0.55 m/s (comparable to the flow velocity) the plume is more peaked than for a stationary source. The maximum flux for a stationary source is about 30 % of the maximum flux for the moving source. Also, the plume's width is about have the width of a the stationary source case.

When the downstream dredging speed is twice the flow velocity (1.33 m/s) the flux results are very similar to the stationary source results. After 230 minutes the plumes have the same width and maximum flux.

For a dredging speed higher than twice the flow velocity (1.67 m/s) the maximum fluxes are lower than for a stationary source. The flux for a moving source is about 33 % smaller than for a stationary source. Also, the plume is somewhat wider for all three considered times. Still, if the width of the plume is the major interest, stationary results are acceptable.

From the three figures can be concluded that in case of an one way moving source the direction of dredging, the dredging speed and source location are the most important factors for decisions on the source term input. If a moving source is schematised as stationary source, the middle of the track should be chosen as source term input location. An upstream moving source term can not be modelled correctly as stationary source. For downstream dredging with a dredging speed twice the flow velocity, the flux results for the stationary situation show best fit with the non-stationary source results.

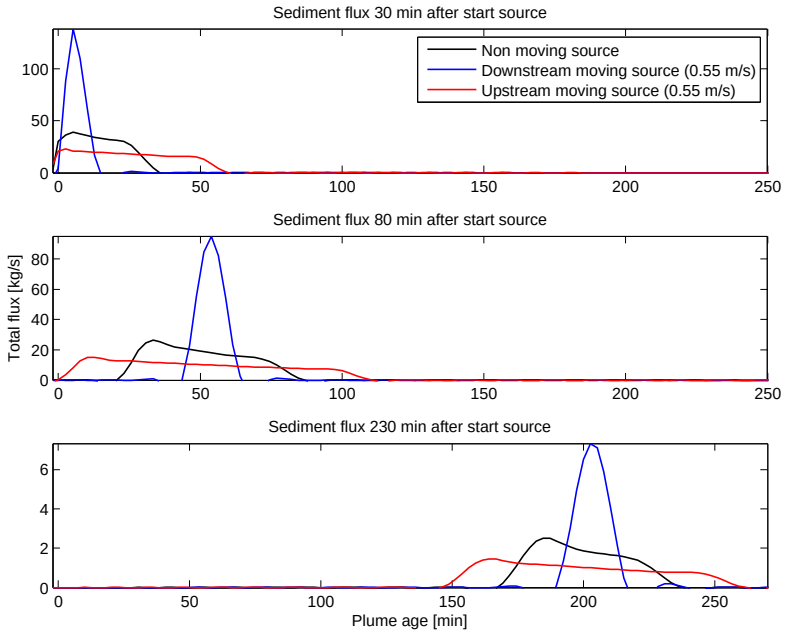

Figure 4.18: Total flux as function of the plume age for a non moving source, downstream moving source and upstream moving source, with a dredging speed of 0.55 m/s (comparable to the flow velocity).

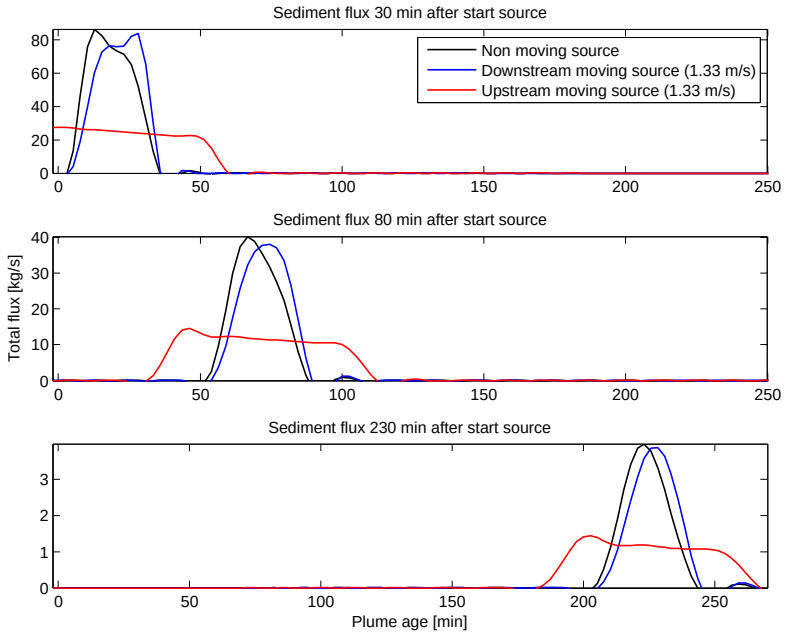

Figure 4.19: Total flux as function of the plume age for a non moving source, downstream moving source and upstream moving source, with a dredging speed of 1.33 m/s (twice the flow velocity).

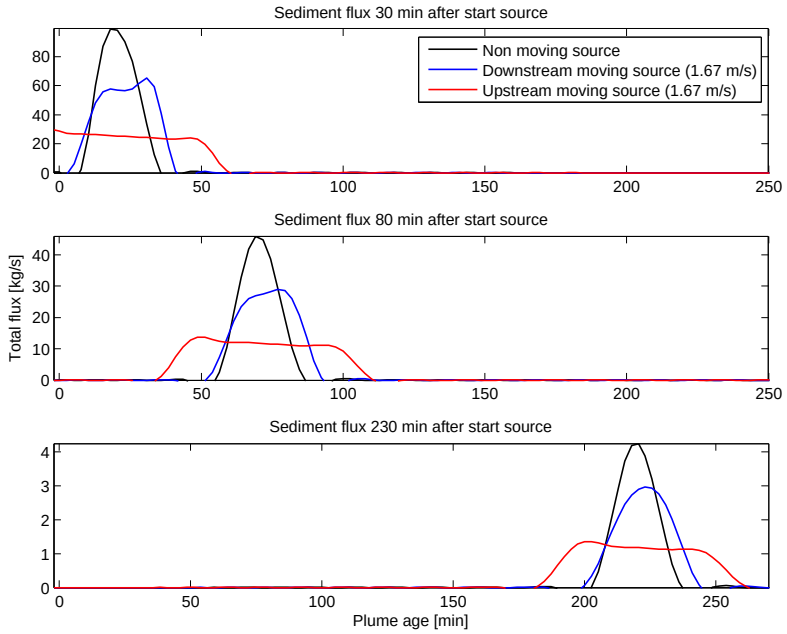

Figure 4.20: Total flux as function of the plume age for a non moving source, downstream moving source and upstream moving source, with a dredging speed of 1.67 m/s (higher than twice the flow velocity).

The above results are only applicable on an one way dredging track, while it is also possible to dredge (and thus overflow) in both down and upstream direction. A two way dredge track (moving up and downstream once) is also investigated for the three dredging speeds. Figures 4.21, 4.22 and 4.23 illustrate the moving source results in comparison to a stationary equivalent for the three dredging speeds.

From the figures can be concluded that in all cases the results are not comparable; the plumes for the non-stationary sources are much wider and peaks are considerably larger. However, as the dredging speed increases, the errors reduce. For a dredging speed of 1.67 m/s the results do show some similarities with the stationary situation. The location of the peak the same as for the stationary source. Especially for older dredge plumes (lower panel) the results do show improvement.

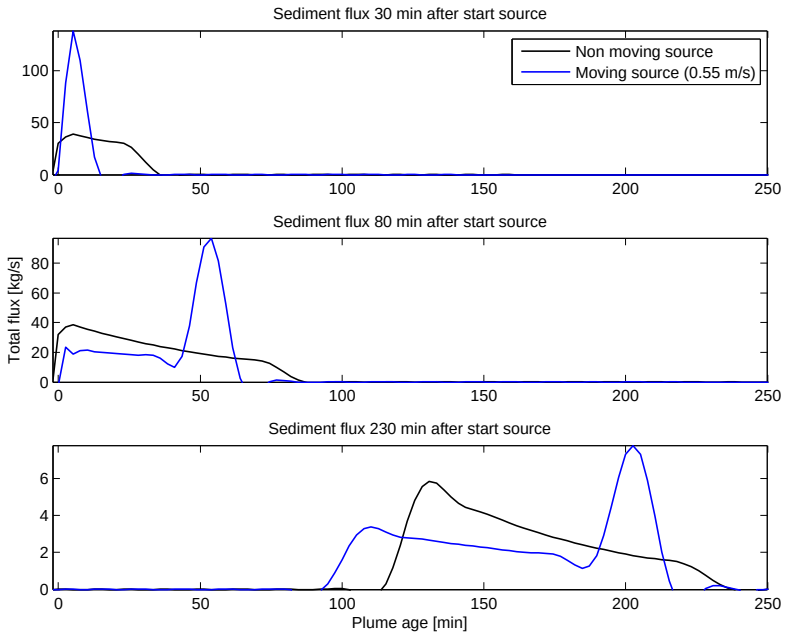

Figure 4.21: Total flux as function of the plume age for a non moving source and an up and downstream moving source (0.55 m/s, comparable to the flow velocity).

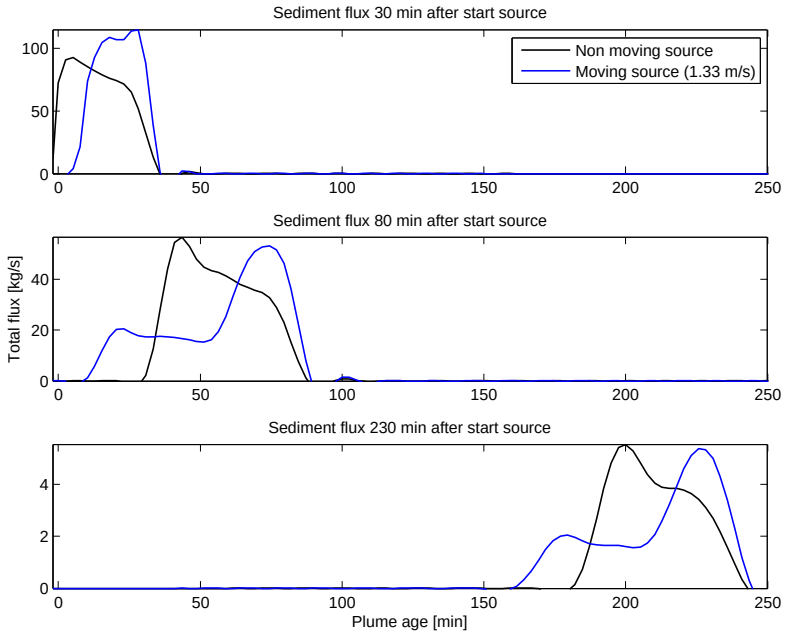

Figure 4.22: Total flux as function of the plume age for a non moving source and an up and downstream moving source (1.33 m/s, twice the flow velocity).

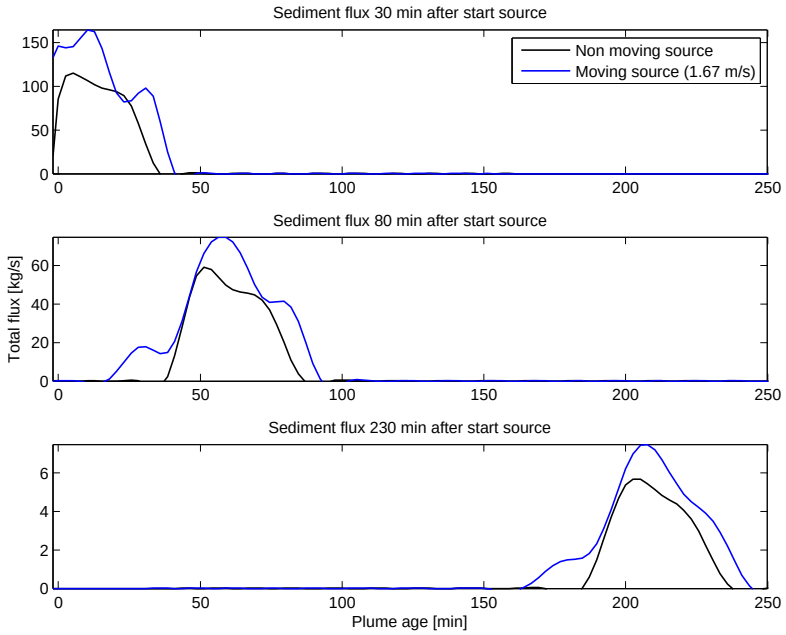

Figure 4.23: Total flux as function of the plume age for a non moving source and an up and downstream moving source (1.67 m/s, higher than twice the flow velocity).

Chapter 5

Comparison with field measurements

5.1 Field measurements

Comparison of the model results with field measurements is executed to test the model's performance and compare model results to real influence of parameters. Data from the EcoShape NW Australia 2011 measurement campaign was used to do so. The dredge plumes measured in this campaign originated from the overflow of a TSHD. The field measurement campaign consisted of measurements on board of the TSHD, to obtain details on the overflow volumes and material. A separate survey vessel was used to measure the plume as transported away from the vessel. A combination of ADCP (Acoustic Doppler Current Profiler) and OBS (Optical BackScatter) measurements were collected by the survey vessel. These can be used to get an overview of the SSC on sailed transects through the plume.

An ADCP is an acoustic system mounted to the survey vessel allowing profile measurements. The ADCP is used to gather flow velocity and concentration profiles. The vertical bin size of the ADCP was 0.5 m, however near the bed and surface a blanking zone exits. The acoustic backscatter measured (in dB) by the ADCP is dependent on the sediment characteristics and site conditions. Calibration to water samples is needed in order to find a relation between the measurements and the actual SSC (in mg/l).

An OBS sensor is often more accurate for measuring turbidity than an ADCP, however, only point measurements are possible. As for the ADCP, the relation between the turbidity measured and the SSC depends on site and sediment characteristics. The field measurements consists of many field trips which include of several ADCP transect measurements through the plume. Along these transects also OBS measurements are available at several water depths.

5.2 Set-up of comparison

Comparing model results to field data requires ambient conditions in the model and field to be comparable. The numerical model simulated a uniform stationary flow case, with no influence of, for instance, wind. These assumptions determine to a large extent which field data is available for comparison. The assumptions require the average flow velocity and direction to be comparable for each transect in a field trip. Also, water depth variation for the considered transects should be minimal. Furthermore, the transects measurements should be more or less perpendicular to the ambient current direction. The field trips were evaluated based on these considerations.

Figure 5.1 shows an overview of the first field trip used for comparison. The colored lines indicate the transects measured during the trip. All transects are measured parallel with respect to each other, which makes comparison to lateral concentration and flux results possible. The thin black line indicates the vessel's dredge track during the measuring time interval. The ambient flow velocity and direction are obtained by taking the average direction and velocity of all measured ambient current data during the trip. For this particular situation this results in a flow velocity of 0.34 m/s and a flow direction nearly perpendicular to the measured transects. The SSC, transect area and ambient flow velocity can be used to calculated a total flux through each transect.

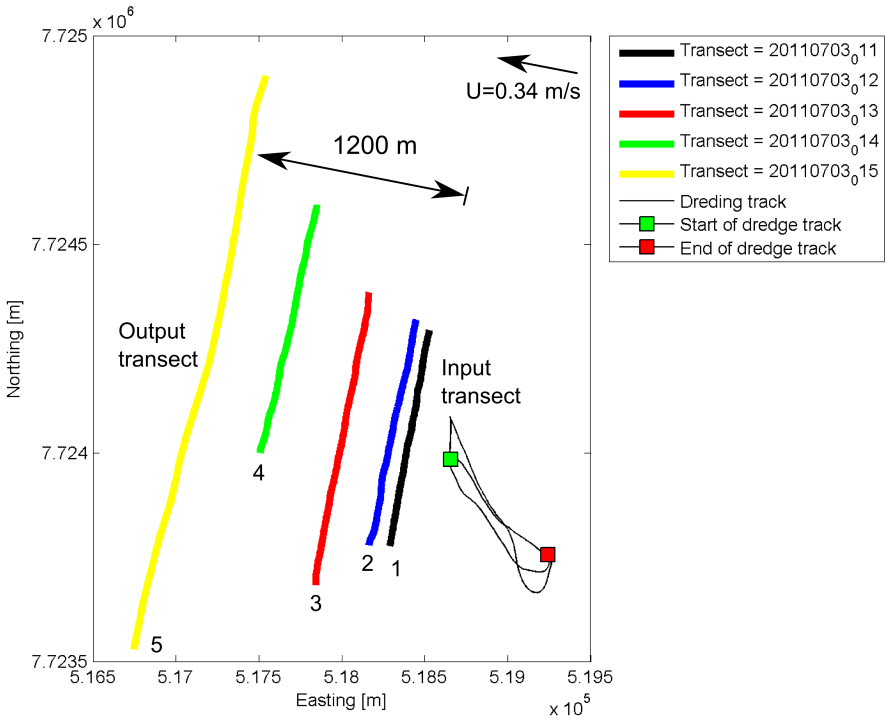

Figure 5.1: Overview of field measurement trip, indicating transects, dredge track and flow velocity.

Comparison of field data to modelled plume dispersion results requires the source term (input) to be derived from the measurements. The first transect (black line) serves as input to the model. It is assumed that all near-field effects have disappeared here. This means that the transect is located just passed, but near, the transition from near- to far-field. Under these assumptions the flux through the transect can be used as input to the far-field model. The other transects, located downstream of the input location, can be used for comparison. In this case the fifth transect (yellow line) is used to calibrate the model results. The distance between the two transects is approximately 1200 m, while the time between origins of the two transects is 54 minutes. Given the flow velocity of 0.34 m/s the plume age at the output transect is approximately 58 min (1200 m * 0.34 m/s / 60 min). The difference between plume age and measuring time interval between the two transects should me minimal. In this way it can be assumed that the plume measured on the output transect originated from the plume measured in the first (input) transect.

The fluxes used as model input and output should only consist of dredge related SSC, not taking

into account any background concentration. In this way the plume can be modelled in ambient water with zero sediment concentration. In reality the ambient water will generally contain some background SSC. This background concentration is determined by plotting the cumulative distribution of all transects. Figure 5.2 shows the cumulative distribution of the sediment concentrations for the considered field trip. The concentration at the bend point of a cumulative distribution curve is considered to be the the background concentration for the transect. This is assumed to be a concentration which is mostly present in the transect, while higher concentrations are related to dredging induced SSC. The overall 'bend point' of the curves (determined by expert judgment) is used to find the background concentration for the whole set of transects. Subtracting this background concentration from the transect concentrations results in the dredging induced SSC per transect.

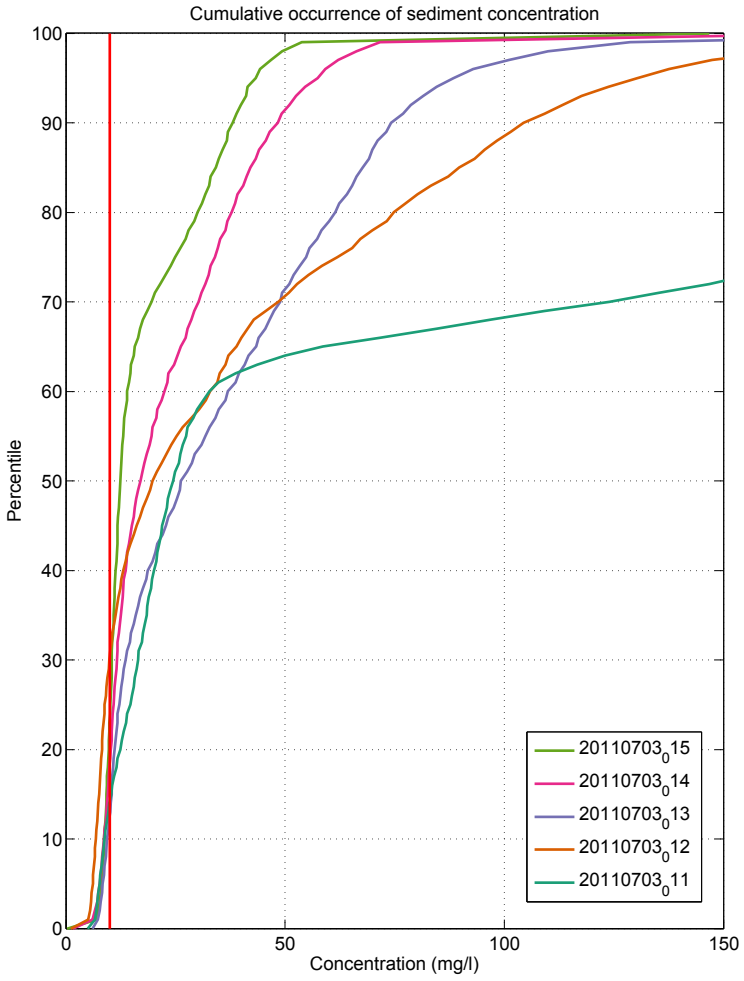

Figure 5.2: Cumulative distribution of sediment concentrations for each transect and the determined background concentration (red line).

Figure 5.3 shows the sediment concentration in both transects as function of the depth and distance from the transect's origin. The colored patches represent the measured ADCP data, while the dots illustrate the OBS measurement results. The measurements generally agree reasonable,

however, in the first transect some differences are noticeable. Reasons for differences can be the explained by the fact that ADCP reacts stronger on coarser particles, while OBS is more sensitive for fine sediment. Also, ADCP is more sensitive for turbulence and air bubbles in the water column De Wit et al. (2014b). As a total flux is calculated, concentration results throughout the whole water column are needed. Therefore, the ADCP measurements are used for further analysis. Any differences between OBS and ADCP measurements are not further discussed as this is not part of this study.

The top figure shows the first transect, from which the input source term will be derived. The fluxes can be calculated by multiplying the concentrations and the ambient velocity. However, the width of the plume is important for implementation on the far-field model. This should be derived by eye from the concentration figure. Clearly two dredge plumes are present in the first transect. This might be a result of the 'two way' dredge track (see Figure 5.1). Therefore, as a first estimation the source term is implemented as two separate plumes with a constant source flux. In the bottom transect the two plumes are still noticeable, but concentrations have dropped and lateral mixing has taken place.

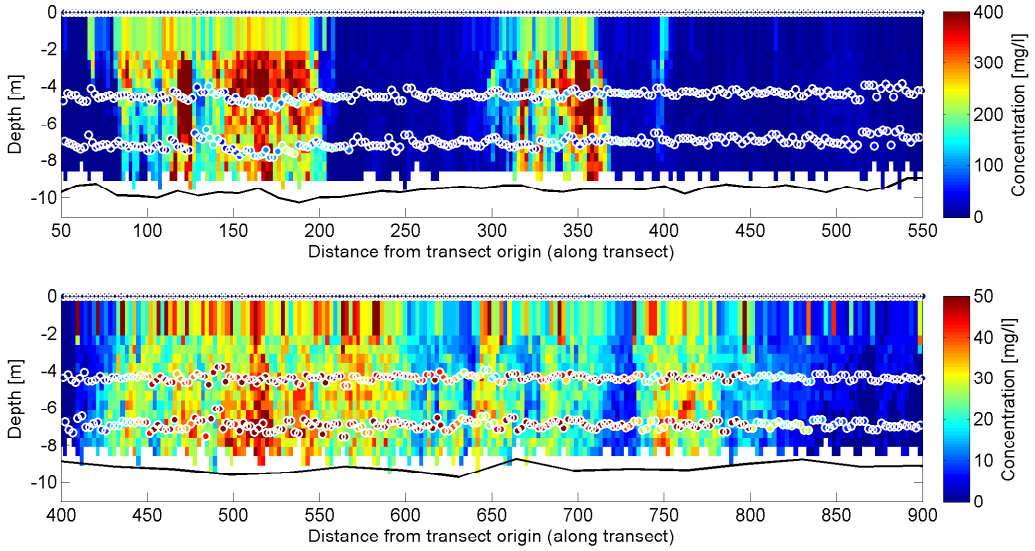

Figure 5.3: Sediment concentration along the transects for both the input (top) and output (bottom) transect.

The numerical model as set up for the experiment is adjusted to serve as a schematisation of the situation present during the field trip. Besides the source term characteristics, the following variables are also determined from the field measurements; the ambient flow velocity, ambient flow direction, water depth and plume age at output location. The bed roughness and slope of the model are calculated based on the steady uniform flow condition. As a first estimation for the eddy diffusivity the same value as in the experiment is used.

Only one sediment type is applied to simulate the plume. No data is available on sediment particles present in the plume, nor on the erosion and deposition parameters. Therefore, the same deposition and erosion parameters as for the experiment are applied; the critical bed shear stress for deposition is set to its maximum value, while erosion is not accounted for in the model. As no information on sediment is known the settling velocity is used to calibrate the model. At first, all

variables, except for the settling velocity, are kept constant. Values are collected in Table 5.1.

	Parameter	Value
Model parameters	Calculation time	1 day
	Time step	60 seconds
	Slope	$2.85\text{x}10^{-6}$
	Water depth	9.6 m
	Bed roughness	65 $m^{1/2}/s$
	Horizontal eddy viscosity	0.021 m^2/s
	Horizontal eddy diffusivity	0.05 m^2/s
	Vertical eddy viscosity	k-ϵ model
	Vertical eddy diffusivity	k-ϵ model
	Upstream boundary	0.34 m/s
	Downstream boundary	9.6 m
Sediment parameters	Sediment type	Cohesive
	Specific density	2600 kg/m^3
	Dry bed density	500 kg/m^3
	Settling velocity	see Section 5.3
	Deposition bed shear stress	1000 N/m^2
	Erosion bed shear stress	4 N/m^2
	Erosion parameter	0.002 kg/sm^2
	Background sediment concentration	10 mg/l
Source term parameters	Source term flux (input)	147 kg/s
	Source term (plume) width	plume 1: 100 m
		plume 2: 50 m
	Sediment flux at 1200 m	38 kg/s

Table 5.1: Model, sediment and source term parameters used for comparison of model results with field measurements.

5.3 Results

To compare the model results with the field data, the sediment fluxes and lateral concentration distributions are evaluated. The two major variables influencing the sediment flux are the settling velocity and the erosion and deposition parameters. The deposition and erosion parameters are taken constant, while the settling velocity is varied to find correct sediment fluxes.

When the sediment fluxes are modelled correctly the sediment concentration is checked. The eddy diffusivity is an important parameter for the lateral concentration distribution. Furthermore, it has been shown that the concentration distribution is dependent on the source term distribution, which is further explored here. At first the total sediment flux along the plume is considered. Also, the model and field data concentration distributions are compared.

Sediment flux

Overflow data suggests that the overflow was used during most of the dredging activity in the time interval of the considered field trip. Therefore, a constant sediment source is applied. Two point sources are added in the model to account for each of the two plumes observed in the input transect.

The most important consideration when interpreting the field data is whether the flux and concentrations measured at the output location indeed originate from the measured plume at the input transect. The time between measurements, distance between transects and flow velocity should match, as was mentioned in Section 5.2. However, even if this is the case, still two different scenarios could be identified, given the fact that a constant source term is considered.

Let's call the start of release of the true source t_0, and look at the development of the plume. After a certain time interval all dynamic plume behaviour will have disappeared and the end of the near-field is reached (t_1). t_1 is also the start time of the far-field plume simulation. Some time later the plume will have arrived at the location of the measured output transect (t_2). The presence of plume concentration and flux at the output transect after a simulation time $\Delta t = t_2 - t_1$ suggests that indeed the front of the plume entered the far-field at t_1 at the input location. This also means that before t_1 the plume was not present in the far-field yet. This further implies that at t_0 the plume is released from the dredging equipment into the near-field.

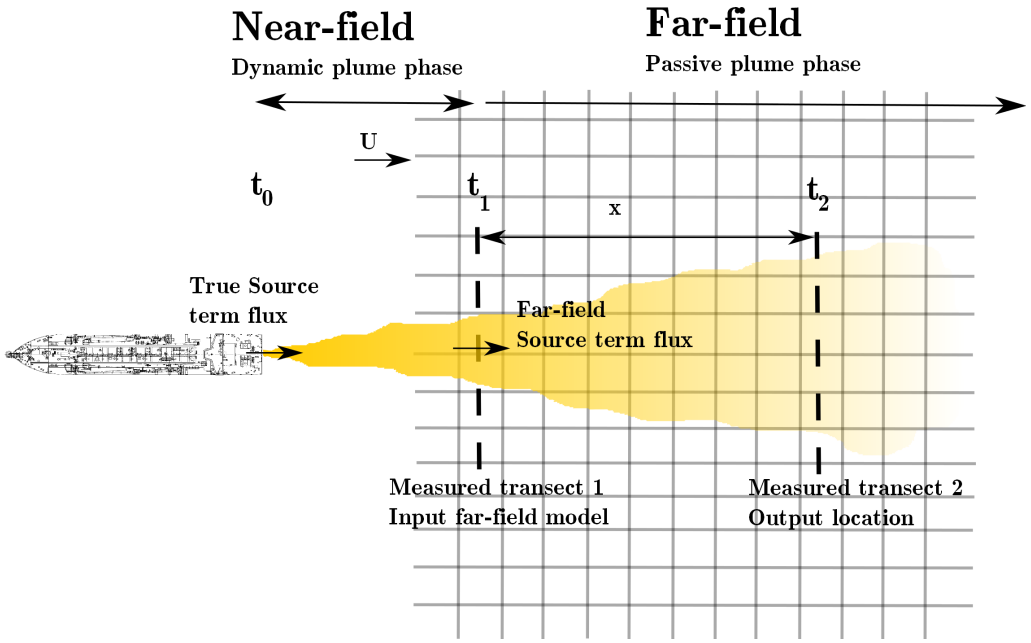

Figure 5.4: Overview of model set up to compare measured transects with model results.

However, in case overflowing started much earlier than the measurement campaign, the plume would have been present in the far-field area before measuring transect 1. This means that the start time of the true source is not t_0, but overflowing started earlier. The front of the plume will have traveled beyond the measuring transects and an equilibrium situation is established before the measurements start. A combination of flow velocity, settling velocity and erosion and deposition parameters determine this equilibrium. This scenario can be simulated by looking at the output transect results at a time $t > t_{equilibrium}$. Where $t_{equlibruim}$ is the time needed to establish the

equilibrium situation. Figure 5.4 shows an overview of the measurements and modelling aspects, indicating transects and corresponding time steps.

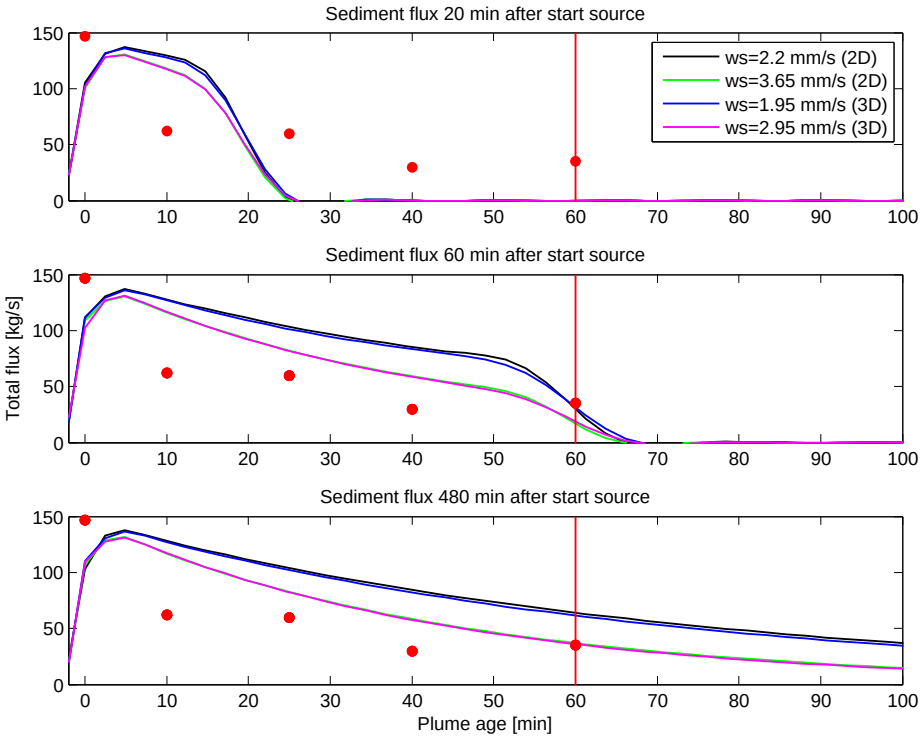

Figure 5.5: Sediment fluxes along the plume for different model simulations at three times after start source (20, 60 and 480 min). The red dots indicate the measured fluxes on the different measuring transects, and the red line illustrates the plume age of the output transect.

Figures 5.5 and 5.6 show longitudinal and lateral results for several 2D and 3D model computations. The output transect was located 1200 m from the source, which corresponds to a plume age of approximately 60 min (red line in Figure 5.5). The red dots indicate the fluxes through the measured transects (starting with the first transect left [1] up to the output transect most right [5]). The measured flux through the output transect is about 38 kg/s. The model is calibrated to this value. The 2D simulations resulted in a settling velocity of 2.2 mm/s and 3.65 mm/s. A settling velocity of 2.2 mm/s gives a flux of approximately 38 kg/s, 60 min after start source (middle panel), corresponding to the first scenario described. Here the front of the plume has just reached the transect location. The plume flux and concentration results 480 min ($t > t_{equilibrium}$) after start source correspond to the second scenario, where the equilibrium has established. Clearly a higher settling velocity is needed to give similar results for a plume age of 60 min (3.65 mm/s for a 2D simulation).

For the 3D simulations the settling velocity needs to be further adjusted to account for the difference in deposition rates between the 2D and 3D simulations. Somewhat lower settling velocities (1.95 mm/s and 2.96 mm/s) result in comparable results as for the 2D simulations. Figure 5.6 demonstrates that the concentration distribution and fluxes for the adjusted 2D and 3D simulations are comparable in both situations.

The model results are based on the assumption of a constant, continuous sediment source.

Therefore, the second scenario, where an equilibrium state has established, seems most valid. The first scenario was based on the assumption that no plume was present before the start of the measurement trip. This can not be verified, but seems implausible.

The determination of the settling velocity presented here is based on conservation of mass. It is assumed that during the field trip no mass has left the considered area. Therefore, the input flux can be related to the output flux through the amount of sediment which has been deposited. It can be concluded that combination of settling velocity and deposition parameters determines the fluxes. The fact that no information is available on sediment properties in the far-field dredge plume during the measurement campaign, justifies the use of the settling velocity as calibration parameter. In this case the last transect information was used to calibrate the model. The performance of the model can be further checked by comparing the other flux measurements (red dots in Figure 5.5. Generally the measurements are lower than the calculated fluxes. This can either be explained by inaccurate measuring and inaccurate interpretation of the measurements or by incorrect representation of the ambient conditions in the model. However, it can be concluded from the results that the equilibrium state (second scenario) shows much better correspondence to the measurements than the first scenario.

The second scenario implied a settling velocity of 2.95 mm/s (3D simulation). This settling velocity corresponds to a sediment particle diameter of approximately 67 μm. Far-field sediment plumes primarily consist of silt and clay particles. This particle is just too big to be classified as silt or clay. However, due to floc formation settling velocities inside the plume could be higher than the settling velocity of the largest particles. Furthermore, seeing the fact that only one sediment particle is used to represent all plume sediment, the found settling velocity are reasonable.

Concentration

The longitudinal plume results illustrated that the flux at the measured output transect can be simulated by the model. However, the concentration distributions did not match. Figure 5.6 shows the lateral concentration distributions (depth averaged) for a plume age of 60 min as simulated by the model. In Figure 5.7 the depth averaged measured concentration is plotted (left figure). The modelled concentration peaks are twice as high as measured. Also, in the model results still two peaks are present, whereas on the measured transect more mixing between the two plumes has taken place. Furthermore, the modelled plume width is smaller than found in the measurements.

The eddy diffusivity used in the first simulations (0.05 m^2/s) followed from the experimental situation. As a uniform stationary flow is assumed, little lateral mixing takes place (see Section 2.1.2). The broader plume and lower concentrations on the measured transect suggest that more lateral mixing has taken place in reality.

Figure 5.7 shows the same measurement results, but now compared to simulated concentration profiles in 2D with a higher eddy diffusivity and adjusted source terms. Fluxes are identical for all simulations, however the width and concentration peaks of the plume do change. The diffusivity was adjusted by calibration of sediment concentration measured in the output transect. The results (middle figure, blue line) show significant improvement by implementation of a higher diffusivity. The two plumes have merged to one plume with two peaks. The total width of the plume is comparable to the measurements, approximately 500 m. However, the peak concentration is still too high. This also results in lower concentrations at the left and right side of the plume.

Figure 5.8 illustrates the sediment concentrations for the measured (top left figure) and modelled transect in 3D (top right figure). These figures also demonstrate that the concentration peaks are

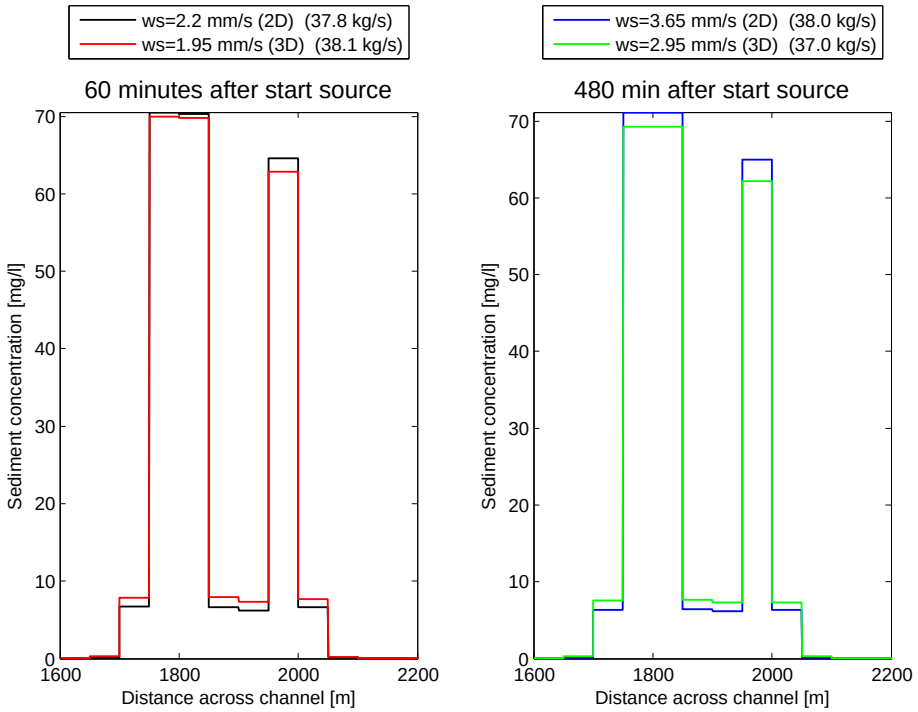

Figure 5.6: Lateral depth averaged concentration profiles and fluxes for different model simulations for a plume age of 60 min observed at two times after start source (60 and 480 min), using a diffusivity of 0.05 m^2/s.

overestimated in the model, while the total width is comparable.

Further adjustments of the model are related to the source term input. Up to now the source was inputted in three grid cells, the first two were used to simulate the biggest plume. A third input cell was used to simulate the smaller plume. This resulted in acceptable flux and concentration output, compared to the measurements. However, even with the adjusted diffusivity, the concentrations were overestimated by the model. Further increasing the diffusivity would lead to too much mixing, and disappearance of the 'two plumes' in the output model results.

Two other configurations of the source term were implemented; a point source and a distributed source based on the lateral concentration distribution in the measured input transect. The point source can be considered a further simplification of the model, while the distributed source is a more detailed approach.

The concentration results are plotted in Figure 5.7. The middle and right figure shows the 2D simulation results for both model inputs. A distributed source with a low diffusivity does not improve results (middle figure, black line). The point source results (right figure, red line) in a similar flux as for the measurements, but the concentration peak is higher and the distribution is, as expected, more peaked. Best results are obtained for a distributed source with increased diffusivity (right figure, green line). The plume width, lateral concentration distribution and peak concentrations are comparable to the measurements. This is further supported by the 3D transect results in Figure 5.8.

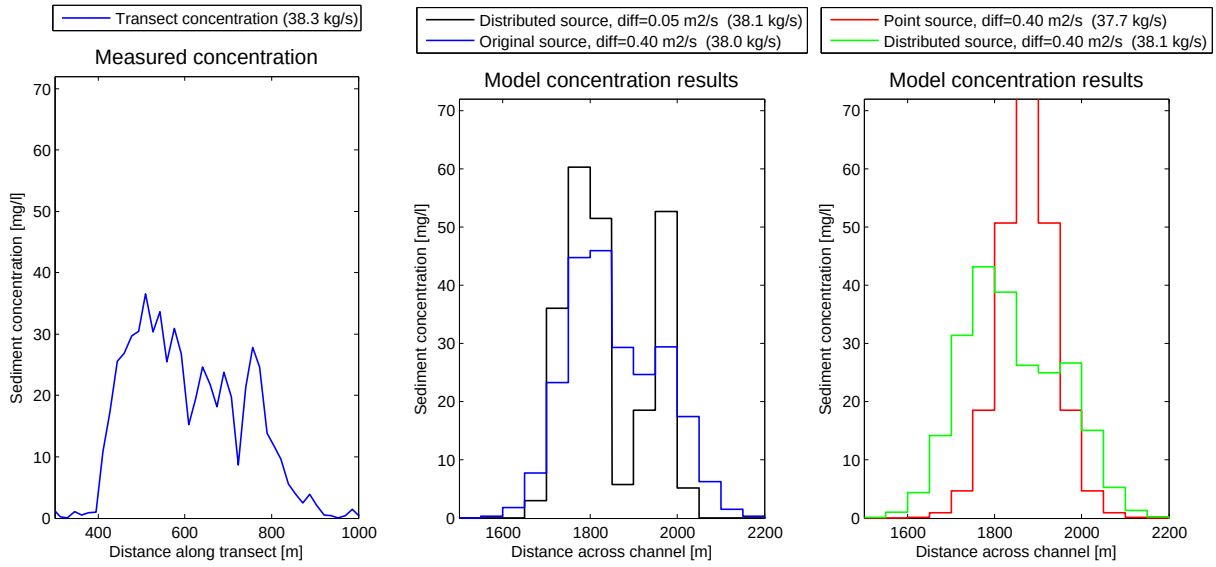

Figure 5.7: Lateral depth averaged concentration profiles and fluxes for a plume age of 60 min, for the field measurement (left panel) and model results with adjusted diffusivity and source term input for 2D simulations with settling velocity = 3.65 mm/s.

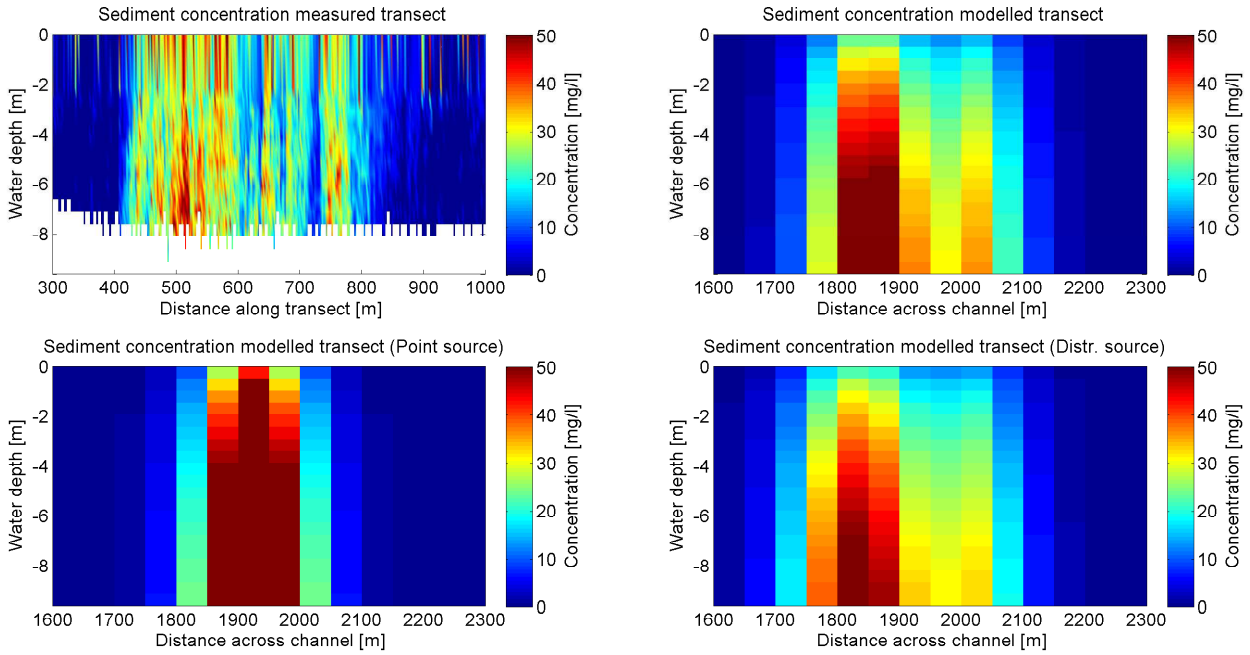

Figure 5.8: Sediment concentration for the measured transect (top left panel), 3D simulation with a diffusivity of 0.40 m^2/s (top right panel), same 3D simulation with point source (bottom left panel) and same 3D simulation with distributed source (bottom right panel).

Comparison with second field trip measurements

The model is adjusted to be able to compare the results to a second measurement field trip. The measurements were taken during the same monitoring campaign, though ambient and plume conditions are slightly different. All model, input and sediment parameters as used in the simulation are either derived from the field data or chosen based on the earlier described assumptions (see Table 5.2). An overview of the transects is given in Figure 5.9, while Figure 5.10 shows an lateral overview of the sediment distribution of the used input [1] and output [6] transects.

	Parameter	**Value**
Model parameters	Calculation time	1 day
	Time step	60 seconds
	Slope	$9.15\text{x}10^{-6}$
	Water depth	9.6 m
	Bed roughness	65 $m^{1/2}/s$
	Horizontal eddy viscosity	0.021 m^2/s
	Horizontal eddy diffusivity	0.05 m^2/s
	Vertical eddy viscosity	k-ϵ model
	Vertical eddy diffusivity	k-ϵ model
	Upstream boundary	0.61 m/s
	Downstream boundary	9.6 m
Sediment parameters	Sediment type	Cohesive
	Specific density	2600 kg/m^3
	Dry bed density	500 kg/m^3
	Settling velocity	See results
	Deposition bed shear stress	1000 N/m^2
	Erosion bed shear stress	4 N/m^2
	Erosion parameter	0.002 kg/sm^2
	Background sediment concentration	15 mg/l
Source term	Source term flux (input)	128 kg/s
	Source term (plume) width	100 m
	Sediment flux at 550 m	61 kg/s

Table 5.2: Model, sediment and source term parameters used for comparison of model results with field measurements of the second field trip.

The flux results for the different simulations are presented in Figure 5.11. The top panel indicates the first scenario, where the plume's front has reached the output transect after 15 min (550 m = plume age of 15 min). For this scenario settling velocities of 1 mm/s (2D) and 0.9 mm/s (3D) were found. The second scenario is shown in the lower two panels, where an equilibrium has established. Significantly higher settling velocities are required for this scenario to occur, 7.8 mm/s (2D) and 6.2 mm/s (3D). Again this second scenario is most reasonable, as it is unlikely that the plume was not present in the far-field before the start of the measuring campaign. Also, the flux measurements along the plume (red dots) correspond closely to the second situation and do not match the results in case of a low settling velocity (blue and black lines).

Subsequently, the diffusivity and source term distribution were adjusted to get more reliable

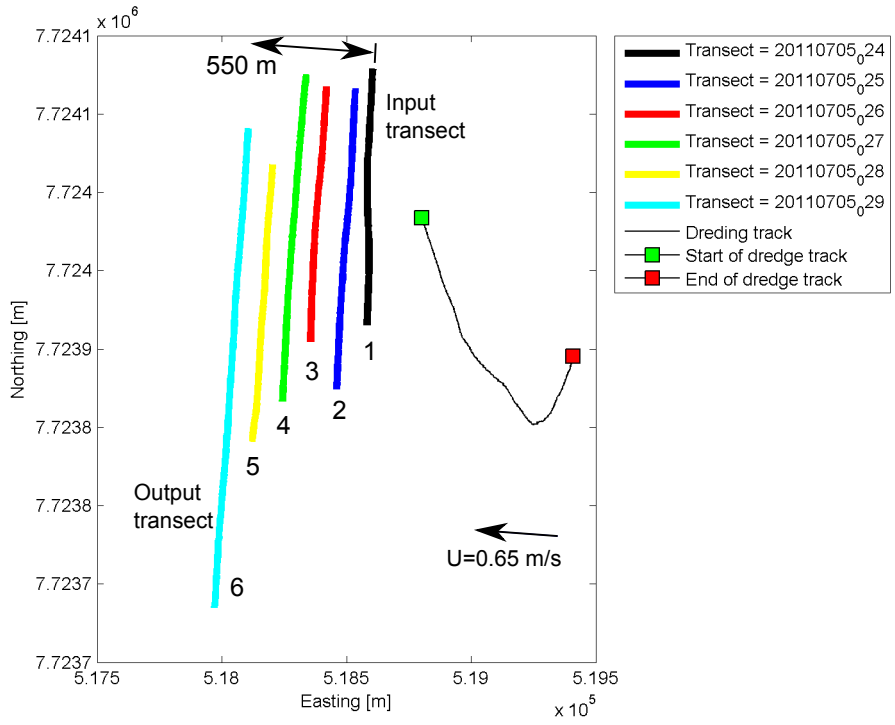

Figure 5.9: Overview of field measurement trip, indicating transects, dredge track and flow velocity for second field trip.

concentration results at the output location. Figure 5.13 shows lateral concentration results for simulations with different diffusivities. Again a higher diffusivity (0.5 m^2/s instead of 0.05 m^2/s) results in a more comparable concentration distribution. Further adjustment of the source term by careful analysis of the input transects improves the results even more (right figure, green line). These 2D results also suggest that in this particular case the plume is also modelled correctly using a point source (right figure, red line). When looking at the depth averaged results this is indeed the case. However, the 3D results show better correspondence for the distributed source with the measured concentrations. A smaller grid size might be needed to capture more detail in the concentration distribution at the output location.

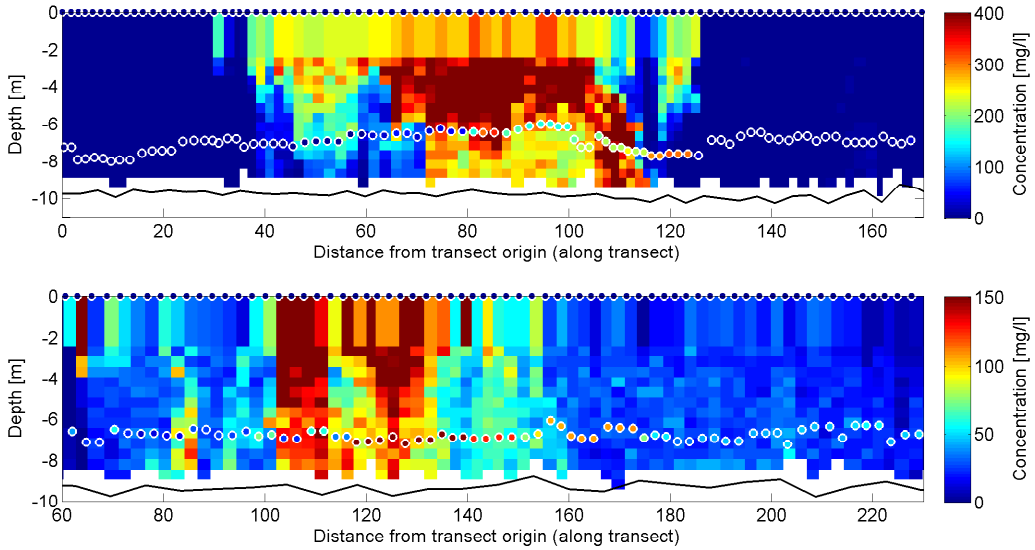

Figure 5.10: Sediment concentration along the transect for both the input (top) and output (bottom) transect for the second field trip.

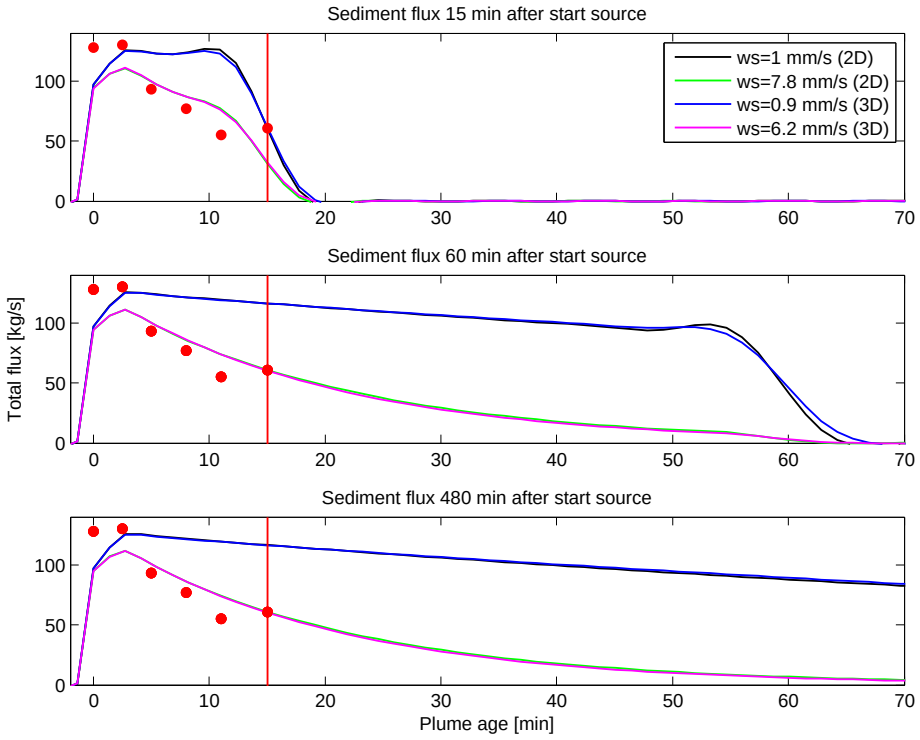

Figure 5.11: Sediment fluxes along the plume for different model simulations at three times after start source (20, 60 and 480 min) for the second field trip comparison. The red dots indicate the measured fluxes on the different measuring transects, and the red line illustrates the plume age of the output transect, for the second field trip comparison.

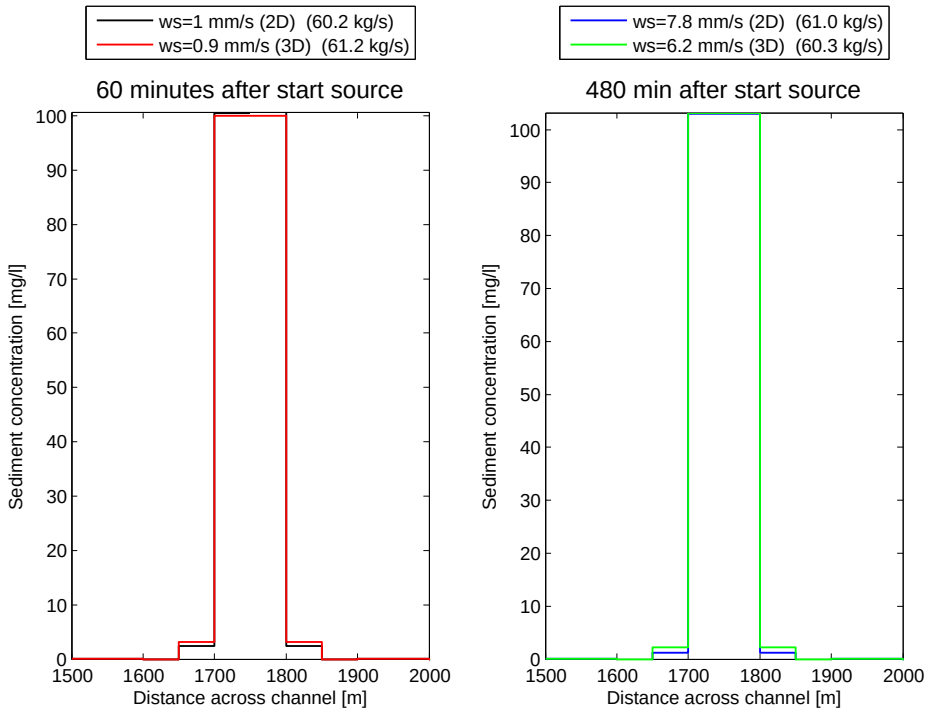

Figure 5.12: Lateral depth averaged concentration profiles and fluxes for different model simulations for a plume age of 60 min observed at two times after start source (60 and 480 min), using a diffusivity of 0.40 m^2/s.

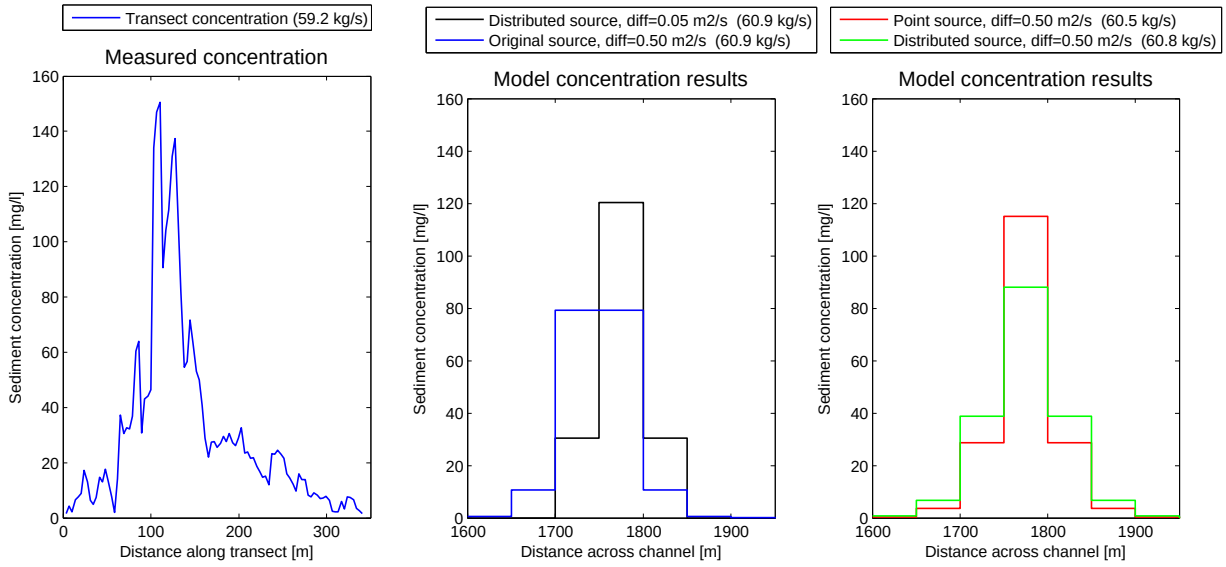

Figure 5.13: Lateral depth averaged concentration profiles and fluxes for a plume age of 60 min for the field measurement (left panel), model results (middle panel) and the model results with an adjusted eddy diffusivity (right panel), for the second field trip comparison.

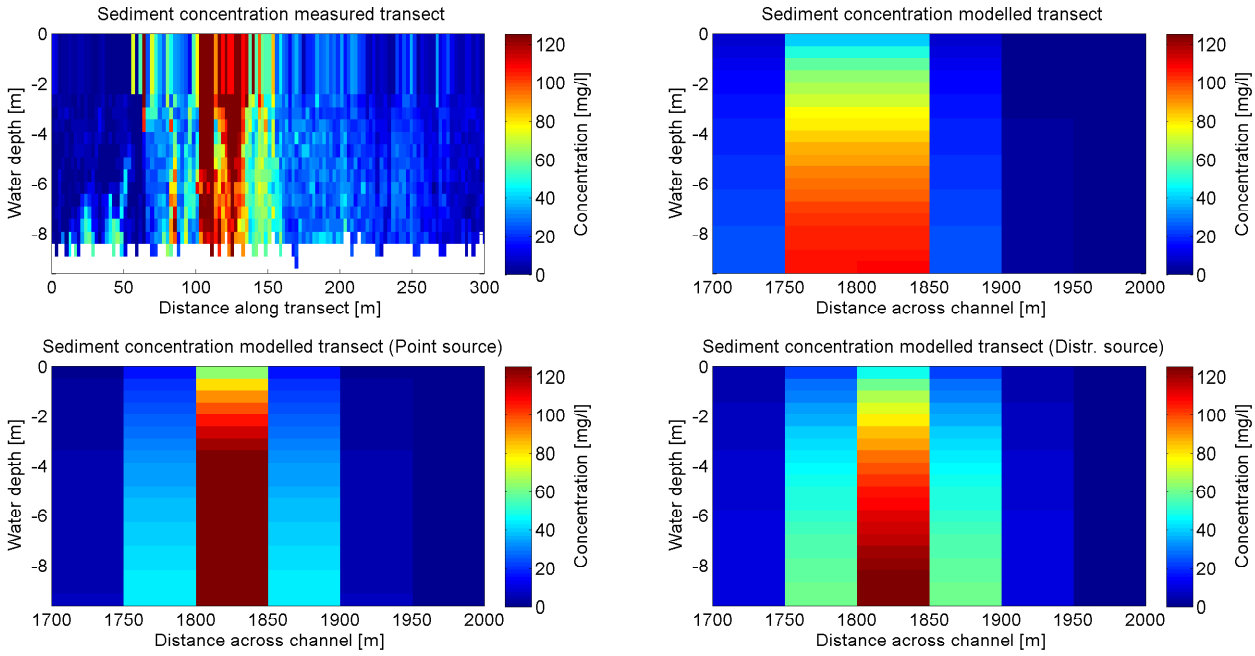

Figure 5.14: Sediment concentration for measured transect (top left panel), 3D simulation with a diffusivity of 0.40 m^2/s (top right panel), same 3D simulation with point source (bottom left panel) and same 3D simulation with a distributed source (bottom right panel).

Chapter 6

Discussion of results

In Chapter 4 the numerical model experiment was set up and the presented results gave insight in the influencing parameters regarding far-field dredge plume modelling. In Chapter 5 the performance of that same numerical model was tested by comparing model results with field measurements. At first, in Section 4.1, the reference scenarios were used to prove the correct performance of the model and find or explain choices on certain parameters. A maximum source discharge was found, aiming at preventing momentum to be added to the flow. Whether momentum is added depends on the input discharge and the computational grid size. No difficulties were encountered in the experimental model and field comparison model. In engineering practice the same is expected, as grids are often rather coarse and far-field source terms small. Subsequently, the influence of model parameters and source input on flux and concentration results in the far-field was investigated in the experiment and further verified in the comparison with field data. In this chapter the obtained results are discussed, aiming to connect outcomes of both chapters.

Influences on far-field fluxes and concentrations are discussed separately. This distinction is made based on lessons learned during the experiment. Whereas some parameters only influence fluxes, other influence both the far-field concentration and flux. When considering the concentration, both the distribution of the concentration in lateral direction and the peak concentration are important. It should be noted that flux and concentration are related to one other. A flux difference also requires a concentration difference (given an equal flow velocity). This suggests that there is no such thing as a distinction between the two output parameters. However, as some parameters do not influence the distribution of the sediment in lateral direction or the peak concentration, still three influence groups can be identified.

At first, the parameters influencing both flux and concentration results are discussed. Subsequently, the influence of parameters on just flux or concentration results are explained separately. Also, the distinction between a young and an old dredge plume is made. In most cases results for a young plume showed differences from results for an old plume, where the plume has been 'released' and more deposition has taken place. The results 80 min after start source give an indication of a young plume (plume age: 26 min), while plume results 230 min after start source were considered old (plume age: 167 min).

Sediment flux and concentration results

The largest influence by model input on the far-field flux was induced by the chosen computational approach. As shown in Section 4.2 the flux for a young plume in a 3D simulation (point source)

was 63.3 kg/s. In the 2D simulation the flux is about 6 % higher, while for a 1D calculation the flux is about 4 % lower. For the old dredge plume only comparison between the 2D and 3D results is possible, as no 1D results were obtained here. The relative flux error for the 2D simulation has grown to more than 40 % of the 3D flux result.

Further investigation in Section 4.3.1 showed that the differences are induced by the difference in deposition rates. Generally the 2D models underestimate deposition and erosion rates. In the experiment only deposition is accounted for. The deposition rate depends on the settling velocity, critical shear stresses (model input), actual bed shear stress (ambient conditions) and the sediment concentration near the bed. For two identical cases in 2D and 3D, the near bed concentration in 2D is underestimated, causing underestimation of deposition rates. Section 4.3.1 illustrated that the settling velocity can be adjusted in a 2D model to match 3D flux results.

Next to the flux error, considerable concentration differences were found in the experimental results. The calculated peak concentrations in 2D were about 1.5 times higher than calculated in 1D. This is induced by the lower fluxes and larger lateral spreading of the plume in 1D. Differences between 2D and 3D concentration results were only related to the peak concentration, and not to the lateral distribution of sediment. The peak concentrations were about the same percentage higher as the fluxes (young plume: 6 % and old plume: 40-45 %). The absolute relevance of this error depends on the actual concentration present.

The difference in fluxes between 2D and 3D simulations were also observed in the data comparison results in Section 5.3. Both chapters showed that if information on the settling velocity and deposition and erosion rates are available, one should be careful in applying those in 2D models. An important notion is the high dependency of the influence of the computational approach on the critical stresses for deposition and erosion. In the experiment only deposition was accounted for, through a maximum critical shear stress for deposition. In case the nett deposition/erosion is zero, there will be no difference between 2D and 3D results. However, through other critical stresses, near bed concentration differences between 2D and 3D can also be bigger than in the experiment. This will then increase the error made in 2D simulations.

Both the experiment and the data comparison demonstrated that the settling velocity should be adjusted in 2D to obtain equal deposition rates, hence equal far-field results. In case no plume sediment properties are known, the settling velocity can be used as calibration parameter. In the field data comparison both 2D and 3D models were adjusted to the measured data, resulting in reasonable settling velocities for far-field dredge plumes. The adjusted settling velocities were calculated by matching the deposition rates and the bed boundary condition. A higher settling velocity also implies a higher near bed concentration (faster settling). In general this resulted in the 2D settling velocity to be approximately 10 % higher than in 3D, which was also calculated in Section 4.3.1. However, as was mentioned before, this only holds for the chosen set of critical stresses for deposition and erosion.

The experiment further showed the influence of the size of the computational grid on both concentration and flux results. Section 4.2 demonstrated that the concentration results are mainly affected by the fact that the grid size determines the number of cells in which the plume can be simulated. The experiment showed that on a coarse grid the plume was not modelled correctly, as the grid size induced a different plume shape (sediment concentration profile). A coarse grid in this case is referred to as a computational grid with a grid size comparable to the plume's width. The lateral concentration distribution leads to this same conclusion; a finer grid leads to more detailed lateral concentration results. However, whether this detail is demanded depends on a number of

other factors; the plume width, lateral/vertical distribution and the eddy diffusivity.

The different grid sizes used in the model experiment did also induce very small differences in peak concentrations, and can be considered insignificant. However, when translated to a flux through a cross section, reasonable difference were observed. For the old dredge plume (after 230 min) the fluxes calculated on a grid of 500x500 m or 250x250 m were about 13 % higher than for the finer grids used, regardless the source term. This can be explained by the fact that a computation on a coarse grid may cause less accurate results. The effect of non physical oscillations, for instance, are enhanced by a coarse computational grid, leading to small concentration deviations. These small deviations induce significant differences when translated to fluxes. Again the terms coarse and fine are related to the plume width. It should be noted that application of the van Leer-2 scheme would prevent the non physical oscillations to arise, hence this issue would not occur. However, since the van Leer-2 scheme is highly diffusive, it was not used in this research (see Section 4.1.1).

A third parameter, related to the source term, is important for simulation of both far-field fluxes and concentrations. Section 4.3.3 demonstrated that the presence of a moving source may induce large differences to the location and magnitude of maximum flux and concentration results, compared to a stationary situation. Depending on the dredging speed/ambient flow velocity ratio and direction of dredging, the implementation of a moving source resulted in a plume at maximum twice wider than the plume resulting from a stationary source. Also, the maximum flux peak was three times higher than the stationary equivalent. For low dredging speeds, compared to flow velocity, application of a moving source does influence far-field results. However, when the dredging speed is twice higher than the flow velocity, and tracks in downstream direction or in both directions (two way) are dredged, a stationary source term shows sufficient results compared to a moving source.

From the results can be concluded that the important factors in decision making on application of a moving source are: the vessel velocity/ambient velocity ratio, direction of dredging and location of the stationary source with respect to the dredge track.

Sediment flux results

The vertical distribution of the source primarily influences the flux, not the concentration distribution. Small impact on far-field peak concentrations is noticeable, but influence is smaller than for the other parameters. Again this is related to the plume width and grid size, as relative influence is larger in absolute sense for higher concentrations. The point source resulted in higher peak concentrations and thus larger differences between the different vertical distributions than simulation with a line source.

Besides the vertically uniform distributed source term, two other vertical distributions were tested in the experiment. Both sources consisted of a higher sediment concentration in the lower half of the water column, leading to a faster settling of the plume. Results of Section 4.2 showed that the distance (and thus time) it takes for sediment to be mixed over the vertical is related to the water depth (500-100 * water depth) and in this case is about 600 m from the input location. Up to that point near bed concentrations are different, and hereby the deposition rates. This causes fluxes for the distributed source to be 5 - 10 % lower than their uniformly distributed equivalents.

As the plume age increases the relative influence of the vertical distribution decreases. Compared to the other parameters the influence of the vertical distribution on flux results in the experiment

is rather small. The influence of the grid size, for instance, is bigger for the old dredge plume.

The second experimental stage (Section 4.3.2) showed the dependency of the plume's settling on the settling velocity, water depth and flow velocity. A higher settling velocity than used in the experiment would enhance the influence of the vertical distribution of the plume, because more sedimenation takes place. The same could be concluded for dredge plume dispersion in deeper water. A larger water depth results in slower vertical mixing of the sediment. This causes the near bed concentrations and thus deposition rates to be different from the uniform distributed case for longer time and spatial scales. Both cases would result in increased differences in far-field fluxes and concentrations.

Sediment concentration results

Both the experiment (Section 4.2) as the comparison with field data (Section 5.3) showed the importance of the lateral distribution of the source term for simulation of far-field concentrations. Calculated fluxes were similar for all tested source terms. Higher concentrations are balanced by narrower plumes, adding up to more or less similar deposition rates. However, the source term did show large influence on peak concentrations and the lateral concentration distribution in the far-field.

The peak concentrations simulated for a source term of 50 m is about ten times higher than for a source term width of 500 m (for a young dredge plume). Thus, implementing a plume of 500 m wide on a grid of 50x50 m, using a point source, leads to an overestimation of the peak concentration by a factor ten. For the experimental situation the error for a young dredge plume can be estimated by dividing the plume source term input width by the actual plume width at the source location.

The influence of lateral distribution is closely related to the actual plume width and computational grid dimensions. A line source on a fine grid (finer than the plume width) may give similar concentrations results as a point source on a coarse grid, as long as the total plume width is the same. However, any lateral variation in the source term can only be applied on a fine grid. The comparison with field data supported the findings of the experiment. Effort put in correct representation of the lateral distribution of the source term improved concentration results in the far-field. The actual difference is dependent on the lateral distribution of the source.

The conclusions based on the simulations with different lateral source term distributions are closely related to the eddy diffusivities. The eddy diffusivities account for exchange of sediment in horizontal or vertical direction, and hereby influence the distribution of sediment. Several eddy diffusivities were tested in the experiment. The vertical eddy diffusivity (and viscosity), accounting for vertical exchange of momentum and matter, are modelled using the k-ϵ model. The physical relevance of the model is doubtful, since dissipation (ϵ) is not a conservative quantity, but it is widely used in engineering practice. Also, the logarithmic velocity profile was correctly modelled. Therefore, the k-ϵ model was used in further simulations.

Selection of a horizontal eddy diffusivity should be done with care. Only one horizontal eddy diffusivity can be applied in Delft3D-FLOW. Throughout the experiment the lowest value was used. As a stationary uniform flow was modelled, no velocity profile was present in lateral direction. This implies only little lateral mixing will take place, represented by a low diffusivity. The reference test showed the sensitivity of the lateral concentration distribution to the applied eddy diffusivity. The eddy diffusivity based on the longitudinal mixing and the Delft-3DFLOW default value resulted in

peak concentrations respectively half and one fifth of the peak concentrations for the lowest lateral eddy diffusivity applied. The relative influence of the diffusivity increases for increasing plume age.

A difficulty regarding the eddy diffusivity is the fact that in engineering practice the value is often estimated. Mixing coefficients are hard to determine as, for instance, upstream velocity profiles can have large effects on mixing downstream. These upstream velocity information is often not known. The comparison with field data demonstrated that the eddy diffusivity as used in the experiment was too low. This resulted in overestimated peak concentrations and narrower plumes. A higher eddy diffusivity gave a better match with the measured data. Clearly the uniform stationary flow assumptions did not hold for the field measurements, implying other mixing effects. This is not unlikely, as a perfectly stationary uniform flow case is seldom found in reality. By adjusting the eddy diffusivity, reasonable concentration results were obtained. Still, the adjusted eddy diffusivities in the data comparison model were considerably lower than the default value used in Delft3D-FLOW (0.4-0.5 $m^{1/2}/s$ instead of 10 $m^{1/2}/s$).

The issue that arises is the fact that while the eddy diffusivity is often hard to derive, it does have significant influence on model results. In a situation where no eddy diffusivity is known, a wrong estimation of this value might result in over- or underestimations of peak concentrations. Furthermore, the eddy diffusivity has shown to have large effects on the influence of other parameters on the concentration results. The influence of lateral distribution of the source term decreases for higher diffusivities, as more lateral mixing takes place and initial plume difference diminish quickly. Simulations showed that for a diffusivity of 1.86 $m^{1/2}/s$ the effects on concentration results further away from the source had decreased significantly. Close to the source the effects of lateral source term distribution were still noticeable.

Considering the large effect of the diffusivity on the lateral distribution of the concentration, it can be considered an important parameter in dredge plume modelling. Though, the effect of diffusivity itself is again dependent on ambient conditions. In case of a high ambient velocity the influence of the diffusivity will decrease. For a high ambient velocity fast advection of the plume will take place, whereas the lateral mixing will be small compared to the longitudinal spreading of the plume.

The comparison with field data showed that the simple numerical model was able to reproduce the fluxes and concentrations derived from the measured transect data. Since no information was available on the settling velocity and diffusivity, these parameters could be used for calibration. Both chapters together give insight in the performance of the far-field plume dispersion model. In forecast modelling of dredge plume fluxes, the knowledge on the settling velocity is crucial. When also far-field concentration distributions are modelled, the application of a correct diffusivity is also important.

Ultimately, the data comparison resulted in reasonable settling velocities, however rather high compared to settling velocities of solely fine sediment. This suggests that a process as floc formation did play a role in the measured far-field plumes. Furthermore, the settling velocities for the two field trips were different (2.95 mm/s compared to 6.2 mm/s). This can be explained by dynamic processes still playing a role in the second field trip. The higher settling velocity then accounts for the dynamic processes which are not accounted for in the model.

Chapter 7

Conclusions and recommendations

7.1 Conclusions

Through literature study, numerical modelling and data comparison, insight in far-field dredge plume dispersion was obtained. In the conclusions and recommendations the research results are evaluated, aiming to support informed selection of modelling techniques and model input. The findings of the research are outlined below, sorted by each of the research questions. The first research question was used to identify a set of model, input and ambient parameters involved in modelling far-field dredge plume dispersion. The second research questions focused on a modelling framework and the actual influence of parameters on model output.

I What are the dominant dredge plume dispersion processes in the near-field, far-field and transition zone and what are the corresponding model schematisations?
Near-field dispersion of dredge plumes is highly dynamic and governed by processes related to the ambient conditions, vessel/plume interaction and the plume's outflow characteristics. Far-field dredge plumes are classified as passive plumes and dispersion happens through a combination of advection, diffusion and sediment deposition and erosion. The differences in spreading mechanisms cause variation in time and spatial scales and demand separate (modelling) approaches for the two areas. The actual transition from near- to far-field is defined by the location where the ambient flow completely governs the spreading of the plume and initial plume characteristics are not important anymore.

Simulation of near-field plume mixing is challenging, since plume behaviour is dynamic and site specific. Nevertheless, near-field model schematisations (process based or semi-empirical) and measuring campaigns are used to calculate near-field plume dispersion. Far-field dredge plume simulations are performed by solving the advection-diffusion equation, together with a correct flow field. In dredge plume modelling, a source term is required to couple the near- and far-field. The use of a virtual source at the location of the dredging activity as source term for far-field modelling was discussed in Section 1.2.3. This research shows that the approach is not appropriate. Near-field processes are not accounted for in a virtual source. The effects of near-field processes on the source term are considerable. Therefore, the use of the proposed far-field source term (at the transition from near- to far-field) is a better approach. Output of near-field modelling or measuring campaigns result in properties of the dredge plume at the transition zone. This output is then implemented on a far-field model. The theoretical framework resulted in the following far-field source term input parameters; the source term magnitude, source term input location, source term sediment

properties, lateral distribution and vertical distribution of the source term.

Ambient parameters as stratification, wind, water depth and flow velocity determine the far-field flow field. Furthermore, schematisation of the flow and model area result in a number of far-field model parameters; computational approach (1D/2D/3D), computational grid size, time step, turbulent viscosity and diffusivity and erosion and deposition parameters.

II What is the influence of model, input and ambient parameters on modelling far-field dredge plume dispersion?

The research presented a modelling framework (Figure 7.1), which gives insight in the sphere of influence of the parameters involved in far-field dredge plume modelling. The computational requirements are determined by the dredge source term, model parameters and ambient conditions (through the model parameters). In the computational requirements stage, choices can be made regarding schematisation of source term, model area and flow field. The influence of the parameters was investigated in this research through a numerical model experiment. Furthermore, comparison with field data gave further insight in the applicability of the results.

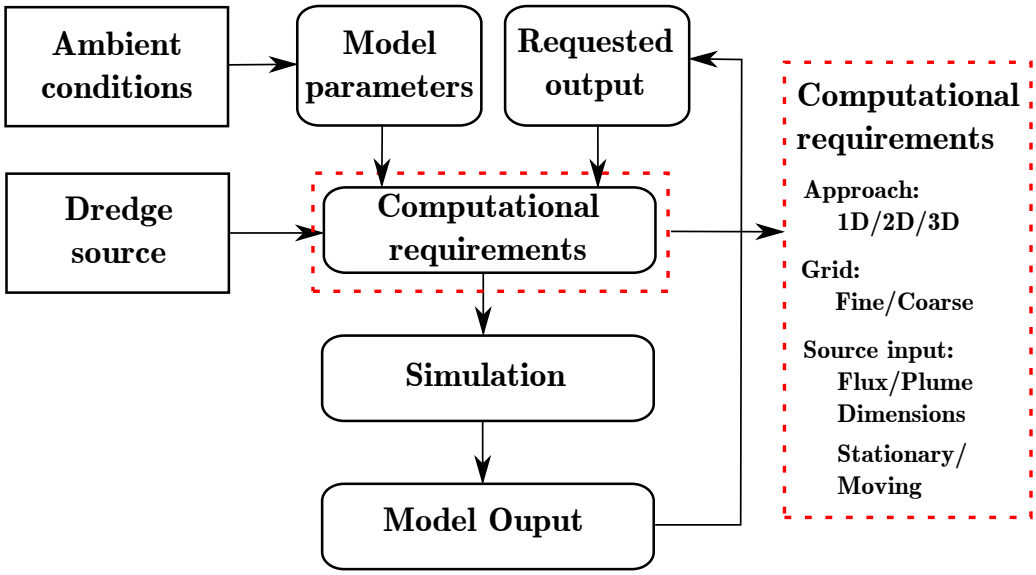

Figure 7.1: Modelling framework for modelling far-field dredge plume dispersion

All model simulations performed in this research confirmed the assumption that requested output is crucial in determination of influence of other parameters. Both the plume age as well as the output parameter showed variability in results. Regarding the output parameter a distinction was made between flux and concentration. For the plume age a distinction was made between a young and an old dredge plume. For a young dredge plume the source term is still continuous. Also, as the plume age depends on both the traveled distance and the flow velocity, a young plume is located relatively close to the source. For an old plume the source term has stopped and the plume is thus 'released' from the source. The dredge plume has been advected further into the far-field. The findings of this research are formulated in nine conclusions;

1. The computational approach has large effects on both on far-field fluxes as well as concentrations. These differences are caused by varying deposition rates in 1D, 2D or 3D, for identical flow and sediment properties. For an old dredge plumes, simulated fluxes in the experiment in 2D were about 40 % higher than simulated in 3D, indicating lower deposition rates in 2D. The deposition rate is determined through the bed boundary conditions by the near bed concentration, settling velocity, the actual bed shear stress and critical shear stress for deposition. In 2D only one vertical grid cell is present, resulting in a concentration which is lower than the near bed concentration for an identical case in 3D, where the sediment profile has adapted to the flow. The effects can be compensated by adjustment of the settling velocity in 2D. For the set of erosion and deposition parameters considered in this research a increase in the order of 10 % resulted in equal far-field fluxes and concentrations.

2. The computational grid size primarily influences far-field fluxes. Four different grid sizes were tested, varying from coarse (comparable to the plume's width) to fine ($1/10^{\text{th}}$ of plume's width). On a coarse grid no lateral plume variation can be applied and the grid is not able to capture the correct sediment plume shape. Furthermore, flux errors for coarse grids increase up to 13 % for old dredge plumes, caused the by applied numerical scheme.

3. The lateral distribution of the source has a large effect on far-field concentrations. Whereas, far-field fluxes are not influenced. This was illustrated by both the experiment as well as the comparison with field data. Any lateral distribution at the source input location will remain intact for both the young as well as the old dredge plume.

4. Vertical distribution of the source term only effects far-field fluxes. Investigation on three different vertically distributed source terms reveals that influence on the young dredge plume is considerable (in the oder of 10 %). For the old dredge plumes the influences become small compared to other contributors on flux variations (computational approach and grid size).

5. Lateral mixing of the plume, expressed by the diffusivity, is hard to verify and detailed knowledge on (upstream) flow conditions is often lacking. The diffusivity primarily influences concentration results. In the experiment a low diffusivity was applied, as a uniform stationary flow was considered (0.05 m^2/s). The comparison to field data revealed higher values were present during the measuring campaigns (0.5 m^2/s). For higher diffusivities the influence of other parameters will be suppressed. The diffusivity alone is then accountable for the lateral distribution of the sediment concentration, especially for old dredge plumes.

6. Ambient conditions (flow velocity and water depth) or settling velocity of the plume's sediment will enhance or suppress influence of other model and input parameters. In deep water or for high settling velocities, the influence of the vertical distribution of the source term is enhanced. A high flow velocity will cause fast advection of the plume, reducing the influence of the diffusivity.

7. Whether application of a moving source term is required, in comparison to a stationary far-field source, depends on the vessel velocity/ambient velocity ratio and direction of dredging. For moving source terms with high dredging speeds (compared to flow velocity) schematisation as a stationary source is sufficient.

8. Far-field concentrations and fluxes are reproducible by the simplified flow case considered in this research. For reproduction of measured fluxes the settling velocity is the determining

parameter. When far-field concentrations are modelled the diffusivity has large effect on correct reproduction. The comparison with field measurements demonstrated the applicability of the model for young dredge plumes, while for older dredge plumes no measurements were available.

9. Two different scenarios should be considered when reproducing measured field data through numerical simulation. A first scenario assumes the plume not to be present in the far-field before the start of the measurements, whereas the second scenario assumes the plume to be present long before the measuring campaign starts. The two scenarios require different settling velocities accounting the plume's sediment. The comparison with field data demonstrated the second scenario to be most reasonable and resulted in plausible settling velocities. Though, the found settling velocities where high compared to typical settling velocities of fine sediments, indicating that processes as flocculation are present in far-field dredge plumes.

Above research conclusions are used to meet the objective of this research; support informed selection of modelling techniques and model input. Recommendations on far-field modelling of dredge plumes can be applied in future forecast modelling studies. This is further elaborated on the recommendations section.

7.2 Recommendations

7.2.1 Recommendation for engineering practice

As per conclusions 1, 2 and 3, a fine gridded 3D model with detailed source term information will result in the most accurate far-field results for both fluxes and concentrations. However, depending on the requested output, other model configurations can be sufficient as well. Based on the research conclusions, recommendations are given for selection of modelling techniques and input. As such, recommendations are based on the uniform stationary flow case as applied in the experimental situation. All recommendations are visualized in Figures 7.2 until 7.5. For these visualizations the modelling framework (Figure 3.3) was used as reference. The recommendations are sorted by the requested output:

Young dredge plume - flux output

In case the requested output location is located close to the source and the source term is still continuous, the plume is considered a young dredge plume. If the fluxes for a young dredge plume are of interest, the solution to the 1D advection-diffusion equation is a recommended alternative for a 3D simulation. Firstly, because application of the analytical solution to the 1D equations is a very simple procedure. Subsequently, the source term can be schematised as a flux and no detailed knowledge on plume dimensions is required. Furthermore, the errors on far-field fluxes are small. However, implementation of the correct flux magnitude is important for the total accuracy of the simulation. As such, it is recommended to put focus on calculation of correct source term flux magnitudes, through near-field modelling or measuring campaigns.

Old dredge plume - flux output

In case the output location is located further into the far-field and the source term has stopped, the plume is considered an old dredge plume. As the source term is not continuous anymore, an

1D approach is not sufficient. If the fluxes for an old dredge plume are of interest, a 2D modelling approach is recommended to serve as alternative for a 3D simulation. However, the observed differences in deposition rates between a 2D and a 3D model require adjustment of the plume sediment's settling velocity. It is further recommended to focus on the magnitude of the source term flux, instead of focusing on plume dimensions or source term distributions. At last, a fine grid is recommended, as the experiment illustrated increasing flux errors for old dredge plumes on coarse computational grids.

Young dredge plume - concentration output

In case the concentrations for a young dredge plume are of interest, a 2D modelling approach is recommended as alternative for a 3D simulation. Any lateral concentration variation present at the source term will affect far-field results. Therefore, focus on correct schematisation of the source term dimensions is important for the total accuracy of the simulation. Subsequently, a fine grid is necessary, as the grid size should be sufficient to capture any source term variation in enough detail.

Old dredge plume - concentration output

In case concentrations for an old dredge plumes are of interest, a 2D modelling approach is again recommended as alternative for a 3D simulation. Since initial variation has large effects on older dredge plume concentrations, correct schematisation of the source term dimensions is advised. Therefore, again a fine grid is essential for accuracy of far-field results. The effect of the vertical distribution of the source term on old dredge plumes is limited. These conclusions result in a fine gridded 2D model being preferred over a coarse gridded 3D model, both being comparably computational efficient.

Varying ambient conditions might change decisions on recommended modelling techniques. In case of strong lateral mixing, the influence of the lateral distribution is suppressed. This means that flux source terms are sufficient for simulating far-field concentrations. Effort in calculation of correct fluxes is than more convenient than effort in application of lateral distributed sources on the far-field model. Also, deep water or high settling velocities will enhance the influence of the vertical distribution of the source term. This will influence far-field flux results, and application of a 3D model is then required.

Other recommendations related to the engineering practice are:

- Application of a moving is highly dependent on the vessel velocity/ambient velocity ratio, direction of dredging and location of the stationary source with respect to the dredge track. The stationary source should always be located in the middle of the dredge track. When dredging upstream tracks only, the movement of the source term is relevant for the far-field results, regardless the dredging speed. This means that application of a moving source is recommendable. In case of dredging downstream tracks only, a stationary source can be sufficient. When the dredging speed is twice the flow velocity or more, the moving source can be considered stationary. If dredging in both up and downstream direction the application of a stationary source is only applicable for high dredging speeds (more than twice the flow velocity).

7.2.2 Recommendation for further research

- It is recommended to extend the model experiment to other flow cases, in order to test influence of processes as tide, wind or stratification. The effects of these ambient conditions in combination with found effects of the source term input will increase insight in the required source term knowledge.

- It is recommended to compare model results to field data measured further away in the far-field. In the research only output for young dredge plumes was considered. This should be extended to data gathered further away from the source input, in order to make comparison for old dredge plumes possible.

- It is recommended for measurement campaigns around dredging activities to lay special focus on certain specific elements, in order to improve data comparison with far-field model results:
  1. Measuring of the plume's sediment properties could improve far-field modelling. From data samples taken within the far-field plume, one or several settling velocities could be derived. These could be used as input for far-field models.
  2. To assess the location of transition from near- to far-field and the age of the plume accurate, more measurements are required. Next to transect measurements, sediment concentrations should also be measured along the trajectory of the plume. These kind of measurement do require careful measuring, as one should capture the whole plume.
  3. At last, the time interval between measuring transects could be linked to the ambient velocity. In this way the plumes measured in the far-field can be accounted to a plume measured in the input transect (at the transition from near- to far-field). This will improve comparison to model results, as a output result can directly be linked to the input transect.

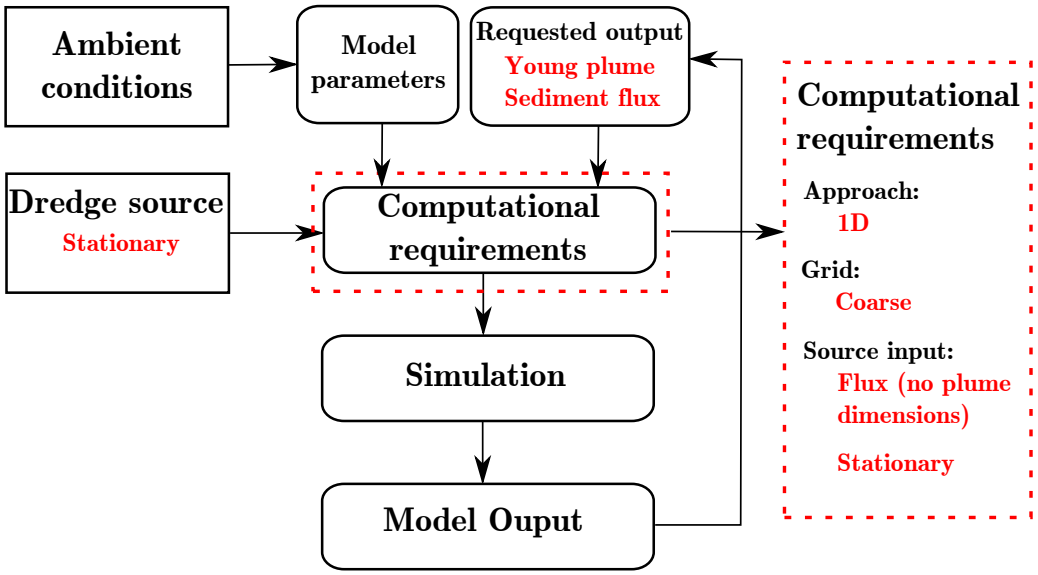

Figure 7.2: Flow diagram indicating recommendations for far-field dredge plume modelling for output situation: flux - young plume.

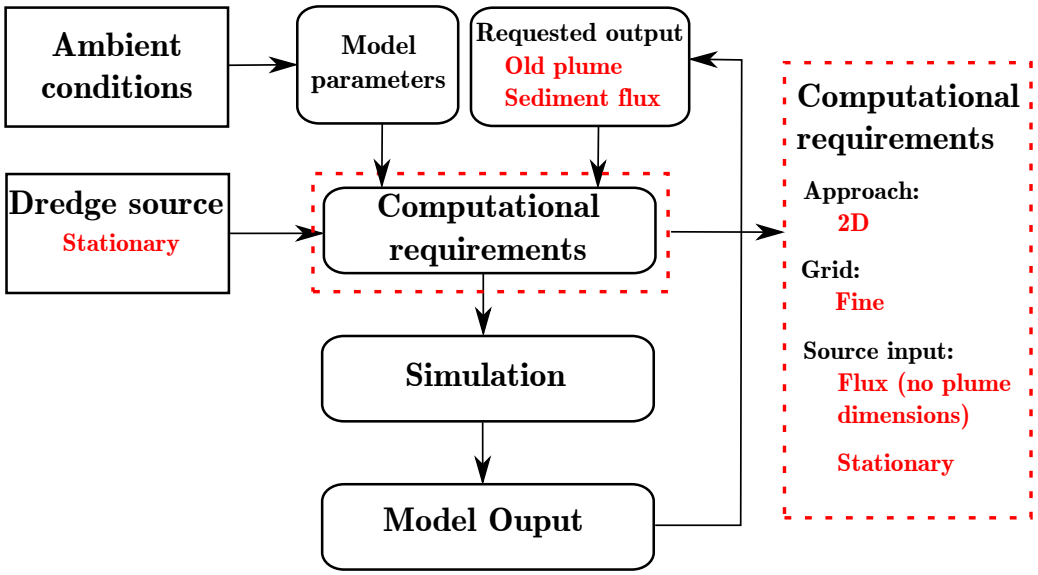

Figure 7.3: Flow diagram indicating recommendations for far-field dredge plume modelling for output situation: flux - old plume.

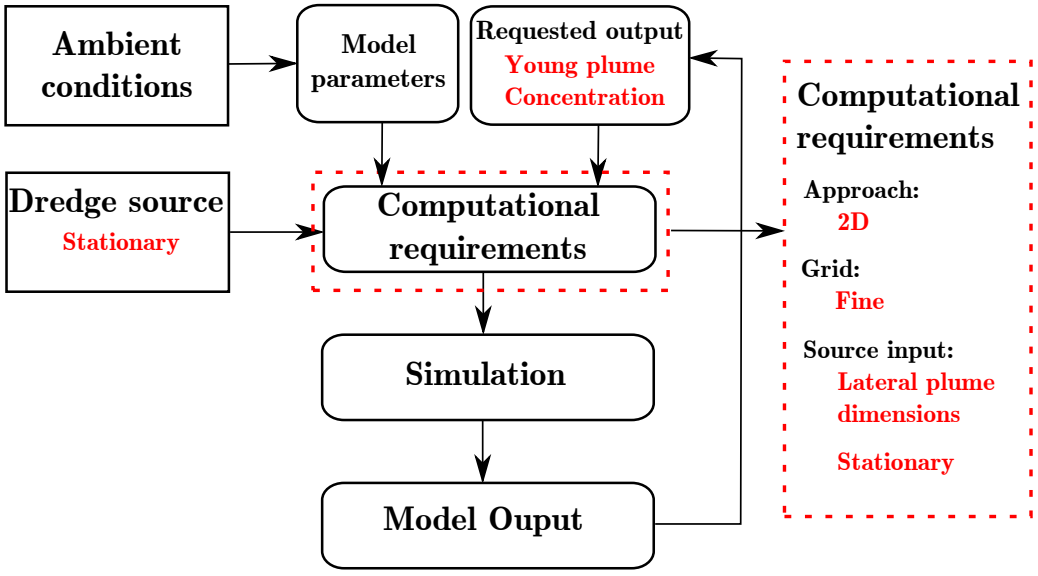

Figure 7.4: Flow diagram indicating recommendations for far-field dredge plume modelling for output situation: concentration - young plume.

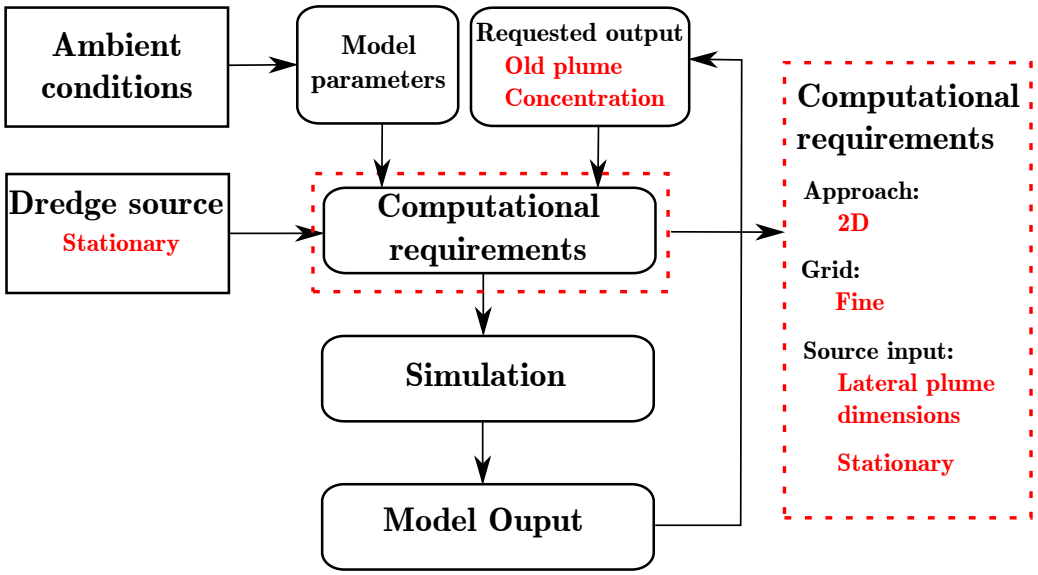

Figure 7.5: Flow diagram indicating recommendations for far-field dredge plume modelling for output situation: concentration - old plume.

References

Aarninkhof, S. G. J. and Luijendijk, A. (2010). Safe disposal of dredged material in an environmentally sensitive environment. By using innovative plume predictions, dredgers can now model the best ways to dispose of environmentally harmful sediment. *Port Technology International*, 47:39–45.

Aarninkhof, S. G. J., Rosenbrand, W. F., Van Rhee, C., and Burt, T. N. (2007). The day after we stop dredging: A world without sediment plumes? In *Proceedings CEDA Dredging Days*.

Akar, P. J. and Jirka, G. H. (1994). Buoyant spreading processes in Pollutant Transport and Mixing, Part 1: Lateral spreading with Ambient Current Advection. *Journal of Hydraulic Research*, 32(6):815–831.

Baird, W. (2004). *MMS Dredge Plume Model User Manual*. W.F. Baird & Associates Ltd.

Becker, J. H. (2011). Dredge plumes: Ecological risk assessment. Master's thesis, Delft University of Technology.

Becker, J. H., Van Eekelen, E. M. M., Wiechen, J. J. J., De Lange, W., Damsma, T., Smolders, T., and Van Koningsveld, M. (2014). Estimating source terms for far field dredge plume modelling. *Journal of Environmental Management*. (Submitted for publication).

Boot, M. (2000). Near-field verspreiding van het overvloeiverlies van een sleephopperzuiger (Near-field dispersion of overflow from a TSHD). Master's thesis, Delft University of Technology, Delft, The Netherlands. In Dutch.

Bray, R. N., editor (2008). *Environmental Aspects of Dredging*. Taylor & Francis/Balkema.

Brooks, N. H. (1972). *Dispersion in hydrologic and coastal environments*, volume No. KH-R-29. W. M. Keck Laboratory of Hydraulic and Water Resources, Californica Institute of Technology, Pasadena, California.

Choi, K. W. and Lee, H. W. (2005). A new approach to effluent plume modelling in the intermediate field. *IAHR Congress, Seoul, Korea*, pages 4303–4311.

Dankers, P. J. T. (2002). The behaviour of fines released due to dredging - a literature review. Technical report, Hydraulic Engineering Section, Faculty of Civil Engineering and Geosciences, Delft University of Technology.

De Wit, L. (2010). Near Field 3D CFD Modelling of Overflow Plumes. In *Proceedings WODCON XIX conference*, page 12. Beijing, China.

De Wit, L., Talmon, A. M., and Van Rhee, C. (2014a). 3D CFD simulation of trailing suction hopper dredge plume mixing: a parameter study of near field conditions influencing the suspended sediment source flux. *Marine Pollution Bulletin*. (Accepted for publication).

De Wit, L., Talmon, A. M., and Van Rhee, C. (2014b). 3D CFD simulation of trailing suction hopper dredge plume mixing: comparison with field measurements. *Marine Pollution Bulletin*. (Accepted for publication).

De Wit, L., Van Rhee, C., and Talmon, A. (2014c). Influence of important near field processes on the source term of suspended sediments from a dredging plume caused by a Trailing Suction Hopper Dredger: the effect of dredging speed, propeller, overflow location and pulsing. *Environmental Fluid Mechanics*. (In press).

Deltares (2009). *User Manual Delft3D-FLOW*. Deltares.

Dimotakis, P. E. (1986). 'Two-dimensional shear-layer entrainment'. *AIAA Journal*, 24(11):1791–1796.

Doneker, R. L. (2008). CORMIX Models for Mixing Processes. In *Mixing Zone Model Workshop*.

Elder, J. W. (1959). The dispersion of marked fluid in turbulent shear flow. *Journal of Fluid Mechanics*, 5:544–560.

Fick, A. (1855). On Liquid Diffusion (abstracted from original paper: Uber Diffusion). *Philosophical Magazine*, X:30–39.

Fischer, H., List, E. J., Koh, R. D. Y., Imberger, J., and Brooks, N. H. (1979). *Mixing in Inland and Coastal Waters,*. Academic Press, San Diego, USA.

Fric, T. F. (1990). *Structure in the near-field of a transverse jet*. PhD thesis, California Institute of Technology.

Groenewold, S. and Dankers, N. (2002). Ecoslib - De ecologische rol van slib. Technical report, RIKZ-RWS.

Hallworth, M. A., Hogg, A. J., and Huppert, H. E. (1998). Effects of external flow on compositional and particle gravity currents. *Journal of Fluid Mechanics*, 359:109–142.

Hinze, J. O. (1975). *Turbulence*. McGraw-Hill, New York, USA.

Jacobs, W., Muller, M., and Van Raalte, G. (2013). Building Block - Assessment of dredging-induced turbity.

Jirka, G. H. (2004). Integral model for turbulent buoyant jets in unbounded stratified flow. Part I: Single Round Jet. *Environmental Fluid Mechanics*, 4:1–56.

Jirka, G. H., Doneker, R. L., and Hinton, S. W. (1996). *User's Manual for CORMIX: A Hydrodynamic Mixing Zone Model and Decision Support System for Pollutant Discharges into Surface Waters*. US Environmental Protection Agency, Tech. Rep., Environmental Research Lab, Athens, Georgia, USA.

Lee, J. H. W. and Chu, V. (2003). *Turbulent jets and plumes - A Lagrangian Approach*. Kluwer Academic Publishers.

Morelissen, R., van der Kaaij, T., and Bleninger, T. (2013). Dynamic coupling of near field and far field models for simulating effluent discharges. *Water Science & Technology*, 67(10):2210–2200.

Nichols, M., Diaz, R., and Schaffner, L. (1990). Effects of hopper dredging and sediment dispersion, Chesapeake bay. *Environmental Geology and Water Sciences*, 15(1):31–43.

Partheniades, E. (1965). *A Study of Erosion and Deposition of Cohesive Soils in Salt Water*. PhD thesis, University of California, Berkeley.

Partheniades, E. (1980). *Cohesive sediment transport mechanics and estuarine sedimentation*. Lecture notes.

Philibert, J. (2005). One and a half centruy of diffusion: Fick, Einstein, before and beyond. *Diffusion Fundamentals*, 2:1–10.

PIANC (2010). Dredging and port construction around coral reefs. Technical report, PIANC EnviCom - Report 108.

Prych, E. A. (1970). Effects of density differences on lateral mixing in open-channel flow. Technical report, California Institue of Technology.

Rademacher, M. (2013). Effectiveness of Silt Screens. Master's thesis, Delft University of Technology, Delft, The Netherlands.

Rodi, W. (1982). *Turbulent buoyant jets and plumes*. Pergamon Press.

Scott, K. J. (1984). *Hindered settling of a suspension of spheres; critical evaluation of equations relating settling rate to mean particle diameter and suspesion concentration*. CSIR, Chemical Engineering Research Group, Report CENG 497.

Smith, S. J. and Friedrichs, C. T. (2011). Size and settling velocities of cohesive flocs and suspended sediment aggregates in a trailing suction hopper dredge plume. *Continental Shelf Research,*, 31(10):S50–S63.

Soulsby, R. L. (1997). *Dynamics of marine sands*. Thomas Telford Publishing, Thomas Telford Ltd.

Spearman, J. R., De Heer, A., Aarninkhof, S. G. J., and Van Koningsveld, M. (2011). Validation of the TASS System for predicting the environmental effects of Trailing Suction Hopper Dredgers. *Terra et Aqua*, 125(3):14–22.

Sreenivas, K. R. and Prasad, A. K. (2000). 'Vortex-dynamics model for entrainment in jets and plumes'. *Physics of Fluids*, 12(8):2101–2107.

Taylor, G. I. (1953). Dispersion of soluble matter in solvent flowing slowly through a tube. *Proceedings of the Royal Society of London, Series A, Mathematical, Physical and Engineering Sciences*, 219:186–203.

Taylor, G. I. (1954). The dispersion of matter in turbulent flow through a pipe. *Proceedings of the Royal Society of London, Series A, Mathematical, Physical and Engineering Sciences*, 223:446–468.

Tennekes, H. and Lumley, J. L. (1972). *A First Course in Turbulence*. The MIT Press.

Torfs, H., Mitchener, H., Huysentruyt, H., and Toorman, E. (1996). Settling and consolidation of mud/sand mixtures. *Coastal Engineering*, 29:27–45.

Turner, J. S. (1973). *Buoyancy Effects in Fluids*. Cambridge University Press, London.

Van Eekelen, E. E. M. (2008). Stripping of dynamic dredge overflow plumes. In *CEDA Dredging Day Conference 2008*.

Van Eekelen, E. M. M. (2007). Experimental research on dynamic dredge overflow plumes. Master's thesis, Delft University of Technology.

Van Ledden, M. and Van Kesteren, W. (2004). A conceptual framework for the erosion behaviour of sand-mud mixtures. *Continental Shelf Research*, 24(1):1–11.

Van Rijn, L. C. (1993). *Principles of Sediment Transport in Rivers, Estuaries and Coastal Seas.* Aqua Publications, Amsterdam.

VBKO (2003). Protocol for the Field Measurements of Sediment Release from Dredgers. *VBKO report*, 1:1–83.

Whitehouse, R. J. S., Soulsby, R. L., Roberts, W., and Mitchener, H. J. (2000). *Dynamics of estuarine muds*. Thomas Telford Publishing, Thomas Telford Ltd, London, UK.

Winterwerp, J. C. (1999). *On the dynamics of high-concentrated mud suspension*. PhD thesis, Delft University of Technology, Delft, The Netherlands.

Winterwerp, J. C. (2002). Near-field behavior of dredging spill in shallow water. *Journal of Waterway, Port, Coastal, and Ocean Engineering*, 128(2):96–98.

Winterwerp, J. C. and Van Kesteren, W. G. M. (2004). *Introduction to the physics of cohesive sediment in the marine environment*, volume 56 of *Developments in sedimentology*. Elsevier.

Zhoa, L., Chen, Z., and Lee, K. (2011). Modelling the dispersion of wastewater discharges from offshore outfalls: a review. *NRC Research Press Web site*.

Appendices

Appendix A

Turbulent transport

Flows are characterised as turbulent or laminar. Laminar flows are an exception, as most flows in nature and built environment are turbulent. The description of turbulence by Hinze (1975) is widely used. He describes turbulent fluid motion as *"an irregular conditions of flow in which the various quantities show a random variation with time and space coordinates, so that statistically distinct average values can be discerned"*. Turbulence is an important phenomenon for the transport of matter. In this appendix transport of sediment by advection and diffusion is explained. First the nature and types of turbulence will be described. Furthermore, a statistical description of turbulence and turbulent diffusion is given as this is used in the theoretical framework of this research.

A.1 Nature of turbulence

In turbulent flow, in contrast to laminar flow, the streamlines do not follow straight lines. Turbulent flow is characterised by an erratic and irregular flow pattern. The Reynolds number can be used to determine whether a flow is turbulent or laminar. It represents the ratio of inertia over viscosity:

$$R_e = \frac{U * L}{\nu}, \tag{A.1}$$

where R_e is the Reynolds number, U the flow velocity, L a characteristic length over which velocity difference is found and ν the kinematic viscosity. For low Reynolds numbers (< 2300) viscosity dominates and the flow can be considered laminar. For high Reynolds numbers (> 4000) flow irregularities can no longer be suppressed by the viscosity, resulting in turbulence. Between these exists an transitional zone. Tennekes and Lumley (1972) give certain characteristics which are widely used in describing turbulence:

- Turbulence is *irregular*, therefore a statistical description is needed.
- Turbulent motion causes large transport of momentum, heat and mass. Therefore turbulence is *diffusive*.
- Turbulent flows have *large Reynolds numbers*.
- Turbulent flows are *three-dimensional* and rotational. Vortex movement could not be maintained if the velocity fluctuations are two-dimensional, since vortex stretching is absent in two-dimensional flows.

- Turbulent flows dissipate energy and are in general more *dissipative* than laminar flows. Energy is transferred from the mean motion to the turbulent fluctuations.
- Large range of length and time scales exist. Turbulent fluctuation length and time scales are far larger than the molecular scale, but even the smallest scales satisfy the *continuum hypothesis*.
- Turbulent flows are *flows*, so turbulence is not a fluid property, but depending on the circumstances a flow can either be laminar or turbulent.

Figure A.1 explains the onset of turbulence in four stages. An initial disturbance is needed to generate turbulence, resulting in a flow which is in a variable state. Laminar flow is followed by turbulent flow. In case of low Reynolds numbers the turbulent structures are suppressed, while for high Reynolds numbers disturbances will continuously create new turbulent structures.

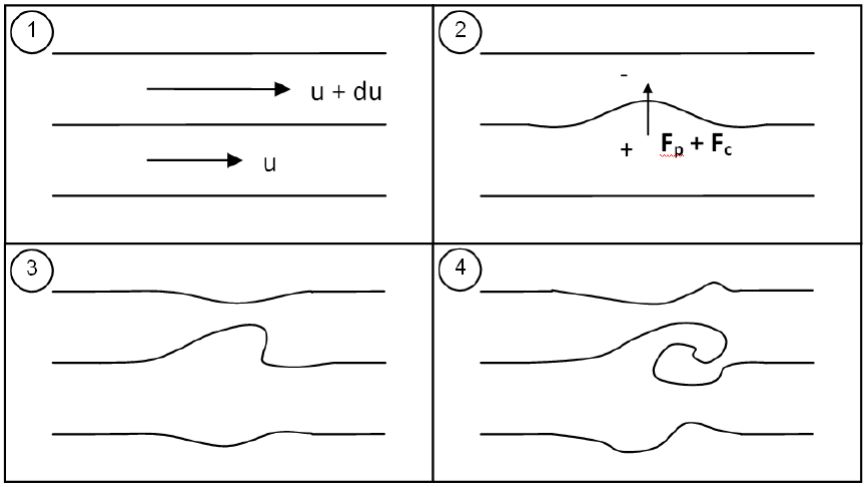

Figure A.1: Onset of turbulence from laminar flow (1) to turbulent flow (4) (Rademacher, 2013).

A.2 Statistical description of turbulence

When looking at a time series of a velocity measurement in a turbulent flow, one will observe a very irregular line. This velocity signal (or signal of any other property) can be interpreted as a mean value and fluctuating component on top of that. In Figure A.2 a velocity time series is shown. The red line characterises the mean velocity and the red arrows represent fluctuations.

Determination of the velocity components from such a time signal can be done by either time averaging or ensemble averaging. Time averaging of a signal results in a mean velocity which is constant in time, together with a time varying fluctuating component. In ensemble averaging the averaging is performed over a number of samples, which can result in a mean velocity which varies in time (e.g. in case of tidal movement). On top of this mean velocity again fluctuations are determined. Which average method and time period to choose is determined by the local properties of the flow. The length of the averaging period should be short with respect to the time scale in which the mean motion varies and long with respect to the time scale of the turbulent

fluctuations. The decomposition of the velocity into a fluctuating and a mean component is called called Reynolds decomposition, resulting in:

$$u = \overline{u} + u' \tag{A.2}$$

$$\overline{u'} = 0 \tag{A.3}$$

$$\overline{\overline{u}} = \overline{u} \tag{A.4}$$

$$\overline{uv} = \overline{u} * \overline{v} + \overline{u'v'} \tag{A.5}$$

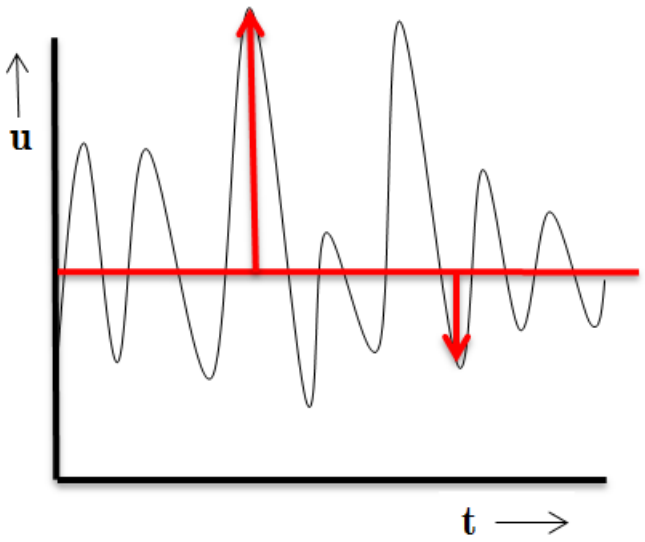

Figure A.2: Time series of a velocity signal with mean velocity (red line) and velocity fluctuations (red arrows).

Due to the irregular motions, a velocity signal of a turbulent flow can only be described using statistics. A velocity signal can be described using a Gaussian distribution (for ideal homogeneous and isotropic turbulence). The mean of the distribution is the mean velocity. The fluctuating component of a property is by nature characterised by its variance: ($\sigma^2 = \overline{(u - \overline{u})^2}$). This is a measure of the kinetic energy contained in the turbulent motions. The kurtosis or flatness of the distribution describes the deviation of the velocity signal from being Gaussian distributed.

In turbulent flows the non-zero product of two fluctuating velocity components seems to be important. This term accounts for the turbulent transport of momentum (when multiplied with the density) and can be interpreted as a turbulent stress. It can be shown that in turbulent flow this turbulent shear stress is much higher than the viscous shear stress. The presence of this non-zero fluctuation velocity term indicates transport of energy from the mean flow to the velocity fluctuations.

A.3 Types of turbulence

Turbulence is present when energy can be transferred from the mean motion to the turbulent fluctuations, which then leads to transport of momentum. This transport is caused by velocity

gradients and corresponding shear stresses. In general two types of turbulence can be identified: wall turbulence and free turbulence.

The first type, wall turbulence, arises from the no-slip condition, stating that the velocity of a fluid at solid boundary is zero relative to that boundary. The shear stresses generated near the wall will cause wall turbulence, provided that the Reynolds number is sufficiently high.

Free turbulence appears in flows where velocity gradients are present, i.e. two adjacent flows having different velocities. Examples are jets, recirculation zones and wakes. At the transition from one flow to the other a mixing layer will be present, where turbulence is generated and transfer of mass and momentum takes place. Grid turbulence is a special type of free turbulence. This type is usually only generated in a laboratory, and present downstream of a grid or wired mesh.

As for laminar flows, the basic equations describing fluid motion, the Navier-Stokes equations, can be used to describe turbulent flows. The Navier-Stokes equations, describing conservation of momentum and mass, are solvable for laminar flows. Turbulent flows, in constrast to laminar flows, are characterised by the presence of many eddies of different time and length scales. In practice the equations could also be solved for turbulent flows, by applying a fine computational grid to catch all these length and time scales. However, up to now, computational power does not allow solving the Navier-Stokes equations for most turbulent flows, since length and time scales result in unsolvable fine grids. Therefore, approximations in the equations have to be made, in order to account for the momentum transfer by the turbulent motions.

By applying Reynolds decomposition the velocity signal (u) is thought to be a summation of a mean velocity ($\overline{u}$) and a fluctuating velocity (u'), as we have seen in the statistical description of turbulence. Introducing the decomposed velocity (and pressure) terms into the Navier-Stokes equation and take the average, results in the so called Reynolds averaged equation. The Reynolds averaged equation describes the fluid motion as a function of the mean velocity. Only a few terms remain in which the fluctuating velocities are present. As stated before, these terms account for the transport of momentum and can be interpreted as stresses, denoted as the Reynold stresses. Due to the presence of these terms approximations are needed to close the set of equations. In turbulent flows the turbulent motions (and corresponding turbulent viscosity) are far more effective in transporting momentum than the molecular viscosity. However, viscosity still is responsible for the dissipation of energy. The turbulent eddies only function as transport mechanism. The whole cycle is referred to as energy cascade; energy from the mean motion is transferred to the large scale turbulent fluctuations, turbulent eddies break up into smaller eddies until the Kolmogorov length scale is reached. At this smallest scale the velocity gradients are high enough and thus viscosity is capable to transfer the energy to heat. This whole cycle is far more effective in draining energy from the mean motion than the direct energy dissipation from the mean motion by viscosity.

Since the turbulent motions are not a property of the fluid, a constant turbulent viscosity can in most cases not be applied. The amount of turbulence has a strong spatial dependency. Following the same analogy as for viscous shear stress the turbulent (Reynold) shear stress can be defined using a turbulent viscosity and a velocity gradient:

$$\tau_t = \rho \nu_t \frac{du}{dy}, \tag{A.6}$$

Assuming a linear shear stress distribution gives a clear dependency between the viscosity profile and the velocity profile. Using a constant turbulent viscosity will result in a parabolic velocity profile, which is not realistic. Several turbulent closure models are derived to come to expressions for the turbulent viscosity in terms of a velocity gradient and a mixing length. For a (fully developed)

steady uniform flow we know a logarithmic profile distribution is present over the water depth. A parabolic viscosity distribution is needed to arrive at this velocity profile. Knowing the velocity profile an expression for the viscosity profile can be derived:

$$\nu_t = \kappa u_* h \gamma (1 - \gamma), \tag{A.7}$$

A.4 Advection diffusion equation

Transport occurs in fluids through a combination of advection and diffusion. The transport by the mean motion of the fluid is called advection, while diffusion is transport associated with the random motions within a fluid. The advective mass flux through the unit area in the yz plane by the velocity component in the x direction is given by the quantity (uC). Here u x *unit area* is the volume per unit time and C is the concentration of mass in that volume. Multiplication gives the quantity uC, which is the rate at which fluid volume passes through the unit area; the advection of mass.

Diffusion can be explained in two ways: either a phenomenological approach can be used, starting with Fickian Diffusion and its mathematical consequences. Also, a physical and atomistic approach can be applied, by considering the random walk of diffusing particles (Philibert, 2005).

First study on diffusion was performed by a Scottish chemist, Thomas Graham, studying diffusion in gasses from 1828 to 1833. Adolph Fick, a German physiologist, extended research on diffusion. The first paragraph of his paper reads (Fick, 1855):

> A few years ago Graham published an extensive investigation on the diffusion of salts in water, in which he more especially compared the diffusibility of different salts. It appears to me a matter of regret, however, that in such an exceedingly valuable and extensive investigation, the development of a fundamental law, for the operation of diffusion in a single element of space, was neglected, and I have therefore endeavored to supply this omission.

Fick (1855) describes how Fourier's heat flow leads to an hypothesis to describe the molecular diffusion process. By following the same mathematical formalism as Fourier's law for heat conduction, Fick's law was derived. The law states that the mass flux of the solute through a unit area per unit time in x direction is proportional to the gradient of the solute concentration in the same direction.

$$q = -D_m \frac{\delta C}{\delta x}, \tag{A.8}$$

where q is the the solute mass flux, C is the mass concentration of the solute and D_m is the coefficient of proportionality. D_m has the dimension ($length^2/time$) and is also called diffusion coefficient or molecular diffusivity. D_m is a property of both the fluid and the diffusing solute. The minus sign indicates transport from high to low concentrations.

Combining Fick's law with conservation of mass gives an equation describing the diffusion process. Conservation of mass leads to a relationship which is true regarding the type of transport process, relating the mass flux ($q(x,t)$) and concentration ($C(x,t)$). Combination of the two relationships gives the diffusion equation (with respect to x), describing mass transfer by Fickian diffusion processes:

$$\frac{\delta C}{\delta t} = D_m \frac{\delta^2 C}{\delta x^2}, \tag{A.9}$$

In this equation the diffusion coefficient is assumed to be constant. This equation can be extended to all three directions (x y z, respective coordinates in parallel, lateral and vertical direction) leading to the diffusion equation:

$$\frac{\delta C}{\delta t} = D_m(\frac{\delta^2 C}{\delta x^2} + \frac{\delta^2 C}{\delta y^2} + \frac{\delta^2 C}{\delta z^2}), \tag{A.10}$$

The second way to describe diffusion is by assuming a random walk. A random walk is a mathematical way of describing a walk of a succession of random steps. Molecules of a fluid are constantly in motion and colliding with each other and other small particles in suspension. Any molecule, or small particle, experiences many collisions every second. The amount of collisions depends on the fluid, the size of the particle and the density and temperature of the fluid. Due to these collisions a particle's motions describes a random path. Given the motion of a particle is completely random, it holds that motions in all directions have the same probability. This would result in zero movement on average. However, after a certain time the particle will have moved fore- or backwards. The motion of such a particle must be described in a statistical way.

Fischer et al. (1979) give an example to demonstrate the random motion of a large number of particles at the same time. Consider two boxes, in which the left box starts with 10 molecules and the right box with 20 molecules, see Figure A.3. The probability of a molecule crossing the line separating the left and the right box in Δt is 0.2. This implies that on average 2 molecules move from left to right and 4 molecules move from right to left. After Δt the left box will have 8 original molecules plus 4 new molecules and the right box will have 16 molecules plus 2 new molecules. In this example transport through the other surfaces is neglected. If we define concentration as the average number of molecules per box, the difference in concentration has lowered from 10 to 6 in the considered time step. A fundamental aspect of diffusion is the fact that differences in mean concentration are, on average, always reduced and never increased.

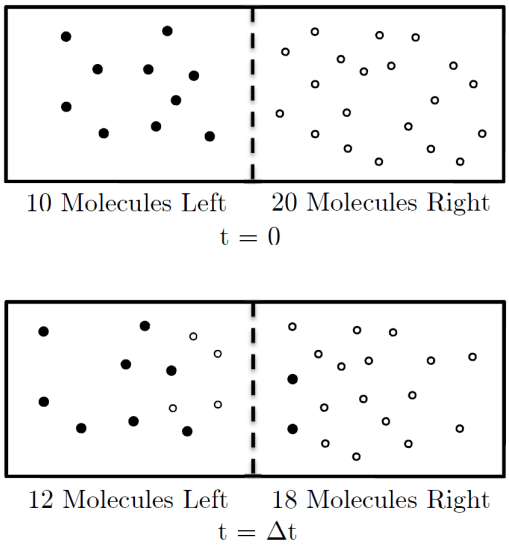

Figure A.3: An illustration of molecular diffusion, showing a probability of 0.2 that molecules will cross into the adjacent box in time interval Δt.

We can define the flux of material moving across the boundary as the rate at which tracer mass is exchanged per time unit and per unit area of the surface. As an example take a unit area

perpendicular to the line separating the left and right box. The total flux of material from left to right is the number of molecules times the mass of the each molecule (assuming all equal), times the probability of transfer. The net mass flux (q) is given by:

$$q = k(m_l - m_r), \tag{A.11}$$

where m_l is the mass of the molecules in the left box, m_r is the mass of the molecules in the right box and k is the probability of transfer. This results, for instance, in a mass flux from left to right; km_l. Now we define the concentration $C_l = \overline{m_l}/\Delta x$ and $C_r = \overline{m_r}/\Delta x$. In which $\overline{m}$ is the average mass in a box. Letting Δx go to zero and filling in C in Equation A.11 gives:

$$q = -k(\Delta x)^2 \frac{\delta C}{\delta x}, \tag{A.12}$$

Equation A.12 shows that the net flux is always down the gradient, from high to low concentrations. The transfer probability is a function of molecular motion and also a function of the size of the box. A larger box means that less molecules are close to the boundary. However, the flux should not be a function of the arbitrarily defined size of the box. By letting $k(\Delta x)^2$ be a constant, q is not depending on the box size anymore (Δx). In this way $k(\Delta x)^2$ is the diffusion coefficient, obtaining from Equation A.12 the same equation as given by Fick's law (Equation A.8).

Equations A.9 and A.10 only considered mass transported by diffusion. Mass transport by the bulk motion, the motion of the fluid itself (advection) is ignored so far. Adding the advective flux to the equation of the solute mass flux (q), Equation A.8 results in the equation describing the total mass transport (in x direction):

$$q = uC + (-D_m \frac{\delta C}{\delta x}), \tag{A.13}$$

Again this equation can be substituted in the equation for mass conservation in all three directions to obtain Equation A.10 plus additional advective terms, which is referred to as the advection diffusion equation:

$$\frac{\delta C}{\delta t} + u\frac{\delta C}{\delta x} + v\frac{\delta C}{\delta y} + w\frac{\delta C}{\delta z} = D_m(\frac{\delta^2 C}{\delta x^2} + \frac{\delta^2 C}{\delta y^2} + \frac{\delta^2 C}{\delta z^2}), \tag{A.14}$$

Turbulent diffusion

Fick's law accounts for mass transport by molecular diffusion in laminar flow. The molecular diffusion coefficient (D_m) in water is typically small, around 10^{-9} m^2/s. The time (t) needed to spread a solute over a distance L depends on this coefficient, and can be estimated with (through scaling):

$$t \approx \frac{L^2}{D_m}, \tag{A.15}$$

Given the small diffusion coefficient, this equation holds very long durations for spreading of a solute. Take for example a cup of tea (height of 10 cm) with some sugar on the bottom of the cup. By only taking into account the molecular diffusion, the time it takes for the sugar to uniformly mix through the cup is in the order of 115 days. By stirring, producing advection and turbulence, this process can be shortened to just a few seconds. In most fluid motions in the environment spreading of a solute happens at a much faster rate than calculated from molecular diffusion alone.

Clearly, other diffusion processes are involved in these fluid motions. Most fluid motions in nature are turbulent, resulting in turbulent diffusion.

Turbulent diffusion is the diffusion of a solute produced by the turbulent motion of the flow. Turbulent motion is characterized by vortices (or eddies) in the flow, with different length scales (or eddy sizes) ranging from the smallest Kolmogorov scale up to to the largest integral scale. The effects of turbulent diffusion are the same as for the random molecular motions, though acting on a larger scale.

Turbulence reduces concentration gradients and transports material. When looking at a patch of solute diffusing in a turbulent flow, the size of the eddies (compared to the patch) is of large influence. Eddies which are smaller than the size of the patch will cause only a little diffusion over the edges of the patch, but will cause mixing within the cloud. The larger eddies (larger than the patch) move the entire patch around, but do not contribute to the mixing process. If we release two patches in the same turbulent water at exact the same location, the movement of the second patch would be quite different from the first one. The small eddies produce steep concentration differences over short distances, which are smoothed out by molecular diffusion. The large eddies, as already stated, will transport the entire cloud, resulting in different motion of the centre of mass of the two patches. The most effective spreading takes place for eddy sizes which are of the same order as the size of the patch.

Transport of energy and momentum in turbulent motions was described before, however, the advection diffusion equation describes transport of matter: heat, smoke, sediment etc. Turbulent transport of momentum along a velocity gradient is practically the same as turbulent transport of matter along a concentration gradient. As for transport of momentum, the turbulent motions account for the most effective spreading of the matter, whereas the molecular diffusion accounts for the actual diffusion on the smaller scales. Therefore, the turbulent diffusion distribution is often taken similar to the distribution of the viscosity. However, due to the fact that the transported momentum is continuously affected by ambient stresses, and passive tracers (as fine sediment) are not, the transport of tracers is more effective than the transport of momentum. Therefore the turbulent viscosity is generally smaller than the turbulent diffusion. The ratio of the viscosity over the diffusivity is given by the Schmidt number (Sc):

$$Sc = \frac{\nu_t}{D_t}, \tag{A.16}$$

Typically the Schmidt number is in the order of 0.5-1.

Spreading of tracer particles injected in water can be described using a dispersion parameter, $\overline{X^2}(t)$. Stating that the mean lateral displacement of the particles can be given in terms of a Lagrangian fluctuating velocity u_L, an equation can be derived for the dispersion parameter in terms of this velocity component and the autocorrelation function (R_L):

$$\overline{X^2}(t) = 2\overline{u_L^2} \int_0^t (t-\tau) R_L(\tau) d\tau, \tag{A.17}$$

where τ is a time interval. The autocorrelation function (R_L) represents the correlation of a velocity with that same velocity when shifted over a certain time interval. This leads to $R_L \approx 1$ for small time intervals, since the the velocity is fully correlated with itself for small time shifts (close to the release location). This leads to $\overline{X^2}(t) \approx \overline{u_L^2} t^2$. Further away from the release location, at larger time intervals, the autocorrelation function integrates to the integral time scale T_L, leading to $\overline{X^2}(t) \approx 2\overline{u_L^2} T_L t$. From this we can conclude that for time scales larger than the integral time

scale the width of the cloud grows linearly in time, which can be considered as a diffusion process with a constant diffusion coefficient $D_t = \overline{u_L^2} T_L$. This can also be written as a product of the integral length scale of the large scale motions and the fluctuating velocity $D_t = l_T \sqrt{\overline{u_L^2}}$. So when the size of the dispersing cloud exceeds the integral length scale, the process can be described using constant coefficients.

After some start up time this criterion often holds for mixing in a stationary homogenous turbulent flow. Therefore it can be described by a diffusion process with a constant diffusion coefficient. The advective diffusion equation (Equation A.14) derived in Section 2.1.2 can be extended for turbulent flows by decomposing the velocity and concentration terms into a mean and a fluctuation component:

$$C = \overline{C} + C', \qquad u = \overline{u} + u', \qquad v = \overline{v} + v', \qquad w = \overline{w} + w', \tag{A.18}$$

In which the overlined components are the time averaged and the primed are the fluctuating components. Filling in the components into Equation A.14 and then take the time average (such that $\overline{\overline{C} + C'} = \overline{C}$) results in:

$$\frac{\delta \overline{C}}{\delta t} + \overline{u}\frac{\delta \overline{C}}{\delta x} + \overline{v}\frac{\delta \overline{C}}{\delta y} + \overline{w}\frac{\delta \overline{C}}{\delta z} = D_m\left(\frac{\delta^2 \overline{C}}{\delta x^2} + \frac{\delta^2 \overline{C}}{\delta y^2} + \frac{\delta^2 \overline{C}}{\delta z^2}\right) - \overline{u'C'}\frac{\delta}{\delta x} - \overline{v'C'}\frac{\delta}{\delta y} - \overline{w'C'}\frac{\delta}{\delta z}, \tag{A.19}$$

The three new terms appearing in Equation A.19 represent the diffusion by turbulent motion (due to the correlation between the fluctuation velocity and concentration components). The molecular transport term is generally much smaller than the turbulent flux and is therefore neglected. This does not mean that molecular diffusion is not important in mixing on the smallest scale, since it accounts for the actual energy dissipation.

The turbulent fluxes can be written as a gradient type transport using an eddy diffusion coefficient (D_t):

$$\overline{u'C'} = -D_{t(x)}\frac{\delta C}{\delta x}, \qquad \overline{v'C'} = -D_{t(y)}\frac{\delta C}{\delta y}, \qquad \overline{w'C'} = -D_{t(z)}\frac{\delta C}{\delta z}, \tag{A.20}$$

where $D_{t(x)}$, $D_{t(y)}$ and $D_{t(z)}$ are the turbulent equivalents to the molecular diffusion coefficient, often referred to as "Fickian turbulent diffusion coefficients", turbulent diffusion coefficents or eddy diffusivities (Fischer et al., 1979). Using the eddy diffusivities, applying the assumption that turbulent transport is much greater than molecular transport and ignoring the overline for average concentration and velocity, Equation A.19 becomes:

$$\frac{\delta \overline{C}}{\delta t} + \overline{u}\frac{\delta \overline{C}}{\delta x} + \overline{v}\frac{\delta \overline{C}}{\delta y} + \overline{w}\frac{\delta \overline{C}}{\delta z} = \frac{\delta}{\delta x}\left(D_{t(x)}\frac{\delta C}{\delta x}\right) + \frac{\delta}{\delta y}\left(D_{t(y)}\frac{\delta C}{\delta y}\right) + \frac{\delta}{\delta z}\left(D_{t(z)}\frac{\delta C}{\delta z}\right), \tag{A.21}$$

For time scales larger than the Lagrangian time scale the above equations can be applied in combination with constant diffusion coefficients.

Shear flow dispersion

Advection by a constant velocity is not effective in mixing a solute since it only carries material, without changing its distribution. However, non-constant advective flows, flows with a velocity gradient (shear flows), are able to stretch and distort a distribution of the material. The cross sectional velocity gradient results in certain parts of the material being carried faster than other

parts, which causes intensification of concentration gradients and therefore dispersion. Dispersion is used to describe diffusion caused by a shear flow.

An example of shear flow dispersion is the combination of a velocity profile over the cross section and diffusion in the direction transverse to the flow direction. Consider a patch of a solute being released in a shear flow (see Figure A.4). The initial patch is transported downstream and distorted by the non-constant advective flow. Transverse diffusion then smears out the material over the cross section resulting in a wider patch of solute downstream, hence the two phenomena have resulted in a longitudinal diffusion of the solute.

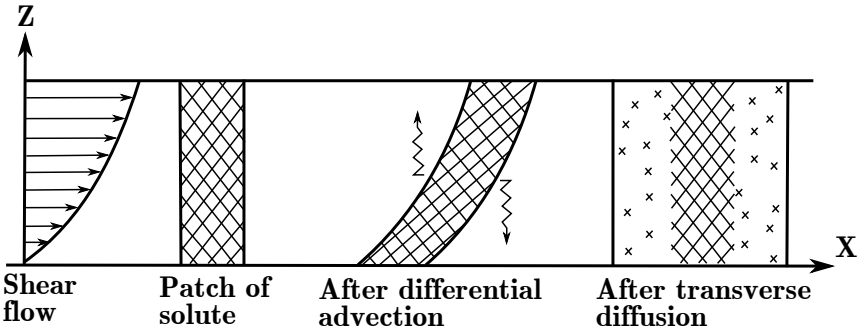

Figure A.4: The dispersion of a patch of solute by a combination of shear flow and transverse diffusion.

Taylor (1953) and Taylor (1954) describe the spread of a solute in laminar pipe flow. This theory is extended over the years to all other kinds of flows to describe dispersion in rivers or estuaries. Taylor (1953) considers dispersion of a solute in laminar flow in a tube. Fischer et al. (1979) applies his concepts to a two-dimensional flow in between two walls, to show that Taylor's theory is applicable to other types of flow.

To describe the theory on dispersion in shear flows first the velocity and concentration profile are divided into a mean and local deviation component ($u = \overline{u} + u'$ and $C = \overline{C} + C'$). The mean concentration and mean velocity at any cross section can be found by:

$$\overline{u} = \frac{1}{h}\int_0^h u dy, \tag{A.22}$$

$$\overline{C} = \frac{1}{h}\int_0^h C dy, \tag{A.23}$$

If first laminar flow is considered, no turbulent fluctuations have to be taken into account. A coordinate system following the mean flow is applied (ξ, τ). In this way the terms including the mean flow can be eliminated from the diffusion equation. Let $\xi = x - \overline{u}t$ and $\tau = t$ (see Figure A.5) and only take into account the local deviations from the mean velocity (u'), this results in the following diffusion equation:

$$\frac{\delta}{\delta\tau}(\overline{C} + C') + u'\frac{\delta}{\delta\xi}(\overline{C} + C') = D_m[\frac{\delta^2}{\delta\xi^2}(\overline{C} + C') + \frac{\delta^2 C'}{\delta y^2}], \tag{A.24}$$

This equation can be rewritten into:

$$\frac{\delta}{\delta\tau}\overline{C} + \frac{\delta}{\delta\tau}C' + u'\frac{\delta\overline{C}}{\delta\xi} + u'\frac{\delta C'}{\delta\xi} = D_m[\frac{\delta^2}{\delta\xi^2}(\overline{C} + C') + \frac{\delta^2 C'}{\delta y^2}], \tag{A.25}$$

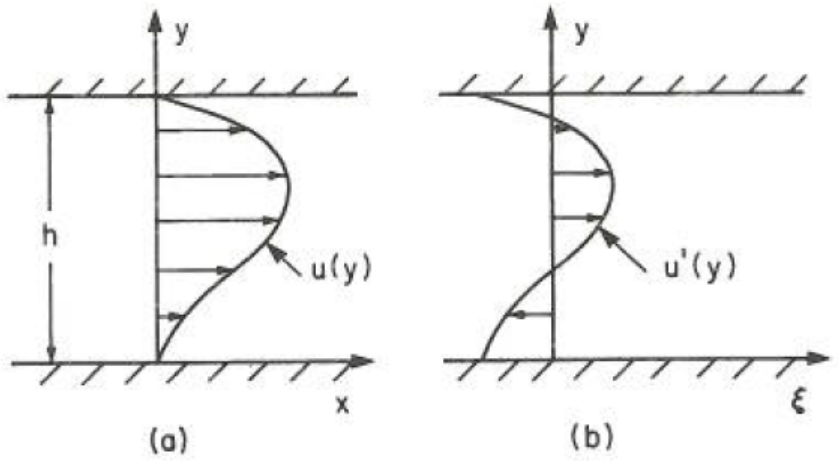

Figure A.5: (a) A possible velocity distribution. (b) The same velocity profile as in (a), but transformed to a coordinate system moving with the mean flow (Fischer et al., 1979).

In this equation the longitudinal diffusion term can be neglected, since the dispersion due to the velocity profile is much larger than due to molecular diffusion in longitudinal direction. Furthermore, Taylor (1953) shows that three of the first four terms can be neglected, based on the order of magnitude of these terms. Hereby, Equation A.25 results into an easily solvable equation for *C'(y)*

$$u' \frac{\delta \overline{C}}{\delta \xi} = D_m \frac{\delta^2 C'}{\delta y^2}, \tag{A.26}$$

With $\frac{\delta C'}{\delta y} = 0$ at $y = 0, h$. The solution to Equation A.26 reads:

$$C'(y) = \frac{1}{D_m} \frac{\delta \overline{C}}{\delta x} \int_0^y \int_0^y u' dy dy + C'(0), \tag{A.27}$$

The mass transfer in stream wise direction is the velocity times the concentration times the cross sectional area resulting in equations A.28 (still relative to the moving coordinate axis). Equation A.28 shows that the mass transported in the stream wise direction is proportional to the concentration gradient in the direction of the flow times some coefficient.

$$M = \int_0^h u' C'(y) dy = \frac{1}{D_m} \frac{\delta \overline{C}}{\delta x} \int_0^h u' \int_0^y \int_0^y u' dy dy dy, \tag{A.28}$$

This is the same result as one will find for molecular diffusion, but now the equation accounts for diffusion due to the whole flow field. An equation can be defined for the bulk transport using the dispersion coefficient:

$$M = -hK \frac{\delta \overline{C}}{\delta x}, \tag{A.29}$$

where h is the water depth, which is the area per unit width of flow and K is the so called (longitudinal) dispersion coefficient. K plays the same role for the whole cross section as the diffusion coefficient D_m does on microscopic scale. From the above it follows that K is:

$$K = \frac{-1}{hD_m} \int_0^h u' \int_0^y \int_0^y u' dy dy dy, \tag{A.30}$$

Now we can write the one-dimensional diffusion equation for cross sectional averages in the fixed (x,y) coordinate system, by reintroducing the mean advective velocity to give the one-dimensional dispersion equation:

$$\frac{\delta \overline{C}}{\delta t} + \overline{u}\frac{\delta \overline{C}}{\delta x} = K\frac{\delta^2 \overline{C}}{\delta x^2}, \tag{A.31}$$

In this equation the longitudinal advective transport is balanced by the cross sectional diffusive transport. This balance can only occur when the mean concentration ($\overline{C}$) varies slowly and the mean concentration gradient ($\frac{\delta \overline{C}}{\delta x}$) is nearly constant over a long period of time. In that case the concentrations fluctuations (C') become small, since cross sectional concentration differences are smoothed by the cross-sectional concentration gradient. These required circumstances take some time to establish. Once established the further spreading can be calculated using Equation A.31

The dispersion equation (A.31) concerns laminar flow only. This equation can be extended for turbulent flow, given the two differences; the velocity profile in turbulent flow differs from laminar flow, and the molecular diffusion coefficient will be replaced by the turbulent diffusion coefficient. Taylor (1954) extents the theory on dispersion in laminar flow to turbulent flow in a pipe. For the case described above the dispersion equation and dispersion coefficient in turbulent flow become:

$$\frac{\delta \overline{C}}{\delta t} + \overline{u}\frac{\delta \overline{C}}{\delta x} = K\frac{\delta^2 \overline{C}}{\delta x^2}, \tag{A.32}$$

$$K = \frac{-1}{hD_t}\int_0^h u' \int_0^y \int_0^y u' dy dy dy, \tag{A.33}$$

Appendix B

Fine sediment

Fine sediment is defined as all particles having a diameter smaller than 63 μm. Fine sediment can be classified as silt or as clay, depending physically on the particle size and mechanically on the plasticity. Several classifications of silts exist. For instance, ISO 14688 grades particles with a diameter between 2 μm to 63 μm as silts. Particles with a diameter larger than 63 μm are sand particles and fraction with a diameter smaller than 2 μm are classified as clay particles.

Besides the size, the nature of silt and clay particles is different. Silt particles consist of quartz material, just like sand. Therefore they have the same properties as sand, and thus act as sand particles with very small diameters. Clay consists of clay minerals, like kaolinite, illite, chlorite and montmorillonite. Important properties of clay are plasticity and cohesion. Plasticity is the property of a clay mass to undergo substantial permanent deformation, at the proper water content, under stresses, without breaking. Cohesion is the property of a material to stick or adhere together (Partheniades, 1980).

Sediment mixtures of silt and clay particles are defined as mud. Mud, furthermore, consists of other organic and anorganic components, water and sometimes gas. The anorganic fractions contain quartz, feldspar, clay minerals, calcite, dolomite, hydroxides, silicates, sulfides and small fractions of other material. The organic material in mud consists of living and dead material as bacteria and remnants or products of fytoplankton, bentic algea, faecel pellets, peat and macromolecules produced by bacteria (Groenewold and Dankers, 2002) (Dankers, 2002). The amounts of material present in mud strongly depends on the origin of the material. In natural sediments commonly more than one sediment type is present, creating a mixture of sand and mud (Whitehouse et al., 2000).

A characteristic of mud is the process of aggregation and break-up taking place, which is referred to as flocculation. The clay particles, organic material and fractions of silt can aggregate to form flocs, which can break up again. Flocs are formed by attractive forces, governed by collision and cohesion. According to Winterwerp (1999) the collision of particles is created by three agents: i) Brownian motions cause particles to collide, ii) particles with larger settling velocity will overtake particles with lower settling velocity causing collision and iii) turbulent motions will carry particles in eddies which also causes collision. The last agent may also cause break up of flocs since turbulent shear may disrupt the flocs. Besides the collision frequency, the stickiness determines the efficiency of the collisions. The stickiness is determined by the particle charge, the ion concentration in the water and by bio polymers and organic coating on the particles (Dankers, 2002). Therefore not all collisions lead to aggregation, since the ability of two particles to stick to each other determines the efficiency of collisions. Flocculation influences the physical parameters of suspended sediment,

as is shown in the section on settling.

Settling

The settling velocity (w_s) of a particle is an important property for research on morphology. Forces acting on particles, gravity flow and chemical forces, determine the settling velocity of that particular particle. When releasing a particle in water the settling velocity will reach a constant value after a start-up phase. The settling velocity differs per material, diameter and flow condition. For massive spherical particles (sand or silt particles) the settling velocity was found by Stokes. The Stokes law states that the final settling velocity of a particle is reached when the drag force on the particle is in equilibrium with the gravity force. This law is only true in low turbulence regimes, where viscosity dominates inertia, resulting in small Reynolds numbers ($Re = w_s d/v$):

$$F_D = F_g, \tag{B.1}$$

$$3\pi\mu d_g w_s = (\rho_s - \rho_w) g \frac{1}{6}\pi d_g^3, \tag{B.2}$$

$$w_s = \frac{(\rho_s - \rho_w) g d_g^2}{18\mu}, \tag{B.3}$$

where F_D is the drag force, F_g is the gravity force, μ is the dynamic viscosity, d is the diameter of the particle, ρ_s is the density of the particle and ρ_w is the density of water. Typical settling velocities for fine sediment are in the order of 0.01 mm/s, while coarser sediment can have settling velocities in the order of 1 cm/s. The small settling velocity for fine sediment is easily overruled by an upward flow, preventing the particles from settling.

For mud flocs the presented formula for settling in a Stokes' regime can not be used, as they are not spherical and their density is not known. Due to the high water content in flocs the density (ρ_f) decreases compared to the particle density, resulting in a lower settling velocity. The aggregation of particles to form flocs results in larger particle diameters, which increases the settling velocity.

Winterwerp (1999) derived an equation for the settling velocities of individual flocs of mud. Based on a literature review he concluded that flocs of mud can be treated as porous, though impermeable, entities.

$$w_s, r = \frac{\alpha}{18\beta}\frac{(\rho_s - \rho_w) g}{\mu} D_p^{3-n_f} \frac{D^{n_f - 1}}{1 + 0.15 Re_p^{0.687}}, \tag{B.4}$$

where α and β are sediment shape factors, ρ_s is the density of the primary sediment particles, D_p is the diameter of the primary mud particles, n_f is the fractal dimension of mud flocs and Re_p is the particle Reynolds number. For spherical ($\alpha = \beta = 1$), massive (n_f=3) particles in Stokes' regime ($Re_p << 1$) Equation B.3 (Stokes law) is obtained from B.4.

For suspensions with high concentrations, particles can influence the settling of neighbouring particles, resulting in hindered settling. Extensive research has been carried out by Scott (1984), focusing on settling of Euclidan (sand) particles. Winterwerp (1999) has extended this research to not Euclidean particles (mud flocs), identifying seven processes affecting the settling velocity of individual particles in suspension:

- Falling particles generate a *return flow and wake formation*, which can affect neighbouring particles. Settling velocities of particles in the near vicinity of this falling particles will be affected, decreasing the overall settling velocity of the suspension.

- The effect of neighbouring particles on the velocity gradients around a falling particle is called the *dynamic flow effect*. This affects the pressure distribution around the particle, hydrodynamic drag and added mass of the particle.
- *Particle-particle collisions* causes additional stresses, hindering the settling of individual particles and therefore decreasing the effective settling velocity.
- *Particle-particle interaction* is the attraction and repulsion between particles, which can result in flocculation.
- Higher particle concentration results in an *increase of viscosity*, which decreases the effective settling velocity of the suspension.
- Individual particles fall in the surrounding suspension, with an *increase of density* the settling velocity of the particle is decreased.
- Particles that are in the wake of other particles will be dragged. As the wake around a group of particles increases, a *cloud of settling particles* will be formed. The cloud can behave as an separate entity, increasing its effective settling velocity.

Hindered settling usually occurs in suspensions with a concentration between 2 g/l and 10 g/l (Whitehouse et al., 2000). Concentrations in passive plumes are generally lower, so hindered settling is in most cases not important.

Another phenomenon occurring in passive plumes is segregation. Segregation relates to the fact that the larger particles settle faster than the smaller particles, resulting in a vertical gradient in particle size (Dankers, 2002). Torfs et al. (1996) studied experiments of earlier research to determine the influence of sand on the settling and consolidation of mud. Segregation occurred in all experiments, by means of sand falling through the mud and being collected at the bottom. But even for mixtures with 0% sand content, segregation was identified. In these cases the larger or more compact flocs sink to the bottom. Segregation leads to layers of mud and sand on the bed, as they are deposited separately.

Appendix C

Delft3D-FLOW

Far-field dredge plume dispersion was modelled using the software engine Delft3D-FLOW, developed by Deltares. It can carry out simulations of flow, sediment transport, waves, water quality, morphological developments and ecology. Delft3D-FLOW simulates hydrodynamics and transport of matter by calculating the non-steady flow and transport phenomena resulting from tidal and meteorological forcing. It solves the 2D (depth-averaged) or 3D non-linear shallow water equations. Delft3D consists of a flow model, a flow field, a transport model and an equation of state which couples the transport model with the flow field and flow model. The system of equations consists of the continuity equation, the momentum equations and the transport equation. To solve the equations boundary conditions, bathymetry, initial conditions and physical parameters are needed.

C.1 Hydrodynamic modelling

The flow equations are derived from the three dimensional Navier-Stokes equations for incompressible free surface flow. Several approximations and assumptions are applied in Delft3D-FLOW. For instance, the shallow water assumption reduces the vertical momentum equation to the hydrostatic pressure relation, following from vertical accelerations being assumed much smaller than the gravitational acceleration. Furthermore, the Boussinesq approximation states that pressure differences are small to the pressure itself.

In the horizontal direction orthogonal curvilinear coordinates are used for which two coordinate systems are supported: Carthesian coordinates (ξ,η) and spherical coordinates (λ,ϕ). In vertical direction two different vertical grid systems are implemented: the σ coordinate system and the Cartesian Z coordinate system. The description of the equations in this appendix is valid for the σ coordinate system. For the Z coordinate system the equations are slightly different. A complete conceptual description can be found in Deltares (2009).

Basic equations

The depth averaged continuity equation is derived by integration of the continuity equation over the total depth, taken into account the kinematic boundary conditions at the water surface and bed level:

$$\frac{\partial \zeta}{\partial t} + \frac{1}{\sqrt{G_{\xi\xi}}\sqrt{G_{\eta\eta}}} \frac{\partial[(d+\zeta)U\sqrt{G_{\eta\eta}}]}{\partial \xi} + \frac{1}{\sqrt{G_{\xi\xi}}\sqrt{G_{\eta\eta}}} \frac{\partial[(d+\zeta)V\sqrt{G_{\xi\xi}}]}{\partial \eta} = (h+\zeta)Q, \qquad \text{(C.1)}$$

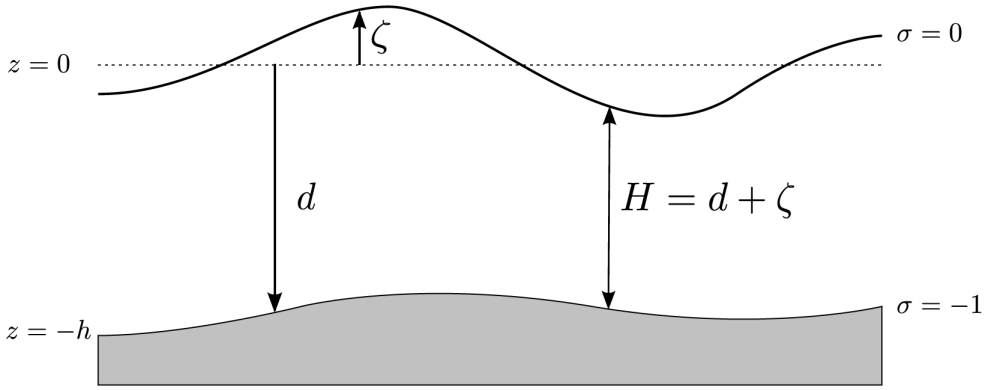

Figure C.1: Definition of water level (ζ), depth (h) and total depth (H) (Deltares, 2009).

where ζ is the water level and d is the depth, $\sqrt{G_{\xi\xi}}$ and $\sqrt{G_{\eta\eta}}$ are coefficients used to transform curvilinear to rectangular coordinates, U and V are depth-averaged velocities in ξ- and η-direction respectively and Q is the water discharge or withdrawal per unit area depending on the discharge, precipitation (P) and evaporation (E):

$$Q = H \int_{-1}^{0} (q_{in} - q_{out}) \mathrm{d}\sigma + P - E, \tag{C.2}$$

The horizontal momentum equations in ξ and η direction are given by:

$$\frac{\partial u}{\partial t} + \frac{u}{\sqrt{G_{\xi\xi}}}\frac{\partial u}{\partial \xi} + \frac{v}{\sqrt{G_{\eta\eta}}}\frac{\partial u}{\partial \eta} + \frac{\omega}{d+\zeta}\frac{\partial u}{\partial \sigma} - \frac{v^2}{\sqrt{G_{\xi\xi}}\sqrt{G_{\eta\eta}}}\frac{\partial \sqrt{G_{\eta\eta}}}{\partial \xi} + \frac{uv}{\sqrt{G_{\xi\xi}}\sqrt{G_{\eta\eta}}}\frac{\partial \sqrt{G_{\xi\xi}}}{\partial \eta} - fv = -\frac{1}{\rho_0 \sqrt{G_{\xi\xi}}} P_\xi + F_\xi + \frac{1}{(d+\zeta)^2}\frac{\partial}{\partial \sigma}(\nu_V \frac{\partial u}{\partial \sigma}) + M_\xi, \tag{C.3}$$

and

$$\frac{\partial v}{\partial t} + \frac{u}{\sqrt{G_{\xi\xi}}}\frac{\partial v}{\partial \xi} + \frac{v}{\sqrt{G_{\eta\eta}}}\frac{\partial v}{\partial \eta} + \frac{\omega}{d+\zeta}\frac{\partial v}{\partial \sigma} + \frac{uv}{\sqrt{G_{\xi\xi}}\sqrt{G_{\eta\eta}}}\frac{\partial \sqrt{G_{\eta\eta}}}{\partial \xi} + \frac{u^2}{\sqrt{G_{\xi\xi}}\sqrt{G_{\eta\eta}}}\frac{\partial \sqrt{G_{\xi\xi}}}{\partial \eta} - fu = -\frac{1}{\rho_0 \sqrt{G_{\eta\eta}}} P_\eta + F_\eta + \frac{1}{(d+\zeta)^2}\frac{\partial}{\partial \sigma}(\nu_V \frac{\partial v}{\partial \sigma}) + M_\eta, \tag{C.4}$$

where u, v and ω are flow velocities in ξ-, η- and σ-direction, ρ_0 is the density of water, f is the Coriolis parameter, P_ξ and P_η represent the pressure gradients, F_ξ and F_η are turbulent momentum fluxes, ν_V is the vertical eddy viscosity coefficient and M_ξ and M_η are external sources or sinks.

The before mentioned shallow water assumption reduces the vertical momentum equation to a balance of the pressure and gravity terms. In this way vertical accelerations due to buoyancy effects or bottom topography are not taken into account. This results in the hydrostatic pressure equation:

$$\frac{\delta P}{\delta \sigma} = -g\rho H, \tag{C.5}$$

Boundary conditions

To get a well-posed mathematical problem with a unique solution for the shallow water equations several initial and boundary conditions for water level and horizontal velocities must be specified. At the surface boundary the momentum equations require a formulation for the shear stress, which is determined by:

$$|\vec{\tau}_s| = \rho_a C_d U_{10}^2, \tag{C.6}$$

where ρ_a is the density of air, U_{10} is the wind speed 10 meter above the free surface (time and space dependent) and C_d is the wind drag coefficient, dependent on U_{10}. In case of no wind the shear stress can be set to zero.

At the bed boundary also a shear stress is required. For 2D depth-averaged flow the shear stress at the bed induced by a turbulent flow is assumed to be given by a quadratic friction law:

$$\vec{\tau}_b = \frac{\rho_0 g \vec{U}|\vec{U}|}{C_{2D}^2}, \tag{C.7}$$

where ρ_0 is the reference density of water, $|\vec{U}|$ is the magnitude of the depth-averaged horizontal velocity and C_{2D} is the Chézy coefficient.

Apart from the bed and surface boundary conditions, boundary conditions have to be specified at all open boundaries of the numerical domain. At any boundary the water level, the normal velocity component or a combination of both should be prescribed.

Grid

To solve the partial differential equations, the equations should be transformed to the discrete space. Therefore the model is covered by a curvilinear grid, which is assumed to be orthogonal and well-structured. Delft3D-FLOW makes use of a special grid pattern, named staggered grid, to arrange the variables describing the flow (u,v,w). On a staggered grid the velocity and water level are not defined at the same locations. The velocity points are always located at the boundaries of the cells, while the water level points (pressure points) are defined in the middle of the cells (Figure C.2). The grid coordinates can be defined either in a Cartesian or in a spherical coordinate system.

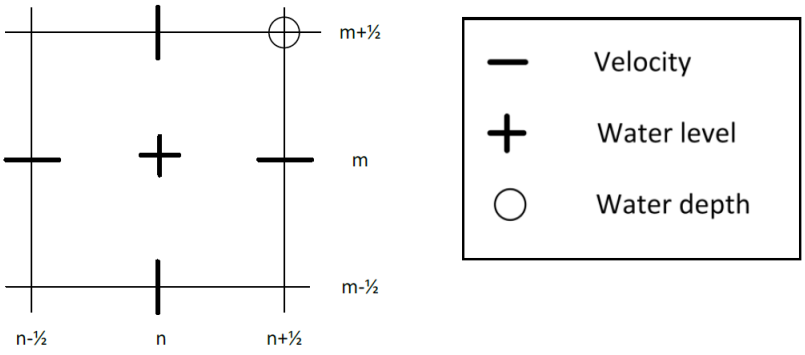

Figure C.2: 2D view of a staggered grid, indicating water level and velocity points.

The numerical grid transformation is implicitly known by the mapping of the coordinates of the grid vertices from the physical to the computational space. The geometrical quantities $\sqrt{G_{\xi\xi}}$ and

$\sqrt{G_{\eta\eta}}$ introduced in Equation C.1, C.3 and C.4, have to be distrectised on the computational grid, as is indicated in Figure C.3.

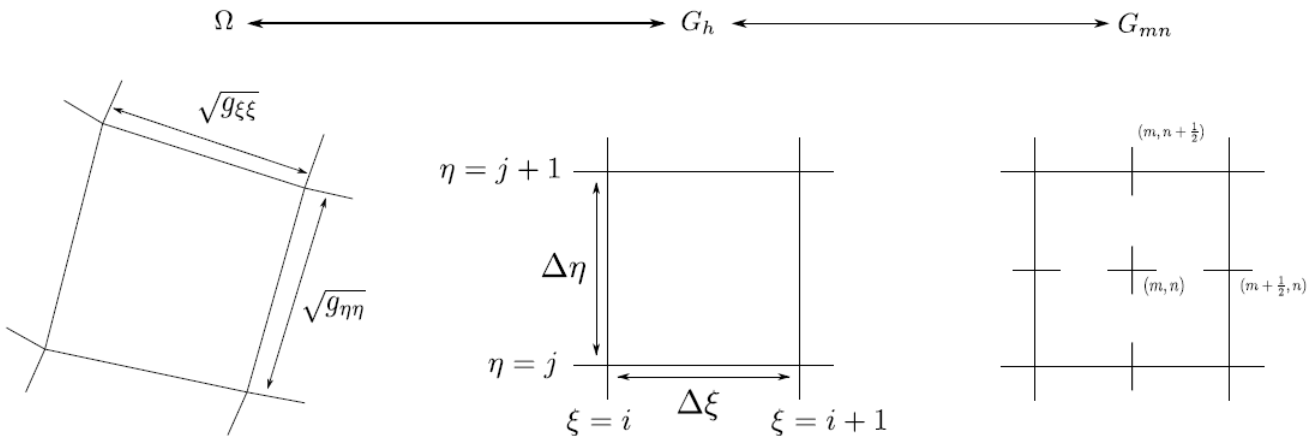

Figure C.3: Mapping of physical space to the computational space (Deltares, 2009).

Time integration

For time integration the ADI-method (Alternating Direction Implicit) is used in Delft3D-FLOW. This is an integration method which splits one time step into two steps, which means that each step consists of half of the time step. In both steps all the equations are solved. For the water level gradient and the advection terms the time levels are alternating. This means that if in one stage a term is taken implicitly in time, in the other stage this term will be taken explicitly in time. Each term has an accuracy of second order in time. The advantage of this model compared with other time-integration methods is that the matrix of equations is reduced to a more structured matrix. The implicitly integrated water levels and velocities are coupled along grid lines. This coupling leads to a system of equations with a small band width.

Because of accuracy and stability for the time integration of the shallow water equations in Delft3D-FLOW, several time step limitations are given. Table C.1 shows an overview of these limitations, in which Δx and Δy are the horizontal grid sizes.

C.2 Sediment transport modelling

Both bed-load and suspended load transport of non-cohesive sediments and suspended transport of cohesive sediments are supported in Delft3D-FLOW. The 3D advection-diffusion equation is solved to calculate suspended sediment transport. This equation is also used to calculate transport of other matter, e.g. heat and salinity. However, there are some major differences between sediment transport modelling and modelling of other constituents. Sediment can be eroded or deposited (exchange between bed and flow), sediment has a settling velocity under action of gravity and the effects sediment has on the local mixture density can be taken into account. The settling velocity, deposition and erosion are processes that are sediment-type specific.

Points per wave period T	$\Delta t \leq \frac{T}{40}$
Accuracy ADI for barotropic mode for complex geometries	$2{*}C_f = 2\Delta t\sqrt{gH(\frac{1}{\Delta x^2}+\frac{1}{\Delta y^2})} < 4\sqrt{2}$
Explicit advection scheme "Flooding scheme" and for the Z-grid model	$2{*}\frac{\Delta t\lvert u\rvert}{\Delta x} < 2$
Stability baroclinic mode internal wave propagation (Z-grid model only)	$2{*}\Delta t\sqrt{\frac{(\rho_{bottom}-\rho_{top})}{\rho_{top}}g\frac{H}{4}(\frac{1}{\Delta x^2}+\frac{1}{\Delta y^2})} < 1$
Explicit algorithm flooding	$\frac{\Delta t\lvert u\rvert}{\Delta x} < 2$
Stability horizontal viscosity term (HLES, partial slip, no slip)	w$2{*}2\Delta t\nu_H(\frac{1}{\Delta x^2}+\frac{1}{\Delta y^2}) < 1$

Table C.1: Time step limitations

Basic equations

The advection-diffusion (mass-balance) equation that is solved for transport of suspended sediment is given by:

$$\frac{\partial C^{(\ell)}}{\partial t}+\frac{\partial uC^{(\ell)}}{\partial x}+\frac{\partial vC^{(\ell)}}{\partial y}+\frac{\partial (w-w_s^{(\ell)})C^{(\ell)}}{\partial z}- \frac{\partial}{\partial x}\left(\varepsilon_{s,x}^{(\ell)}\frac{\partial C^{(\ell)}}{\partial x}\right)-\frac{\partial}{\partial y}\left(\varepsilon_{s,y}^{(\ell)}\frac{\partial C^{(\ell)}}{\partial y}\right)-\frac{\partial}{\partial z}\left(\varepsilon_{s,z}^{(\ell)}\frac{\partial C^{(\ell)}}{\partial z}\right)=0, \quad \text{(C.8)}$$

where $C^{(\ell)}$ is the mass concentration of sediment fraction (ℓ), u, v and w are flow velocity components, $\varepsilon_{s,x}^{(\ell)}$, $\varepsilon_{s,y}^{(\ell)}$ and $\varepsilon_{s,z}^{(\ell)}$ are eddy diffusivities of sediment fraction (ℓ) and $w_s^{(\ell)}$ is the (hindered) sediment settling velocity of sediment fraction (ℓ).

Initial and boundary conditions are needed for Equation C.8. The boundary conditions consist of a water surface boundary condition, a bed boundary condition and open inflow and outflow boundary conditions. The boundary condition at the bed is given by:

$$-w_s^{(\ell)}C^{(\ell)}-\varepsilon_{s,z}^{(\ell)}\frac{\partial C^{(\ell)}}{\partial z}=D^{(\ell)}-E^{(\ell)}, \text{ at } z=z_b, \quad \text{(C.9)}$$

where $D^{(\ell)}$ is the sediment deposition rate of sediment fraction (ℓ) and $E^{(\ell)}$ is the sediment erosion rate of sediment fraction (ℓ). This equation relates the suspended sediment concentration in the bottom layer to these fluxes. In every cell a source and sink term is applied. The calculated fluxes are also applied to the bed, in order to update the bed level. The description of the deposition and erosion fluxes is different for cohesive and non-cohesive sediments.

At the surface the vertical flux through the free surface is set to zero, resulting in:

$$-w_s^{(\ell)}C^{(\ell)}-\varepsilon_{s,z}^{(\ell)}\frac{\partial C^{(\ell)}}{\partial z}=0, \text{ at } z=\zeta, \quad \text{(C.10)}$$

where $z=\zeta$ is the location of the free surface. For the open inflow boundaries, conditions for all conservative constituents need to be specified. A Thatcher-Harleman return time can be specified

to simulate re-entry of material that flowed out of the model. Another option allows to specify equilibrium concentration profiles for sediment fractions to be applied to inflow at the open boundaries. At the outflow boundaries, no conditions are applied, which means that only advection is considered.

Erosion and sedimentation

For cohesive sediment fractions the exchange between water phase and bed is calculated using the Partheniades-Krone formulations (Partheniades, 1965):

$$E^{(\ell)} = M^{(\ell)} S(\tau_{cw}, \tau_e^{(\ell)}), \tag{C.11}$$

$$D^{(\ell)} = w_s^{(\ell)} C_b^{(\ell)} S(\tau_{cw}, \tau_d^{(\ell)}), \tag{C.12}$$

$$C_b^{(\ell)} = C^{(\ell)}(z = \frac{\Delta z_b}{2}, t), \tag{C.13}$$

where $E^{(\ell)}$ is the erosion flux, $M^{(\ell)}$ is the erosion parameter and $S(\tau_{cw}, \tau_e^{(\ell)})$ is the erosion step function, given by:

$$S(\tau_{cw}, \tau_e^{(\ell)}) = \begin{cases} (\frac{\tau_{cw}}{\tau_e^{(\ell)}} - 1), & \text{when } \tau_{cw} > \tau_e^{(\ell)} \\ 0, & \text{when } \tau_{cw} \leq \tau_e^{(\ell)} \end{cases} \tag{C.14}$$

where $D^{(\ell)}$ is the deposition flux, $w_s^{(\ell)}$ is the settling velocity, $c_b^{(\ell)}$ is the average sediment concentration in the near bottom computational layer and $S(\tau_{cw}, \tau_d^{(\ell)})$ is the deposition step function, given by:

$$S(\tau_{cw}, \tau_d^{(\ell)}) = \begin{cases} (1 - \frac{\tau_{cw}}{\tau_d^{(\ell)}}), & \text{when } \tau_{cw} < \tau_d^{(\ell)} \\ 0, & \text{when } \tau_{cw} \geq \tau_d^{(\ell)} \end{cases} \tag{C.15}$$

where τ_{cw} is the maximum bed shear stress, $\tau_e^{(\ell)}$ is the critical erosion shear stress and $\tau_d^{(\ell)}$ is the critical deposition shear stress.

The calculated erosion and deposition fluxes are applied to the near bottom computational cell by setting the appropriate sink and source terms to that cell. Advection, particle settling and diffusion through the bottom of this cell are all set to zero to prevent double counting these fluxes.

Appendix D

Supporting figures

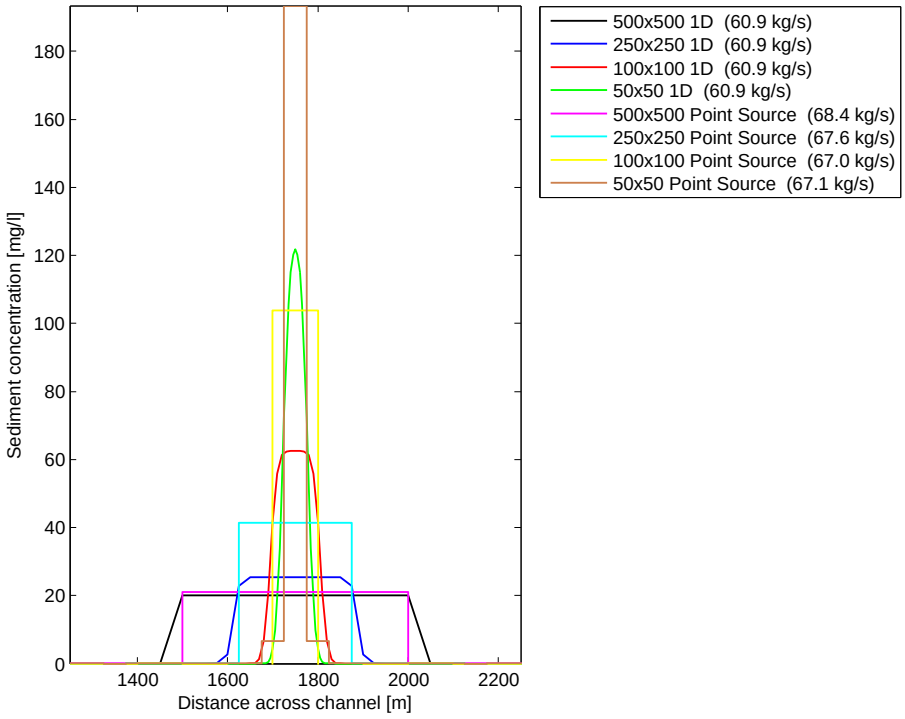

Figure D.1: Lateral concentration profiles and sediment fluxes observed 80 min after start source for a plume age of 26 min for several 2D and 1D simulations.

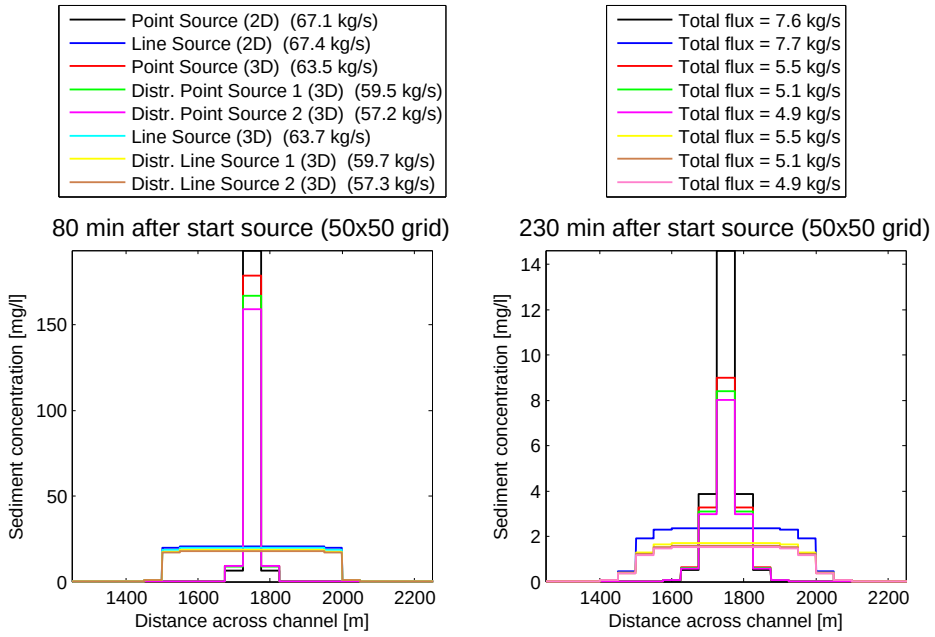

Figure D.2: Lateral concentration profiles and sediment fluxes observed 80 min after start source, for a plume age of 26 min (left figure) and observed 230 min from start source, for a plume age of 167 min (right figure) for several source terms.

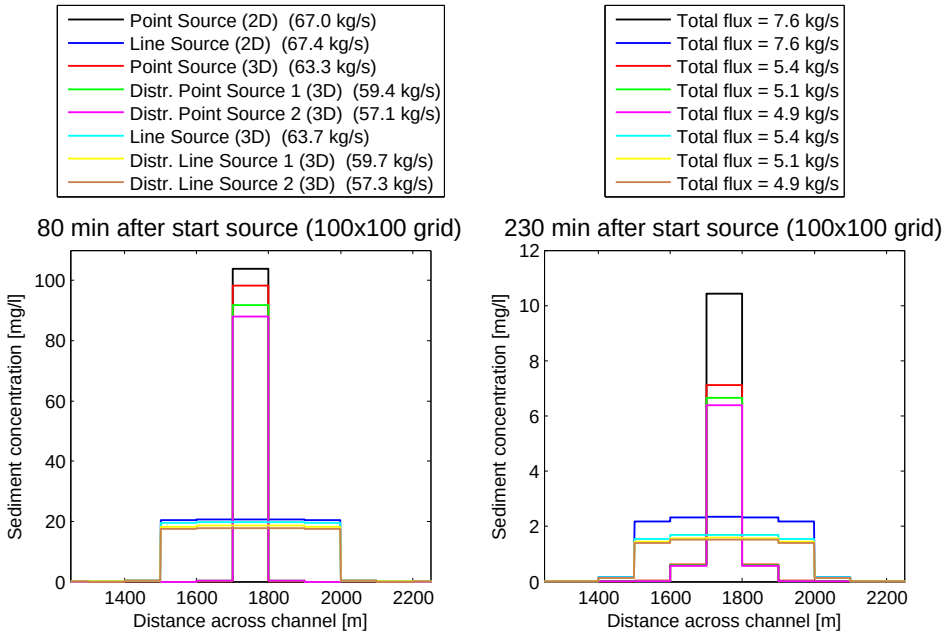

Figure D.3: Lateral concentration profiles and sediment fluxes observed 80 min after start source, for a plume age of 26 min (left figure) and observed 230 min from start source, for a plume age of 167 min (right figure) for several source term.

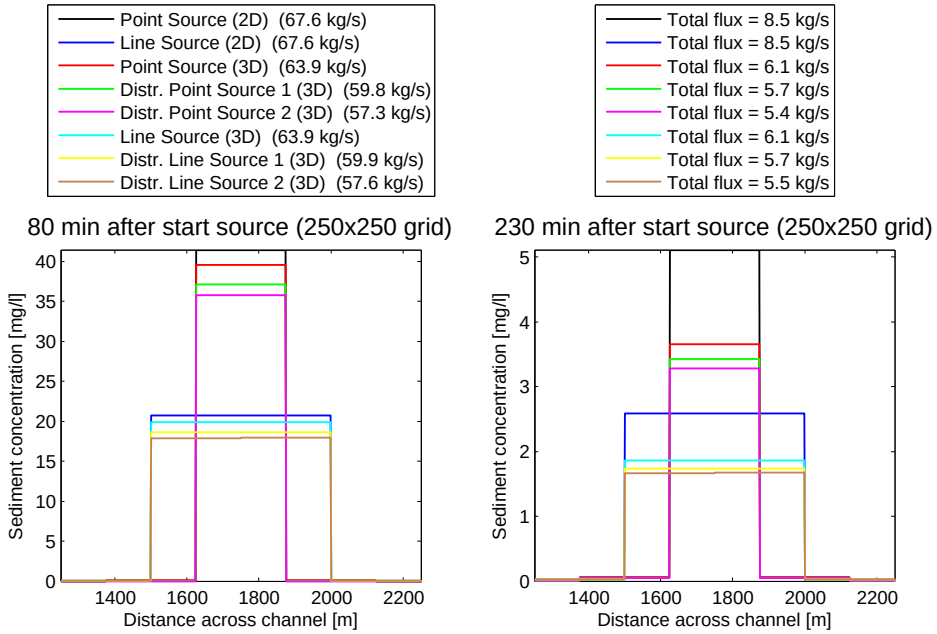

Figure D.4: Lateral concentration profiles and sediment fluxes observed 80 min after start source, for a plume age of 26 min (left figure) and observed 230 min from start source, for a plume age of 167 min (right figure) for several source term.

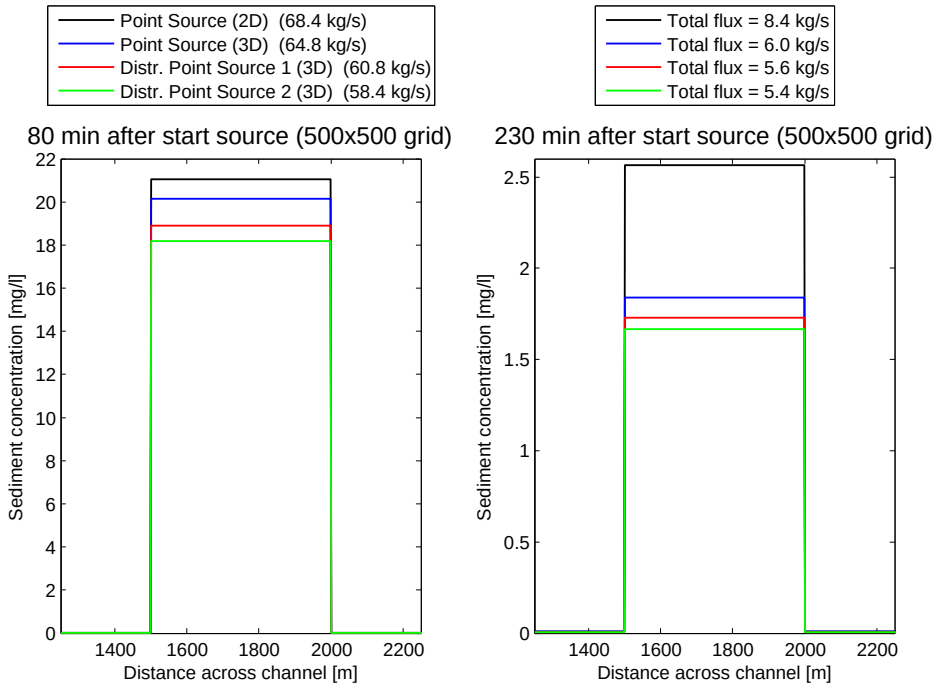

Figure D.5: Lateral concentration profiles and sediment fluxes observed 80 min after start source, for a plume age of 26 min (left figure) and observed 230 min from start source, for a plume age of 167 min (right figure) for several source term.

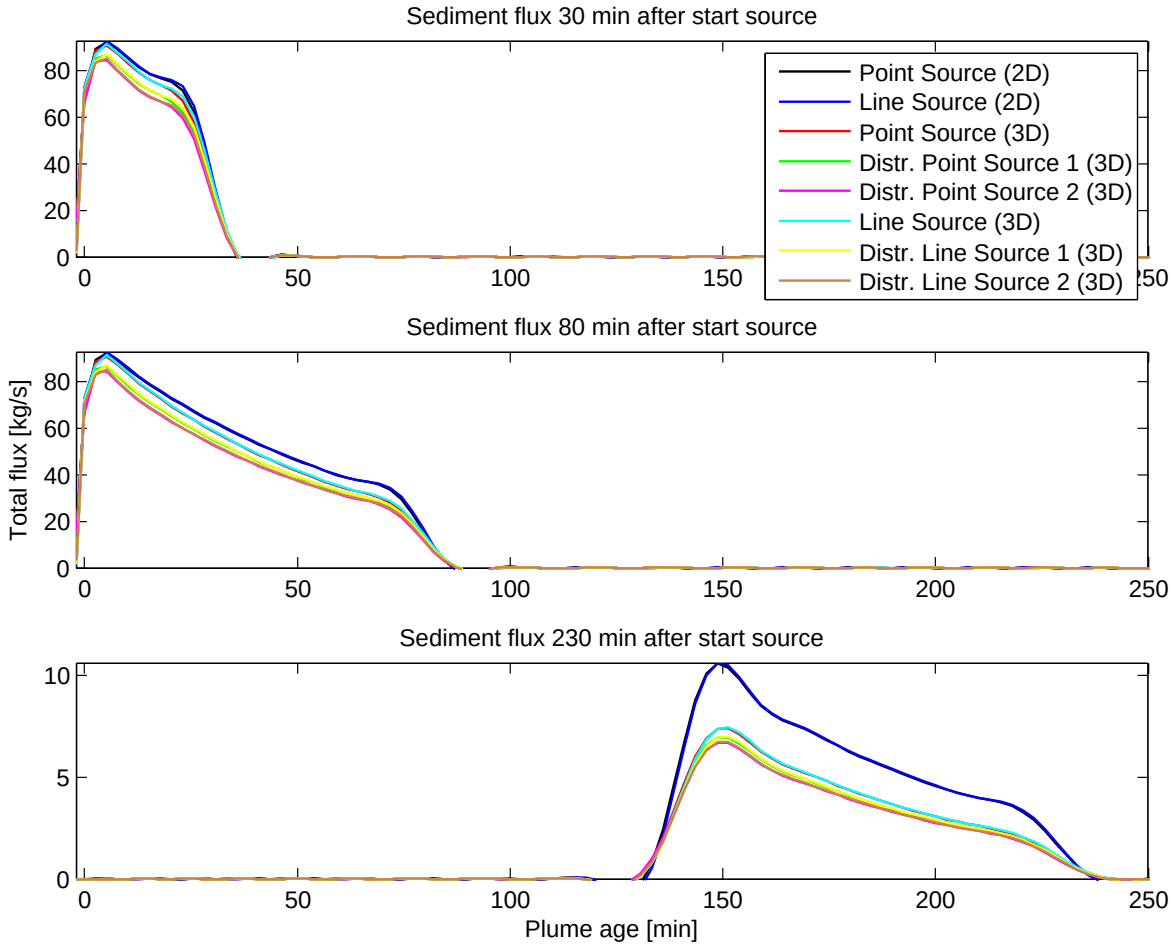

Figure D.6: Total flux as function of the plume age along the channel for 2D and 3D simulations observed 30, 80 and 230 min after start source.

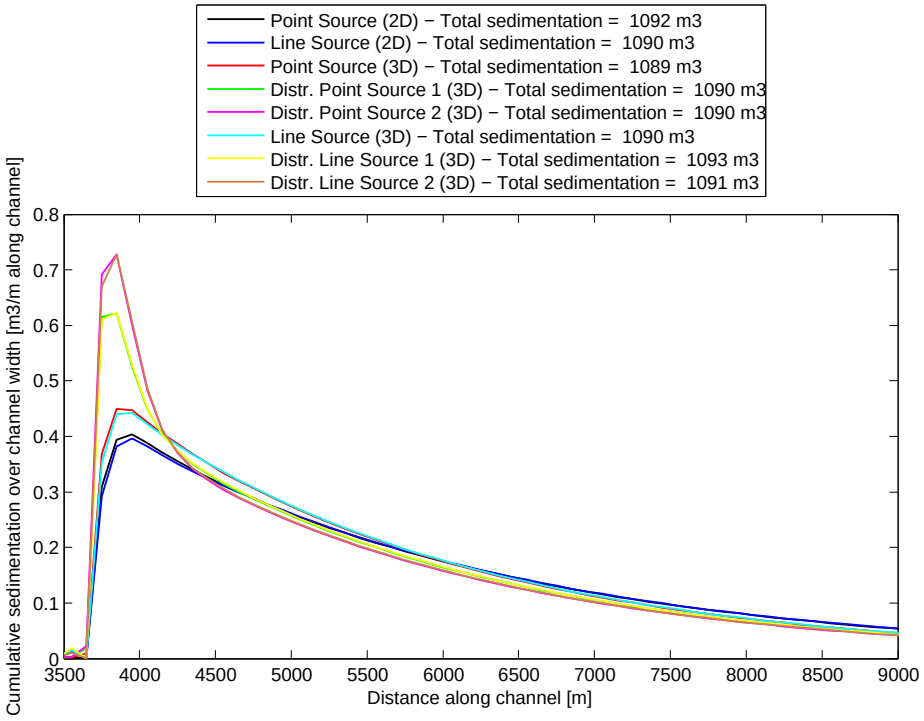

Figure D.7: Cumulative sedimentation/erosion along channel for several source terms on 100x100 grid.

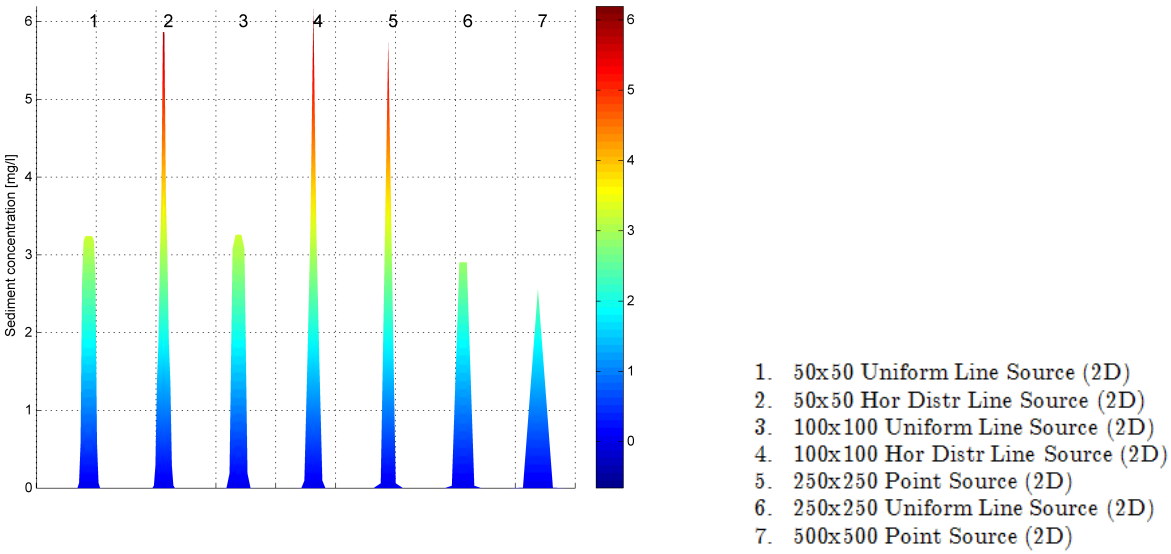

Figure D.8: Sediment concentration profiles observed 230 minutes after start source for different sources and on different grids.

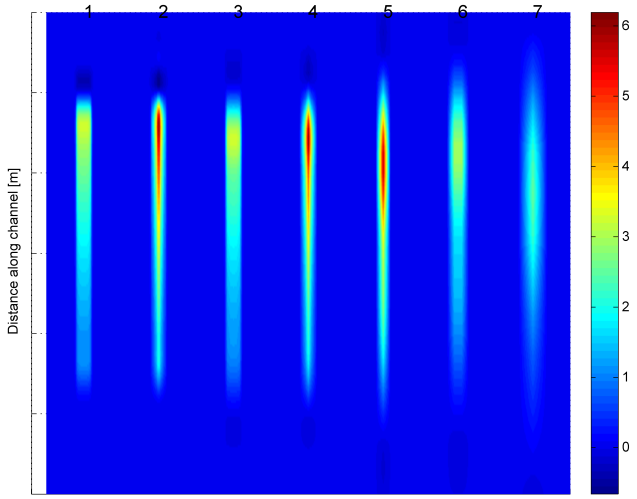

1. 50x50 Uniform Line Source (2D)
2. 50x50 Hor Distr Line Source (2D)
3. 100x100 Uniform Line Source (2D)
4. 100x100 Hor Distr Line Source (2D)
5. 250x250 Point Source (2D)
6. 250x250 Uniform Line Source (2D)
7. 500x500 Point Source (2D)

Figure D.9: Top view of sediment concentrations observed 230 minutes after start source for different sources and on different grids.

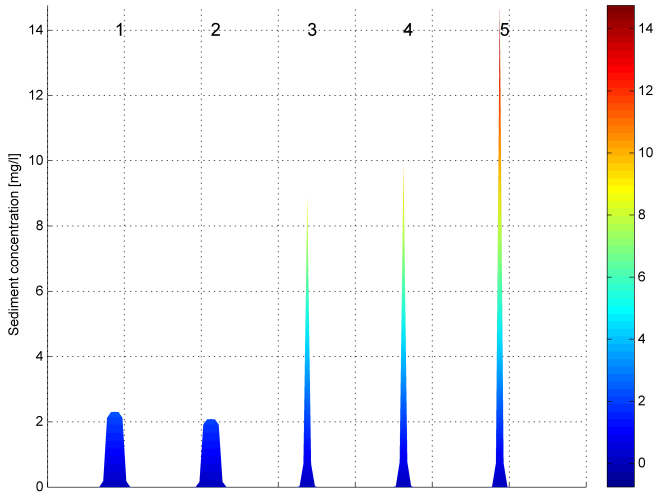

1. Uniform Line Source (3D)
2. Vertical Distr Line Source (3D)
3. Vertical Distr Point Source (3D)
4. Point Source (3D)
5. Point Source (2D)

Figure D.10: Sediment concentration profiles observed 230 minutes after start source for different sources on 100x100 grid.

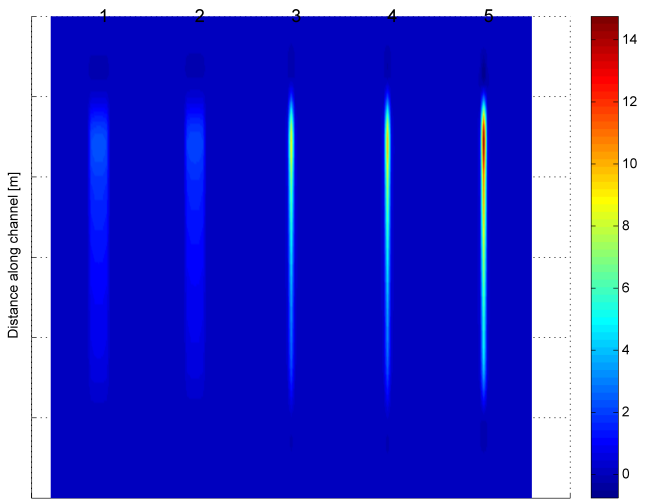

1. Uniform Line Source (3D)
2. Vertical Distr Line Source (3D)
3. Vertical Distr Point Source (3D)
4. Point Source (3D)
5. Point Source (2D)

Figure D.11: Top view of sediment concentrations observed 230 minutes after start source for different sources on 100x100 grid.